Using UAV-Based Imagery to Determine Volume, Groundcover, and Growth Rate Characteristics of Lentil (*Lens culinaris* Medik.)

A Thesis Submitted to the College of Graduate and Postdoctoral Studies

In Partial Fulfillment of the Requirements for the Degree of Master of Sciences in the Department of Plant Sciences

University of Saskatchewan

Saskatoon, Saskatchewan, Canada

By

Karsten M.E. Nielsen

PERMISSION TO USE

In presenting this thesis/dissertation in partial fulfillment of the requirements for a Postgraduate degree from the University of Saskatchewan, I agree that the Libraries of this University may make it freely available for inspection. I further agree that permission for copying of this thesis/dissertation in any manner, in whole or in part, for scholarly purposes may be granted by the professor or professors who supervised my thesis/dissertation work or, in their absence, by the Head of the Department of Plant Sciences or the Dean of the College of Agriculture and Bioresources. It is understood that any copying or publication or use of this thesis/dissertation or parts thereof for financial gain shall not be allowed without my written permission. It is also understood that due recognition shall be given to me and to the University of Saskatchewan in any scholarly use which may be made of any material in my thesis/dissertation.

Requests for permission to copy or to make other uses of materials in this thesis/dissertation in whole or part should be addressed to:

Head of the Department of Plant Sciences

College of Agriculture and Bioresources, University of Saskatchewan

Room 4D36, Agriculture Building 51 Campus Drive

Saskatoon, Saskatchewan S7N 5A8 Canada

or

Dean

College of Graduate and Postdoctoral Studies

University of Saskatchewan

116 Thorvaldson Building, 110 Science Place

Saskatoon, Saskatchewan S7N 5C9

Canada

Abstract

Plant growth rate is an essential phenotypic parameter for crop physiologists and plant breeders to understand in order to quantify potential crop productivity based on specific stages throughout the growing season. While plant growth rate information can be attained though manual collection of biomass, this procedure is rarely performed due to the prohibitively large effort and destruction of plant material that is required. Unmanned Aerial Vehicles (UAVs) offer great potential for rapid collection of imagery which can be utilized for quantification of plant growth rate. In this study, six diverse lines of lentil were grown in three replicates of microplots with six biomass collection time-points throughout the growing season over five site-years. Aerial imagery of each biomass collection time point was collected from a UAV and utilized to produce stitched two-dimensional orthomosaics and three-dimensional point clouds. Analysis of this imagery produced quantification of groundcover and vegetation volume on an individual plot basis. Comparison with manually-measured above-ground biomass suggests strong correlation, indicating great potential for UAVs to be utilized in plant breeding programs for evaluation of groundcover and vegetation volume. Nonlinear logistic models were fit to multiple data collection points throughout the growing season. The growth rate and G50, which is the number of growing degree days (GDD) required to accumulate 50 % of maximum growth, parameters of the model are capable of quantifying growth rate, and have potential utility in plant research and plant breeding programs. Predicted maximum volume was identified as a potential proxy for whole-plot biomass measurement. Six new phenotypes have been described that can be accurately and efficiently collected from field trials with the use of UAV's or other overhead image-collection systems. These phenotypes are; Area Growth Rate, Area G50, Area Maximum Predicted Growth, Volume Growth Rate, Volume G50, and Volume Maximum Predicted Growth.

Acknowledgements

I would like to express most sincere gratitude to my supervisors Dr. Kirstin Bett and Dr. Steve Shirtliffe. Their constant support and encouragement throughout my entire experience as a graduate student have helped to drive my academic development and aided tremendously in the completion of this thesis. I am grateful to my advisory committee, Dr. Ravindra Chibbar, Dr. Kevin Stanley, and Dr. Kate Congreves, for their valuable suggestions and constructive criticism throughout this project.

I would like to sincerely thank Dr. Hema Duddu and Monglu Wang for all of their suggestions and assistance with image collection and image processing, as well as the Agronomy and Weed Ecology crew and the Pulse Crop Breeding crew for their support and friendship. I would also likely to thank my fellow graduate students for their support, suggestions, and friendship throughout this experience.

I sincerely acknowledge the financial support provided for this research by the Saskatchewan Pulse Growers, Genome Prairie, the Government of Saskatchewan, Canada First Research Excellence Fund, Western Grains Research Foundation, the University of Saskatchewan Plant Imaging and Research Center, Application of Genomics to Innovation in the Lentil Economy (AGILE), and Genome Canada. I would also like to show my most sincere appreciation to the family and estate of Dr. Robert Knowles for the support I received through the Robert P. Knowles Scholarship Fund during my studies.

Dedication

To my family, friends, and peers for their limitless support and encouragement throughout my graduate studies. To my parents, for instilling the love and appreciation of the outdoors which has led to my interest in this field.

Table of Contents

List of Tables

List of Figures

List of Abbreviations

2-D – Two Dimensional

3-D – Three Dimensional

AGILE – Application of Genomic Innovation in the Lentil Economy

AGL – Above Ground Level

AIC – Akaike Information Criterion

ALS – Airborne Laser Scanner

ANOVA – Analysis of Variance

B.C.E. – Before the Common Era

bNDVI – Blue Normalized Difference Vegetation Index

CPWC – Critical Period for Weed Control

DSM – Digital Surface Model

DTM – Digital Terrain Model

DW – Dry Weight

FAO – Food and Agriculture Organization

G × E – Genotype by Environment

GCP – Ground Control Point

GDD – Growing Degree Days

GLONASS – Global Navigation Satellite System

gNDVI – Green Normalized Difference Vegetation Index

GPS – Global Positioning System

GSD – Ground Sample Distance

GWAS – Genome-Wide Association Mapping

HI – Harvest Index

IR – Infrared

LAI – Leaf Area Index

LiDAR – Light Detection and Ranging

LOF – Local Outlier Factor

MP – Megapixel

NDVI - Normalized Difference Vegetation Index

NGRDI – Normalized Green Red Difference Index

NIR – Near Infrared

OBIA – Object-Based Image Analysis

RGB – Red Green Blue

RTK – Real Time Kinematic

SfM – Structure from Motion

TIFF – Tagged Image File Format

UAV – Unmanned Aerial Vehicle

VI – Vegetation Index

VTOL – Vertical Take-off and Landing

WW – Wet Weight

List of Equations

Equation 2.1

$$Phenotype = Genotype + Environment + (Genotype \times Environment)$$

Equation 2.2

$$NDVI = \frac{NIR - Red}{NIR + Red}$$

Equation 2.3

$$gNDVI = \frac{NIR - Green}{NIR + Green}$$

Equation 2.4

$$bNDVI = \frac{NIR - Blue}{NIR + Blue}$$

Equation 2.5

$$NGRDI = \frac{Green - Red}{Green + Red}$$

Equation 4.1

$$f(x, (b, c, d, e)) = c + \frac{d - c}{1 + \exp\left(b(\log(x) - \log(e))\right)}$$

Equation 5.1

$$w = C.p^{-3/2}$$

1.0 Introduction

The current demand for an increase in global food production is enormous. The Food and Agriculture Organization (FAO) estimates the need for a 70 % increase in global food production before 2050 in order to feed the rapidly growing population (FAO, 2009). A production increase of this magnitude will require a multifaceted approach involving increased production area, improved agronomic practices, more efficient production and transportation systems, and the development of improved crop varieties (Tilman et al., 2011).

In recent years, the cost of genotyping has dramatically declined and the ability to efficiently and accurately identify a large number of genes has become possible (Ingvarsson and Street, 2011; Shendure and Hanlee, 2008). Association studies aim to compare large sequenced germplasm collections with corresponding phenotypic information, enabling researchers to connect phenotypic responses with their controlling genes. By including evaluation of phenotypes across multiple environments, genotype × environment (G×E) interactions can be deduced. Understanding G×E interactions is essential to determine the effect identified genes will have over multiple environments (Brachi et al., 2010).

In order for new crop varieties to be developed, plant breeders expend significant resources identifying and quantifying traits which may be of use in future varieties. Data must be manually collected on a large number of breeding lines, often with multiple replications and locations (Miladinović et al., 2015). This much data is generally not possible for one individual to collect, so multiple people may be employed for the collection of trait information. Factors such as fatigue, variability of observers, and changes in plant morphology over time can result in inconsistencies in data collection, causing errors and inefficiencies in the breeding program (Daniel et al., 2017). Additionally, this large labour requirement comes at a significant cost and represents a major expense in any breeding program (Furbank, 2009; Reynolds et al., 2019).

Remote sensing techniques have the potential to dramatically improve the quality of data collected in plant breeding programs, while also reducing the labour required to collect the same amount of data. The use of technology which allows rapid imaging of research trials may permit the collection of multiple phenotypic traits at one time, and collection of those same traits multiple times throughout the growing season (Andrade-Sanchez et al., 2013). Plant height in a typical research program utilizing human data collectors, for example, may be collected one or

two times during a growing season and require a substantial amount of labour (Jiang et al., 2016). However, utilizing remote sensing technologies, multiple traits may be collected concurrently as frequently as desired and require only a few minutes per day of in-field activity (Han et al., 2019; Hu et al., 2018).

Above-ground biomass is an important trait for plant breeders to understand for a number of reasons that may differ based on the end-goal of the crop. In crops where the entire plant contributes to an end-use such as forage for livestock feed, bioenergy, or textiles, above-ground biomass can be used to directly measure yield potential. In crops where only a portion of above-ground biomass is desired, total above-ground biomass can still provide useful information regarding yield (Grüner et al., 2019). In lentil (*Lens culinaris* Medik.), as well as other crops grown for seed, plant biomass is a measurement which often correlates with seed yield (Whitehead et al., 2000) and other traits useful to breeders (Donald and Hamblin, 1976). Under sub-optimal growing conditions, excessive above-ground biomass may be considered undesirable as resources put into biomass might be better utilized for the production of seed yield (Dixit et al., 2017). Conversely, insufficient above-ground biomass will limit the crops ability to collect resources and result in reduced yield potential.

Despite clear reasons for measuring aboveground crop growth, directly associated traits such as biomass are seldom measured in breeding programs due to the large cost and labour requirements for their collection. Multiple measurements throughout a season are of even greater value due to the ability to accurately calculate parameters such as plant growth rates, competitive advantage against weeds, and to determine ideal fertility and irrigation regimes. Multiple biomass collections, however, are essentially unheard of in breeding programs due to the destructive nature of collection and prohibitively high cost and time requirements.

The objectives of this study were to compare parameters of plant growth rate obtained by conventional methods and high-throughput phenotyping techniques, and to evaluate their potential utility in plant breeding programs. High-resolution aerial images were collected on a diverse panel of lentil (*Lens culinaris* Medik. spp.) produced in Saskatchewan, Canada, in 2017 and 2018. By utilizing several high-resolution overlapping overhead images, 2-dimensional (2-D) orthomosaics and dense 3-dimensional (3-D) point clouds were produced.

2-D orthomosaics are produced by stitching multiple overlapping high-resolution images together into a single large image. Analysis of these orthomosaics can produce measurements of digital groundcover by quantifying pixels of certain spectral values which identify plant tissues. By making assumptions on plant architecture and density, these orthomosaics may also be used as a proxy for biomass.

3-D point clouds can be produced from the same set of overlapping images as a 2-D orthomosaics using Structure from Motion (SfM) methodology. SfM software works by automatically matching key features in multiple images to extrapolate 3-D structural information (Doneus et al., 2011; Neitzel and Klonowski, 2011; Pix4D, Switzerland; Verhoeven et al., 2012). Analysis of 3-D point clouds can be used to quantify digital canopy volume. In many field and tree crop species, plant dimensions and canopy volume are important factors which may limit yield (Hill et al., 1987; Underwood, et al., 2016; Morgan et al., 2001). In addition, digital canopy volume may be used as a proxy for biomass. Using this estimate of volume, biomass and plant growth rate can be quantified at a higher level of accuracy than though a 2-D approach due to increased information. Because this data can be collected quickly and efficiently at a high temporal frequency, it is possible to interpret crop changes over time. Plant growth rate can be extracted from structural changes undergone by the crop throughout the growing season, giving highly valuable insight into differential performance of various genotypes throughout a growing season.

2.0 Literature Review

2.1 Lentil

Lentil is one of the oldest crops known to human civilization (Sonnante et al., 2009), and among the first domesticated agricultural crops. It was likely domesticated during the Epipaleolithic period in the Near-East around 8900 to 8600 B.C.E. (Lev-Yadun et al., 2000). Lentil is a small bushy annual diploid (2n=2x=14) legume that produces small pods 1-2 cm long (Sarker and Erskine, 2006). Plant height ranges from 15 cm to 75 cm depending on genotype and environmental conditions (Saxena, 2009). Cultivated lentil can be classified as large-seeded (macrosperma) or small-seeded (microsperma) (Sandhu and Singh, 2007), with large variation in seed colour and cotyledon colour. Market classes are defined by seed size and colour, with specific demands for various market classes (Erskine et al., 2009b). Each pod contains one to two lens-shaped seeds, which are protein-rich and contain many vitamins and minerals important for humans (Erskine et al., 2009a). Lentils can be consumed as a meat substitute, and are popular in Europe, much of the Middle East, and India (Sandhu and Singh, 2007). Lentils contain high levels of tryptophan and lysine and will result in a balanced intake of essential amino acids in the human diet when partnered with wheat or rice (Erskine, 1983).

The largest producers of lentil are Canada, India, and Turkey (FAOSTAT, 2017). Lentil production and volume increased dramatically on a global scale between 1961 and 2006 (Bekkering, 2015). Canada is the largest global exporter of lentils, and exported 2 053 528 t in 2016, contributing over 50 % of the total global share, considerably more than all other observed nations (FAOSTAT, 2016). The majority of Canadian lentils are produced in the Province of Saskatchewan (Government of Saskatchewan, 2018).

Lentil produces relatively low biomass compared to other field crops due to their short height and insubstantial stems. Whitehead et al. (2000) identified a strong positive correlation in four lentil genotypes between seed yield and biomass in Pullman, WA, USA and Reading, UK. Erskine (1983) also identified a positive relationship between straw yield and seed yield in a collection of 3 586 genotypes of lentil. This correlation suggests that by identifying plant growth rate and predicting biomass early in the growing season, yield potential may be predicted. There is a large variability of biomass and harvest index (HI), which is the yield proportion of the crop compared to all aboveground biomass, in cultivated lentil varieties (Dixit et al., 2017). Jogloy et

al. (2011) determined that in peanut (*Arachis hypogaea*), another member of the Fabaceae family, crop growth rate and partitioning efficiency had significant broad-sense heritability. Therefore, in order to produce high-yielding lentil varieties, germplasm displaying high biomass and HI potential should be identified and selected for use in breeding programs (Dixit et al., 2017).

2.2 Traditional Growth Analysis in Crop Research

Research done on plant populations nearly always requires some amount of phenotypic characterization (Boote and Sinclair, 2006; Dongwei et al., 2018; Golzarian et al., 2011; Haile et al., 2019). Plant phenotypic information may be useful for documentation and description purposes, and may be required for variety registration (Canadian Food Inspection Agency, 2019) and for germplasm submission to gene banks (Agriculture and Agri-Food Canada, 2018). Accurate and thorough plant phenotyping is essential in most crop research studies affecting plant health and productivity, as phenotype is a strong indicator of plant health.

Furthermore, plant phenotyping plays an essential role in plant breeding programs due to the relationship between phenotype, genotype, and environment which can be expressed as;

$$Phenotype = Genotype + Environment + (Genotype \times Environment) \quad (2.1)$$

The use of the terms "genotype" and "phenotype" and the description of their relationship can be traced to Wilhelm Johannsen, a Danish plant physiologist, beginning in 1909 (Wanscher, 1975). With accurate phenotypic and environmental information, plant breeders can take advantage of this relationship to understand the underlying genetics of the populations they work with. By combining genotypic and phenotypic information, it is sometimes possible to identify the gene or genes responsible for a given phenotype (Lande and Thompson, 1989; Cardon L and Bell J, 2001; Slavov et al., 2013). Ultimately, high-quality genotypic and phenotypic information enable plant breeders to develop and make use of tools such as marker-assisted selection or genomic selection. These tools allow the selection of germplasm likely to display a desirable phenotype at a very early stage, drastically increasing efficiency in the breeding program (Wang et al., 2019).

Conventionally, physical phenotypic characteristics commonly collected in a field environment such as height, colour, days until maturity, are collected manually by skilled personnel (Boote and Sinclair, 2006; Dongwei et al., 2018; Golzarian et al., 2011; Haile et al., 2019). Manual collection of this information is tedious and time-consuming (Boote and Sinclair, 2006; Chen et al, 2012a). Traits being collected, as well as the level of accuracy required, dictate the amount of effort needed to acquire data for meaningful analysis and interpretation. Forest health, for example, can be estimated by visually classifying needle loss into five categories, and needle discolouration into four classes (Innes, 1988). While these observations may be made relatively quickly with minimal physical effort, there is great potential for variation between observers and at different times and locations. Subjectivity between different observers, as well as by the same observer over a period of time, can induce large amounts of variation into data collected. Innes (1988) notes the main sources of this variation to be affected by observer experience, trait observed, observer bias, weather, quality of light, and direction of light relative to the observer. While some of this variation may be reduced through training, reference material, and incorporation of check varieties, Innes (1988) demonstrated that differences do not remain constant and therefore are challenging to account for effectively. Additionally, while replication and randomization may be used to statistically reduce some of this variation, increased data collection comes at a significant time and likely monetary cost therefore resulting loss of efficiency in the research program. It is therefore desirable to collect this data in a matter which increases consistency and reliability without the need for human observers.

Structural traits such as height, lodging, biomass and branching/tillering are frequently collected in plant research programs (Haile et al.; 2019, Xinhua et al., 2011) for analysis as well as general characterization and variety registration (Canadian Food Inspection Agency, 2019). These traits are easier to quantify, and therefore may be less affected by observer subjectivity. However, their collection tends to be very tedious and time-consuming. Height is conventionally collected by manually measuring height from the ground to the top of the plant or a specified location (Tullu et al., 2008). Branches and tillers may simply be counted. Biomass quantification adds a further level of complexity, because material needs to be collected and removed from the field to be dried prior to weighing (Zhang and Flottmann, 2016). The requirement for destruction of the biomass sample makes any future field data from that sample impossible to confirm, increasing uncertainty of the experimental design by requiring alternatives such as split-plot

designs or a number of specific plots destined for destruction and other plots intended for season-long data collection. Removing material from the field for further analysis also increases the risk of mislabelled or lost samples which can complicate analysis and interpretation.

Structural traits such as height and biomass may be utilized in the calculation of plant growth rate. The ability to calculate plant growth rate can allow researches to make several predictions regarding plant performance including inter- and intra-specific competitive ability (Deng et al., 2012), resource-use efficiency (Villar et al., 2005), and yield potential (Andrade et al., 2005; Sadras et al., 2013). As proper evaluation of biomass-based plant growth rate is extremely resource-intensive, requiring manual evaluation of plant biomass at multiple time-points (Villar et al., 2005), various studies have attempted to estimate plant growth rate based on parameters such as incident radiation (Andrade et al., 2005) and spectral indices of vegetative material (Sadras et al., 2013). As these approaches aim to indirectly evaluate plant growth rate, there is high potential for error due to the large amount of environmental variation experienced under field conditions (Villar et al., 2005).

2.3 Image Acquisition Platforms

Numerous sensors and cameras exist that can be utilized for field-level phenotyping applications. These sensors can be carried by various platforms in order to efficiently capture useful data. Each platform has its own strengths and weaknesses, and it is essential that platform selection thoroughly considers all requirements of the research program. In many scenarios, multiple platforms may be necessary to best capture all traits of interest.

2.3.1 Ground-Based Platforms

In its simplest form, ground-based image-acquisition may involve nothing more than a person holding a camera for the purpose of image-acquisition. Much more complex approaches are well-documented and include sensor-carrying carts pushed by humans (Crain et al., 2016; White and Conley, 2013), human-operated vehicles (Busemeyer et al., 2013; Montes et al., 2011), and autonomous vehicles (Madec et al., 2017; Xu et al., 2018). The cost of these

platforms ranges from very low, utilizing off-the-shelf, consumer-grade goods, to very high, utilizing top-of-the-line sensors and autonomous guidance systems (Madec et al., 2017). Generally, ground-based platforms are very stable due to their relatively slow rate of travel and the potential to include advanced stabilization systems (Andrade-Sanchez et al., 2013). Additionally, due to their close proximity to vegetation being inspected, extremely high spatial resolution is possible when compared with other field-level platforms. While size and weight are important considerations with regards to adverse soil conditions such as mud, soil compaction, plant damage, power requirements, and general ease-of-use, self-propelled ground-based platforms do not significantly limit sensor weight and dimensions. Therefore, multiple sensors can often be combined on a single ground-based platform to provide a large amount of high-resolution data (Jimenez-Beril et al., 2018). Pushcart-type platforms are more restrictive of sensor size and weight due to the manpower requirement to move the platform through the field. Weight can rapidly accumulate as multiple and higher-resolution sensors are added due to the requirement for additional data storage and power supply provisions.

One of the most important considerations for ground-based phenotyping platforms is the amount of time required for data collection of an entire experiment. As the environment surrounding the phenotyping platform is constantly changing, sensors may detect changing information unrelated to the crop phenotype being evaluated. This may be due to air movement, changes in incident light quality or quantity, or temperature fluctuations. These environmental fluctuations must be accounted for and corrected for in order to produce accurate and consistent data (Araus and Cairns, 2014).

A major drawback of ground-based platforms is their potential interference with crop growth and development. Because of their design, many ground-based platforms operate within a few centimeters of the plant material being observed. When plants are small early in the growing season, impact to plants may be minimal. However, as plants growth though the season, some machine designs in certain crops are likely to either have a significant impact on plants observed, or will not be capable of data collection past a certain plant size (Andrade-Sanchez et al., 2013). Effects on plant growth and development may result from the machine physically touching plant material, or due to soil compaction affecting soil water mobility and root growth (Ma et al., 2013). Despite these challenges, there are several occasions where ground-based platforms have

been successfully utilized to collect plant traits in high throughput applications (Jimenez-Beril et al., 2018; Yuan et al., 2018a; Khan et al., 2018; Haghighattalab et al., 2016; Comar, 2012; Andrade-Sanchez et al., 2013; White and Conley, 2013).

2.3.2 Cable, Crane, and Gantry-Based Platforms

Various platforms exist which suspend sensors above crop research trials for the purpose of high-throughput phenotyping. These platforms have many benefits over ground-based and aerial-based systems. As their footprint is outside of the field environment, field conditions which may limit operation or cause damage to the research trial have no impact on operation (Kirchgessner et al., 2016). These systems cause minimal impact to the research trial as it is not in contact with the crop or nearby soil. They are not significantly impacted by weather phenomena, and data collection can generally be performed under normal growing conditions (Kirchgessner et al., 2016). While payload size may be somewhat restricted by engineering limitations, sensor size and weight restrictions are generally much less limited than with other platform types (Kirchgessner et al., 2016). Because of this, several high-quality sensors may operate concurrently, providing data with extremely high spatial and spectral resolution (Virlet et al., 2017). NU-Spidercam is an example of a fixed system consisting of a sensor platform suspended by pole-mounted cables. The platform is capable of operating with a payload up to 30 kilograms, with sensors typically outfitted to evaluate canopy temperature, vegetation indices (VI), and plant architectural characteristics (Bai et al., 2019). Field Scanalyzer is a gantry-based platform with a payload capacity of 500 kg (Virlet et al., 2017; LemnaTec GmbH).

In addition to payloads located on the machine, suspended platforms typically include on-site control rooms with essentially unlimited capacity for housing instruments and system-related equipment. Because suspended systems are generally permanently fixed in location, research trial size is limited by the size that the system is able to cover as well as by requirements for proper crop rotation and fallow periods (Virlet et al., 2017). Additionally, long-lasting effects of treatments such as disease inoculation, herbicide application, and soil alterations must be considered. Careful planning is also required for field maintenance activities, as overhead machinery is a serious consideration for equipment and workers in the field (Kirchgessner et al., 2016).

2.3.3 Aerial Platforms

Aerial platforms include tethered balloons, blimps, satellites, manned aircraft, and unmanned aerial vehicles (UAVs) (Deery et al., 2016). Aerial platforms are generally able to cover an area more rapidly than other platforms because a larger area can be effectively captured in a single image, and because many aerial platforms such as UAVs and manned aircraft are capable of travelling much more quickly than ground-based units.

Due to a larger distance between the camera and the subject, a larger ground sample distance (GSD) and lower spatial resolution results when comparing similar sensors on aerial platforms to ground-based sensors. GSD describes the ground area portrayed in a single image pixel, and is an important consideration for remote sensing due to the potential loss of information associated with high GSD (Felipe-Garcia et al., 2012). This is especially relevant in small-plot research, as a single pixel from satellite imagery may be significantly larger than an entire plot, making it impossible to accurately interpret plot-level information (Pettorelli et al., 2005). The maximum acceptable GSD will depend on the size of the smallest object that must be identified and what procedures are used to identify the object of interest (Neumann, 2008). While satellites and manned aircraft can rapidly acquire imagery for many large-scale endeavors including ecological, geological, and commercial agricultural mapping (Duveiller and Defourny, 2010), GSD tends to be excessively large to meet application requirements at a plant research scale. A single pixel from satellite imagery can range from a few meters to several thousand meters, depending on which satellite and sensor was utilized (Pettorelli et al., 2005). Additionally, water vapour and particulate matter in the atmosphere can have a significant effect on light scattering, resulting in difficulties obtaining accurate indices-based information from the large distances associated with satellites and high-altitude manned and unmanned aircraft flights (Gao, 1996).

Many previous studies have utilized manned aircraft as a platform for various sensors with the goal of rapid information gathering of general crop health. Elliot et al. (2007) utilized a manned fixed-wing aircraft at an altitude of 610m above ground level as a platform for a multispectral camera observing 3m × 3m wheat plots and was able to identify crop damage based on Normalized Difference Vegetation Index (NDVI) calculations. Each plot in the study contained approximately 100 pixels, which was sufficient for the indices-based crop health

approximation desired. Deery et al. (2016) utilized a manned helicopter as a platform for an airborne thermography study in canola and pea plots. As helicopters generally have greater maneuverability and are capable of operating at lower speeds than fixed-wing aircraft, the study was able to produce repeatable results based on thermal imagery data collected from altitudes of 60m-90m without significant risk to the pilot or excessive craft-induced downwash resulting in crop movement.

Small UAV's have many advantages over manned aircraft. Purchase and operating costs are generally much lower than for manned aircraft. They are typically capable of take-off and landing at the research location and do not require specialized take-off and landing zones such as airports. While special certifications and permissions are required for the operation of UAV's for research and business in Canada, they are generally much more easily attained than for the operation of manned aircraft (Government of Canada, 2019). Most small UAVs are capable of flying at extremely low altitudes, with limitations imposed only by crop movement resulting from craft-imposed downwash. Low altitude operation, between approximately 5 m to 50 m above ground level, can allow sufficiently low GSD to produce high-resolution imagery capable of distinguishing fine crop details with negligible atmospheric effect on light-scattering (Rasmussen et al., 2016). Large UAVs capable of very high-altitude operation for longer duration flights and with higher payload capacities than small UAVs may offer imagery similar to manned aircraft or satellites, but at lower operating costs (Herwitz et al., 2002). The maximum altitude a UAV can be legally operated in Canada without special authorization is 122 m above ground level (AGL) (Government of Canada, 2019), which is sufficient to allow very rapid collection of medium-resolution imagery for a variety of commercial agricultural uses. As GSD will depend on camera resolution, a higher resolution camera may be carried to a higher altitude while still producing sufficient GSD for useful analysis.

A variety of UAV designs are available, including fixed-wing crafts, blimps, helicopters, and multicopters, or crafts with multiple rotors. Blimps, being lighter than air, allow stable and energy-efficient platforms that may cause less disturbance to plants when operated at extremely low altitudes close to the canopy surface. Depending on their size, they can have significant payload capacities enabling multiple sensors to be carried at once (Inoue et al., 2000). However, the large craft size required to carry such payloads may be prohibitive for use in multiple field

locations. Because of their size and shape, blimps are also difficult to control in windy conditions (Sankaran, et al., 2015). Helicopters and multicopters are capable of vertical take-off and landing (VTOL), reducing the space required for operation. Additionally, they are capable of hovering which may allow more stable images at specific locations with reduced motion blur compared to fixed-wing UAVs and manned aircraft (Sieberth et al., 2014). Fixed-wing UAVs, however, tend to fly at higher speeds and be more energy-efficient, allowing longer endurance and therefore more productive data collection missions. Due to their simpler construction, they are less prone to mechanical failure and may even be able to continue gliding to a safe landing location in the event of a propulsion system failure (Senthilnath et al., 2017). Multicopters and helicopters, in contrast, tend to undergo significant damage when mechanical failures occur at altitude.

Operators typically control UAVs with radio-based control systems, and in Canada are legally responsible for safe operation and separation from other air traffic throughout the flight (Government of Canada, 2019). Autonomous or semi-autonomous flight may be possible with UAVs containing on-board navigation systems. These systems may include Global Positioning System (GPS), global navigation satellite system (GLONASS), cellular network towers, or various other radio navigation methods (Miko et al., 2013). Using on-board navigation systems, the UAV can be controlled along a pre-planned flight plan without the need for operator inputs throughout the flight, enabling a high degree of accuracy along the ground while reducing the workload of the operator.

2.4 Image Acquisition Sensors

Various sensors can be utilized on high-throughput phenotyping platforms. Significant consideration should be expended on sensor-selection when designing a high-throughput phenotyping platform due to the wide variation of cost, durability, and ability of various sensors to identify relevant traits in crop research plots.

2.4.1 Digital Photogrammetry Utilizing Consumer-grade Cameras

Digital photographic images may be captured using consumer or professional-grade cameras and sensors. The ability to utilize cameras from the consumer market is especially desirable due to their relatively low cost compared with scientific or industrial-grade sensors such as Light Detection and Ranging (LiDAR) or hyperspectral sensors. Consumer-grade Red-Green-Blue (RGB) cameras capture red, green, and blue bands of the visible light spectrum and are commonly utilized because of their low cost, availability, and high spatial resolution (Rasmussen et al., 2016). Additionally, these cameras can easily be converted to collect near infrared (NIR) bands which may be useful in the calculation of various vegetation indices (Lelong, 2008).

Structure from Motion (SfM) allows the interpretation of an object's structure from a series of 2-D images which capture the object of interest from different points of view (Ullman, 1979). The use of SfM algorithms for the purpose of crop phenotyping are becoming increasingly popular with proven potential for the identification of plant structural and architectural traits (Holman et al., 2016). While this approach does not require specific spectral bands, it does require high-resolution imagery in order to allow highly-detailed structural analysis. Consumer RGB cameras and converted consumer RGB cameras are therefore very useful because they are able to provide cost-effective high-resolution imagery for 3-D structural analysis of research plots, as well as basic spectral information that can be utilized for the calculation of various VIs. Sun et al. (2018) found relatively high coefficients of determination between LiDAR-derived volume of cotton (*Gossypium spp.*) and crop yield using similar methodology to the present study, suggesting both LiDAR and SfM techniques have utility in measuring volume for the purpose of biomass and yield estimation.

2.4.2 Hyperspectral Sensors

Hyperspectral sensors collect a greater number of narrower bands than multispectral sensors. Generally, data is considered to be hyperspectral if it contains greater than 7 bands (Yang and Everitt, 2011), and may contain well in excess of 100 bands. Previous studies have utilized hyperspectral sensors for evaluation of various crop research-based parameters including

disease quantification (Muhammed, 2005), crop residue identification (Yue et al., 2019), yield estimation (Yang and Everitt, 2011), crop stress detection and identification (Estep et al., 2004), and herbicide damage (Huang et al., 2016). While hyperspectral imaging has a high level of demonstrated potential for rapid phenotyping of various plant traits with a high level of accuracy (Ge et al., 2016), equipment required to collect hyperspectral imagery is generally significantly more expensive than more simple sensor options (Proctor and He, 2015). Additionally, a significant proportion of hyperspectral imagery tends to be entirely unused in analysis (Yang and Everitt, 2011). This results in an unnecessary requirement for large data storage solutions, further increasing the costs and weight associated with hyperspectral data collection. While hyperspectral sensors can be utilized on most high-throughput phenotyping platforms, their weight, increased GSD, and cost often limit their use on UAVs (Proctor and He, 2015).

2.4.3 Multispectral Sensors

Sensors capturing 3-7 relatively wide spectral bands are generally considered to produce multispectral imagery (Yang and Everitt, 2011). Several commercial manufacturers produce multispectral cameras for crop analysis, including Micasense (Seattle, USA), Hiphen (Avignon, France), and Tetracam (Chatsworth, USA), among others. These specialized cameras are generally quite light-weight and durable, and are frequently utilized on various ground and aerial-based phenotyping platforms. Some manufacturers are able to provide customized sensors to obtain specific spectral data based on the needs of the user. In many instances, it is likely that once relevant bands have been identified from hyperspectral data for a specific purpose, a customized multispectral sensor may be used in future, applied applications (Calvini et al., 2017; Yang and Everitt, 2011; Mewes at al., 2009). While the high cost and relatively low spatial resolution of multispectral cameras relative to consumer-grade RGB cameras is a major drawback, the increased spectral resolution available from multispectral and hyperspectral sensors is highly valuable to many applications. Increased spectral resolution can allow identification of subtle differences between experimental treatments either on a single spectral band or through calculation of various spectral indices.

Multispectral sensors have significant, demonstrated potential for use in high-throughput plant phenotyping systems on various platform types. Multispectral cameras are frequently

utilized on UAV-based platforms because of their desirable compromise between spatial resolution, spectral resolution, weight, and cost. Various studies to date have utilized multispectral imagery in plant breeding programs to provide relevant information to plant breeders in applied plant breeding programs (Sankaran et al., 2018; Haghighattalab et al., 2016)

2.4.4 Thermal Detection

Canopy temperature can give insight into differential tolerance to drought and heat stress among genotypes (Maleki et al., 2014). As water potential and turgor pressure decrease due to drought stress, stomata close and the rate of transpiration decreases (Blum et al., 1983) leading to reduction in plant growth rate (Gonzalez-Dugo et al., 2019). Therefore, identification of genotypes capable of maintaining low canopy temperatures under heat and drought stress is important for identification of germplasm with high yield potential under such stresses.

Canopy temperature may be quantified using infrared (IR) thermometers or from thermal cameras (Hoffmann et al., 2016; Gonzalez-Dugo et al., 2019; Kumar and Tripathi, 1990). As IR thermometers are cheap, lightweight, and durable, they can quite easily be integrated into ground-based phenotyping platforms to obtain plot-level canopy temperature readings. Thermal cameras have a larger field of view than IR thermometers, and are ideal for comparing multiple plots at a single moment in time to identify differences in canopy temperature among genotypes (Gonzalez-Dugo et al., 2019). For the analysis of large areas while maintaining high resolution, multiple thermal images may be stitched together into an orthomosaics (Gomez-Candon et al., 2016).

2.4.5 Light Detection and Ranging

LiDAR is able to identify surface points by calculating the time of flight for laser pulses travelling between the sensor and the target, and back to the sensor (Chen et al., 2012b). With enough points relating to the surface of an object, structural information can be deduced and a virtual representation of the object can be created. Measurements can then be made on the virtual structure. LiDAR has been previously utilized on ground-based (Madec et al., 2017) and aerial-

based (Brede et al., 2017; Hill et al., 2014) platforms for height quantification in crop plots as well as for forest evaluation.

Wallace et al. (2016) compared the capability of airborne laser scanner (ALS)-derived point clouds to SfM-derived point clouds produced using a consumer-level digital camera. While the forest structure study found ALS point clouds to provide more accurate tree height and groundcover information, it concluded that SfM was an adequate method for measuring forest structural parameters. SfM is highly desirable for high-throughput phenotyping applications, especially when utilizing UAV platforms, because lightweight high-resolution cameras can be obtained for low costs when compared with LiDAR sensors. Additionally, SfM-derived point clouds may be derived from imagery obtained by a consumer or scientific-grade multispectral or single-band camera, enabling a single sensor on a single flight to obtain both 3-D and spectral information.

2.5 2-Dimensional Overhead Image Analysis of Plant Groundcover and Biomass Estimation

Data useful to plant scientists can be extracted from the spectral information contained in relatively simple 2-D imagery of the crop being investigated. Chappelle and Kim (1992) identified low reflectance in soybean (*Glycine max*) in the visible light range, which is approximately 400 to 700 nm. Gausman (1977) identified high reflectance of near-infrared radiation due to scattering by cellular sub-structures. Condit (1970) shows that soils tend to produce a relatively consistent increase in reflectance with longer wavelengths generally reflecting a higher proportion of radiation. Dry soils are generally more reflective than moist soils, but this increase is relatively consistent across the visible and NIR spectrum. Daughtry et al. (1996) suggests that crop residues and soil follow similar spectral trends and can be difficult to distinguish from one-another. Collectively, this information can be utilized in a model to identify various parameters of plant growth, health, and productivity potential.

Various indices which capitalize on the unique spectral differences between vegetation and non-vegetative material may be calculated and used to differentiate between plant material and non-plant materials such as soil and straw. These indices, such as normalized difference

vegetation index, can be used to differentiate between green plant material and non-plant materials.

$$NDVI = \frac{NIR-Red}{NIR+Red} \quad (2.2)$$

These indices capitalize on the unique spectral properties possessed by healthy plant material and those of non-plant material. Green NDVI and Blue NDVI are variations of NDVI that may be of particular use when a converted camera lacking the red band is utilized.

$$GNDVI = \frac{NIR-Green}{NIR+Green} \quad (2.3)$$

$$BNDVI = \frac{NIR-Blue}{NIR+Blue} \quad (2.4)$$

Normalize Green-Red Difference Indices is useful to identify green vegetation using an RGB camera where no NIR information is available.

$$NGRDI = \frac{Green-Red}{Green+Red} \quad (2.5)$$

A large number of indices exist for use in the analysis of vegetation, with many of them comparing NIR bands with various portions of the colour spectrum (Hunt et al., 2013).

A study by Bendig et al. (2015), which attempted to predict barley biomass using spectral indices and height information collected by a UAV, was able to achieve reasonably high accuracy (R^2 =~0.59-0.84). This approach, however, showed reduced effectiveness when applied late in the season due to canopy colour changes associated with maturity. A very minor increase in accuracy was seen when UAV-based height estimates were included in the calculations. Using similar methodology in dry bean, Sankaran et al. (2018) noted increasing correlation between area and biomass from early to mid-season data collection but significantly reduced correlation during late pod-fill

Torres-Sanchez et al. (2015) used an object-based image analysis (OBIA) procedure utilizing Otsu's method of thresholding (Otsu, 1979) to determine vegetation parameters, and found a poor ability to differentiate between vegetation and soil on some occasions. Otsu's method of thresholding is based on gray-level histograms, and allows unsupervised automatic thresholding for the purpose of foreground and background separation.

2.6 3-Dimensional Overhead Image Analysis for Biomass Quantification and Yield Prediction

3-D data may be acquired either through digital aerial photography or LiDAR techniques. Each offers its own distinct advantages and disadvantages.

SfM techniques enable several overlapping images from multiple perspectives to be combined into a single 3-D point cloud which, portray the 3-D environment that was captured (Snavely, 2007). Various software packages exist to produce 3-D point clouds from multiple overlapping 2-D images using this method, including Pix4D and Agisoft Photoscan (Agisoft LLC, St. Petersburg, Russia; Doneus et al., 2011; Neitzel and Klonowski, 2011; Pix4D SA, Lausanne, Switzerland; Verhoeven et al., 2012). This SfM technique works by automatically identifying matching key features among various images. These features are then combined automatically by the program in the manner most likely to produce the smallest error. This will result in a point cloud with points that are correctly located relative to one-another but lacking real-world scale from the scene. True scale information can be incorporated using ground control points (GCPs) with an accurate known position, or by identifying each image with GPS information (Westoby et al., 2012).

LiDAR is able to identify surface points by calculating the time of flight for laser pulses travelling between the sensor and the target, and back to the sensor (Chen et al., 2012a). By determining the relative location of a large number of points, a 3-D point cloud is generated. Following the generation of 3-D point clouds, various methods can be used to provide useful data for quantification of crop traits. For height estimation, a range of points most-likely to correspond with manually-identified canopy height simply needs to be identified. This will primarily involve the removal of outliers from data. Outliers may result due to points fully penetrating the canopy or points located higher than the actual crop canopy due to non-target species or off-types located within the plot. Generally, a specific percentile should be selected depending on the crop species examined to provide optimal correlation with manually-collected phenotypic measurements (Yuan et al., 2018b). In some cases a tessellation of the 3-D point clouds, also referred to as a "mesh," may be applied to all vegetation points that should be included in analysis (Leeper, et al., 2011). This mesh provides a smooth 3-D shape on which further analysis on its physical structure may be performed. Several commercial 3-D imagery

processing programs are capable of this process. Pix4D software (Pix4D, Switzerland) has built-in features to identify volume which are user friendly, but designed in favor of large-scale, low replication analysis as would be used for applications such as industrial mining stockpile estimation or environmental monitoring, among others. The “R” package library “alphashape3d” (R Foundation) and Python library “scipy.spatial.ConvexHull” (SciPy Community, 2017) are programs that allow the user to apply a mesh to exterior points in a point cloud. While these methods may be less intuitive to users not experienced with command line programs, they offer potential for more efficient performance that is essential for the repetitive nature of research plot analysis. Chen et al. (2012b) identified that outliers within the point cloud can be a significant problem. Breunig et al. (2000) identified Local Outlier Factor (LOF) as a potential method for identifying and removing outliers. Removing outliers ensures that the mesh is fit to the point cloud as accurately as possible, to produce more accurate results. Digital Terrain Models (DTMs) and Digital Surface Models (DSMs) can be created from 3-D point clouds for use in further analysis (Heurich, 2008). A DSM is a 3-D image representing all vegetation and structures (Sole and Valanzano, 1996). A DTM eliminates vegetation and structures and displays only the terrain. Therefore, any volume filled by vegetation can be quantified by subtracting DTM from DSM (Holman et al., 2016). A study by Torres-Sanchez et al. (2015) utilized a similar approach on images collected from a UAV to estimate olive tree volume, and was able to predict crown volume successfully. Walter et al. (2018) utilized point clouds created from UAV-based photogrammetry to predict biomass and yield in wheat plots, with relative success.

3.0 Using UAV-based Images to Quantify Crop Growth in Lentil

3.1 Introduction

A wide range of experimental studies aim to quantify various parameters of plant growth and development in an efficient and accurate manner in order to determine a treatment-induced or genotypic effects on plant growth and development. Oftentimes, as a direct result of time and cost constraints, growth parameters collected may be insufficient or minimally acceptable to conclusively prove or disprove the biological hypothesis in question. Obtaining accurate parameters pertaining to plant growth rate, plant size, and plant development tends to be exceptionally difficult due to multiple factors including a large effect of sub-sampling error, significant time commitment, subjectivity of evaluators, the need for sequential measurements, and requirement for destructive processes. In a large number of plant research trials where the quantification of plant size and growth rate would be a useful parameter in analysis and result interpretation, it is presumed that these traits are simply not collected due to their prohibitively high data-collection time and cost requirements. As an alternative, studies often examine traits such as stem length, canopy height, and seed yield as indicators of plant growth rate and productivity.

A UAV platform may be utilized to rapidly collect overhead images of a research trial which can be analyzed to produce parameters relating to plant size and growth. By collecting and analyzing a series of overlapping overhead imagery of lentil research plots, this experiment was designed to produce plot volume and vegetation area parameters. It is expected that these traits will be strongly related to traits such as early-season plant vigour (Kipp et al., 2014), groundcover, and plant biomass and as such, may be used as a high-throughput proxy for in-field measurements. With reduced peak-season time commitments to non-destructively collect this trait information, it is presumed that numerous research programs would realize a great deal of value from these procedures.

While 2-D analysis has been used to effectively determine groundcover in various crops (Calera et al., 2001; Duan et al., 2017), it was hypothesized that as the crop continued to increase in height and density, as well as change in architecture, a 3-D analysis approach would be able to produce more accurate and robust biomass estimations in lentil plots. 3-D analysis allows variably in plant architecture to be identified and accounted for independently of other factors,

rather than relying on assumptions of plant architecture and shape as is required when utilizing 2-D analysis approaches. Experiments by others have evaluated the utility of 3-D analysis techniques for agricultural research (Torres-Sanchez et al., 2015, Neumann et al., 2015, Wallace et al., 2016) but limited literature is currently available examining 3-D analysis on crops similar in both size and architecture to lentil for the purpose of volume estimation.

3.2 Materials and Methods

3.2.1 Germplasm

The material utilized was derived from the lentil diversity panel from the Application of Genomic Innovation in the Lentil Economy (AGILE) trial (Haile et al., 2019). The lentil diversity panel consisted of 324 lentil genotypes planted in 1 m^2 microplots. These genotypes included various cultivars and landraces from the Mediterranean, South Asian, and temperate climactic zones. A diverse subset of six genotypes from this panel were selected for biomass and high-throughput phenotyping analysis. The subset was selected specifically based on diversity of biomass, canopy height, plant architectural traits, and groundcover. Genotypes included in the study were: CDC Asterix, CDC Cherie, CDC Redcoat, ILL 7716, ILL 9888, and PI 490288 LSP. In Rosthern 2018, CDC Asterix was omitted and only five genotypes were analyzed due to an error at the time of seeding.

3.2.2 Experimental Design

The trial was arranged in a Randomized Complete Block Design (RCBD) with three replicates separated by a single range of pea plots (Figure 3-1). Each microplot was seeded at a rate of 70 seeds per plot and was approximately 1m^2 consisting of three rows. No fertilizer or inoculant was applied at the time of seeding. Five site-years were observed with locations at Rosthern and Kernen Research Farm in 2017 and at Rosthern, Kernen Research Farm, and Nasser Farm in 2018 (Table 3-1). Weeds were manually controlled to ensure weed-free imagery and biomass samples, and to eliminate interspecific competition. Soil condition at the time of seeding, soil texture, and soil classification are shown in Table 3-1. Six plots of each genotype

were established per replication to allow whole-plot biomass analysis approximately once every two weeks throughout the growing season (Figure 3-1).

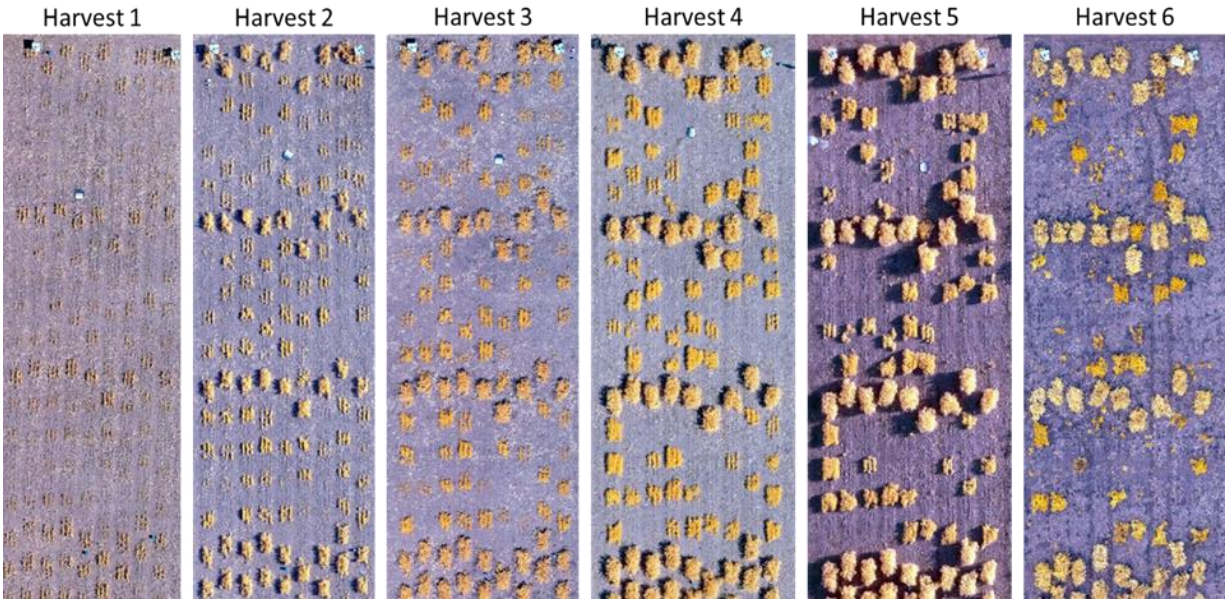

Figure 3-1: Overhead image of the trial layout taken with a Sony α5100 24.3MP camera, converted to utilize NIR, green, and blue channels to enable calculation of NDVI, within 2h prior to biomass sampling. Six diverse lentil genotypes were grown in a Randomized Complete Block Design (RCBD) with three replicates at five site-years. Each replicate is separated by a row of pea plots. Whole-plot biomass was measured approximately every two weeks throughout the growing season resulting in elimination of select plots.

Table 3-1: Site location and soil information for all site-years of data collection (SKSIS Working Group, 2018).

Site-Year	GPS Coordinates	Soil Surface Texture	Soil Classification	Seedbed Condition
Sutherland 2017	52°10'12.4457"N, -106°30'39.9089"W	Clay	Orthic Dark Brown Chernozem CH	minimum till
Nasser 2017	52°09'53.2956"N, -106°30'45.9547"W	Clay	Orthic Dark Brown Chernozem CH	dry, cultivated
Rosthern 2017	52°41'27.5423"N, -106°17'25.5372"W	Very Fine Sandy Loam	Orthic Black Chernozem CH	minimum till
Nasser 2018	52°09'50.7261"N, -106°30'36.4198"W	Clay	Orthic Dark Brown Chernozem CH	dry, cultivated
Rosthern 2018	52°41'16.7208"N, -106°18'04.0860"W	Very Fine Sandy Loam	Orthic Black Chernozem CH	minimum till

3.2.3 Field Data Collection

Whole-plot biomass was measured by cutting all above-ground material at ground-level on an approximately bi-weekly basis. Canopy height was measured at each plot immediately prior to destructive sampling by placing a measuring stick vertically in a representative interior portion of each plot and measuring the height of the canopy without manipulating any vegetative material. Leaf area was measured using a LI-COR LI-3100 (LI_COR Biosciences, Lincoln NE, USA) area meter at Nasser 2017, Sutherland 2017, and Nasser 2018. To do this, a sub-sample of three representative plants was randomly collected during whole-plot biomass collection and leaf area was measured immediately following transportation to the lab. Individual leaflets were flattened and fed into the leaf area meter, with the value for each complete plant being recorded and utilized in further analysis. Leaf area measurement collection was concluded once plants had senesced and no photosynthesizing material remained. Plants were collected for biomass analysis within the 24 hours prior to overhead images being collected. Data collection was targeted to occur every 14 days. Flight delays occasionally occurred due to poor weather conditions or mechanical issues, which delayed biomass collection as well. Wet weight biomass and leaf area were measured within two hours of collection. Samples were then dried at 71 ^{o}C for 72 hours or until oven moisture was below 2 %. Dried samples were weighed immediately following removal from the drying oven. Growing degree days (GDD) were calculated at each trial location using hourly-recorded temperature data collected from respective trial locations. The equation used to describe GDD was:

$$Accumulated\ GDD = \sum[\left(\frac{T_{MAX}+T_{MIN}}{2}\right) - T_{BASE}] \qquad (3.1)$$

where T_{MAX} is the maximum recorded daily temperature, T_{MIN} is the minimum recorded daily temperature, and T_{BASE} is assumed minimum temperature where growth occurs. For this experiment, T_{BASE} of lentil was assumed to be 5ºC (Alba, 2019; Neupane, 2019). If T_{MAX} or T_{MIN} were less than T_{BASE}, they were considered to be zero as described by McMaster and Wilhelm (1997). GDD accumulation was considered to begin on the date of seeding. Climactic data for trial locations shown in Table 3-2 indicates that temperatures in both years of the study were relatively similar to the historical average, and that precipitation was below the historical average in both years of the trial.

Table 3-2: Climactic information at Rosthern and Kernen research trial locations in 2017 and 2018 (Environment Canada, 2018).

		Mean Temperature (ºC)			Mean Precipitation (mm)		
Location	Month	2017	2018	Historical Average	2017	2018	Historical Average
Kernen Crop Research Farm (Saskatoon)	May	11.6	14.1	11.2	56.0	36.4	34
	June	16.0	17.1	15.8	47.8	15.8	64
	July	19.3	18.7	18.5	32.4	52.6	54
	August	17.8	17.1	17.6	30.0	27.0	44
	TOTAL	-	-	-	166.2	132.0	196
Rosthern	May	11.0	13.6	10.8	51.2	28.5	40
	June	15.3	16.8	15.6	39.4	28.4	66
	July	18.7	18.0	18.3	29.0	60.9	65
	August	17.1	16.1	17.2	27.6	34.6	53
	TOTAL	-	-	-	147.1	152.0	224

3.2.4 Image Acquisition

UAVs were utilized as rapid overhead image collection platforms. Two DraganFly UAVs (Draganfly Innovations, Saskatoon, SK, Canada); one Draganflyer X4-P model and one Draganflyer Commander model (Figure 3-2), were used interchangeably to collect images. Both UAVs were quadcopters outfitted with a gimbal-stabilized camera mount designed to accept various cameras.

Figure 3-2: Draganflyer Commander carrying a gimbal-mounted high-resolution consumer grade camera, one of the UAV's used to capture in season images of lentil field plots.

Most images were collected using either a consumer-grade 24.3MP Sony α5100 series camera (Sony Corporation, Minato, Tokyo, Japan) or with a consumer-grade 20.1MP Sony QX1 series camera (Table 3-3). Both were converted to utilize NIR, green, and blue channels. On two flight dates in this study, a 20.1MP Sony RX100MIII capturing red, green, and blue bands was utilized due to technical issues with the converted cameras (Table 3-3). As the NIR band was not available, different indices were required to determine vegetation area. Trends in data suggest that the use of a different camera on the final flight had a negligible effect on the volume and groundcover estimations. Ground sample distance for each potential camera and altitude combination is shown in Table 3-3.

$$GSD = \frac{Sensor\ Pixel\ Size \times Altitude}{Focal\ Length} \qquad (3.2)$$

Table 3-3: Ground Sample Distance (GSD) of each camera/altitude combination used throughout the experiment.

Camera (lens, focal length, f-stop)	Altitude (m)	Ground Sample Distance (mm)
Sony RX100MIII 20.1MP	15	4.1
(24-70mm, 8.8mm, f/1.8-2.8)	20	5.5
Sony QX1 20.1MP	15	5.3
(16mm, 24mm, f/2.8)	20	4.0
Sony α5100 24.3MP	15	4.9
(16mm, 24mm, f/2.8mm)	20	3.7

Take-off and landing of the UAV was executed manually by the pilot, but the image acquisition portion of flights was performed utilizing a pre-programmed flight plan created with DraganFly Surveyor software. The Surveyor software automatically produces a flight plan with optimum speed and routing to obtain operator-prescribed parameters including altitude, image overlap, and GSD. Images were collected from a nadir perspective with the payload saddle in surveyor mode. Flight altitude was set either to 15m or 20m to allow relatively low GSD providing high-resolution imagery (Table 3-3). Image overlap was maintained at 70 % or greater to allow orthomosaic and 3-D point cloud development. Permanently placed reference targets with a known location measured using a Trimble 5800 model R8 real time kinematic (RTK)-corrected GPS system were located within each trial. At Rosthern, a Trimble (Sunnyvale, California, U.S.A) GeoXT – GeoExplorer 2008 series GPS was used.

3.2.5 Image Processing

Images acquired from the UAV platform were first converted to tagged image file format (TIFF) using Adobe Photoshop version CC 2018 (Adobe, www.adobe.com). Stitched orthomosaics (Figure 3-1) and 3-D point clouds (Figure 3-3) were then produced for each location and flight-date using Pix4D software Version 4.3.3.1 (SA, Lausanne, Switzerland, 2018) following the workflow shown in Figure 3-4.

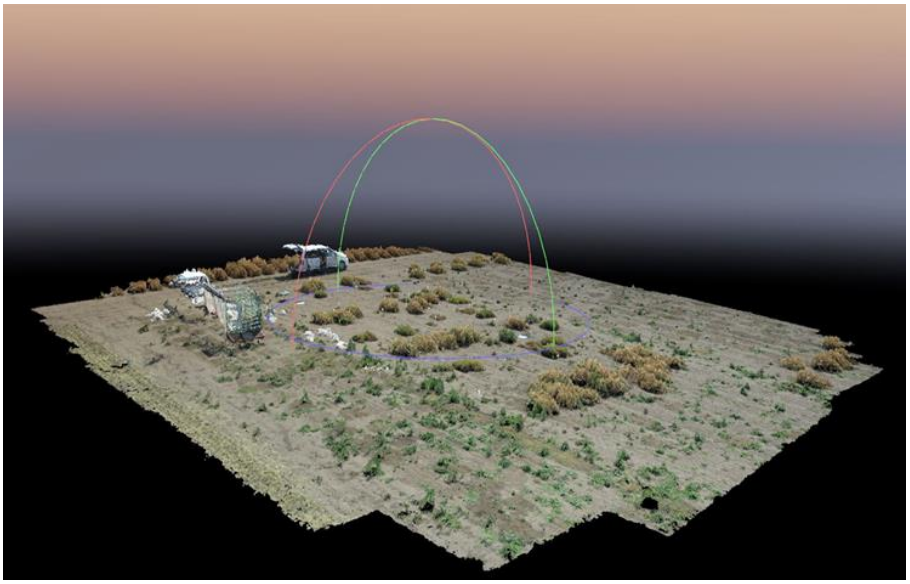

Figure 3-3: Sample of a three-dimensional point cloud generated from overlapping UAV images using Pix4-D software.

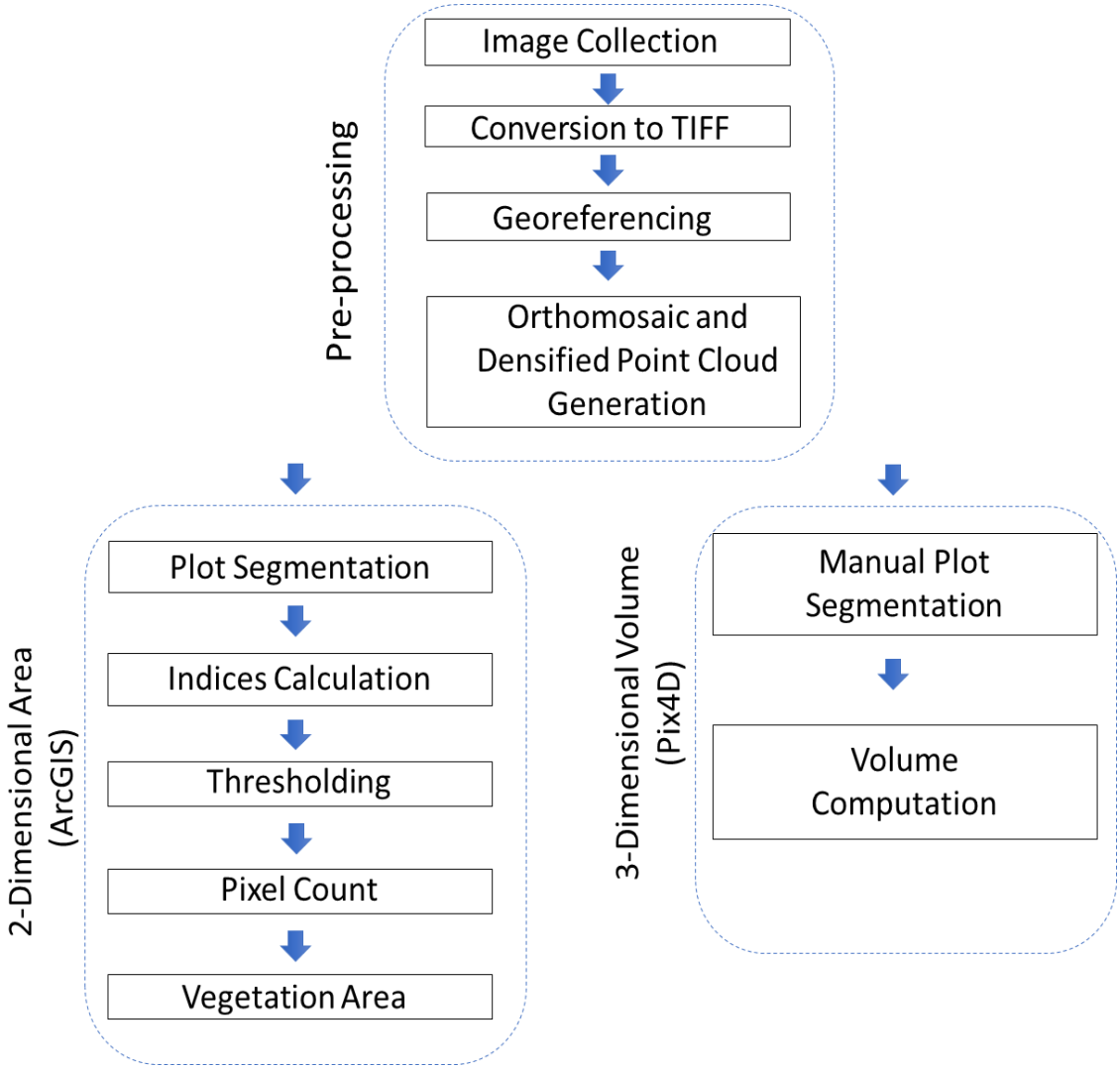

Figure 3-4: Overhead image analysis protocol utilized to quantify vegetation area and volume based on overhead images.

3.2.6 Image Analyses

3.2.6.1 2-Dimensional Analyses

2-D analysis was utilized to determine the area of ground covered by vegetation as viewed from a nadir perspective. ArcGIS software version 10.4.0.5524 (ESRI, 2015) was utilized first for plot segmentation by manually creating bounding polygons on a 2-D orthomosaic around each plot, then to apply indices to identify plant material from non-plant material (Figure 3-4). gNDVI (Equation 2.3) was quite effective in identifying green pixels while eliminating shadows and other non-green material (Table 3-4). On some image dates (Table 3-5), bNDVI (Equation 2.4) was determined to be a better basis for green pixel identification based on visually-observed indices characteristics. On biomass sample 6 at Sutherland 2017, only RGB imagery was available so NGRDI (Equation 2.5) was utilized. Rasmussen et al. (2016) suggested that the use of NGRDI compared with NDVI did not significantly inhibit the ability to assess green vegetation. Therefore, for the purposes of quantifying ground covered by green vegetation in this study bNDVI, gNDVI, and NGRDI were considered to produce equivalent results as indices selection and threshold value selection was determined independently at each image analysis timepoint. Once indices were calculated, thresholds were applied to eliminate all non-green pixels from the image. Thresholds were determined by user-based visual inspection on each imaging date. By manually determining thresholds, the present study had high success in separating vegetation from non-vegetative backgrounds such as soil and crop residue. To compare with standardized threshold values, the average threshold value from all site-years and image dates as well as the average threshold value from Nasser 2018 were determined and compared with independently selected threshold values at Nasser 2018 (Table 3-4). Nasser 2018 was chosen as an average trial location representative of all site-years. A reduced ability to differentiate vegetation from background materials such as soil and crop residue, especially when compared to the average of thresholds applied to all site-years, was identified. Although indices results were highly correlated between individually determined thresholds for each date and the average of thresholds applied to Nasser 2018, the averaged threshold appears to underestimate early-season vegetation area and overestimate mid-season vegetation area based on visual comparison of threshold results (Table 3-4). While early and mid-season vegetation pixels were separated from background pixels relatively easily due to a large contrast between

pixel value, vegetation was much more difficult to accurately separate from background material due to crop senescence and corresponding loss of chlorophyll. As a result, a small difference in threshold values applied to late-season imagery had potential to dramatically change the vegetation area value. Therefore, data for further analyses were derived from independently determined threshold values as this method was determined to most accurately quantify vegetation area. Pixel count and calculated green pixel area were then determined for each plot using the raster calculator in ArcGIS based on pixels categorized as being representative of vegetation. These values were then used in further analysis, negating variance between actual indices values calculated. Rasmussen et al. (2016) observed the stitching process of Pix4D to have an effect on NDVI values at high altitudes greater than 30 m above ground level in cloudy conditions but did not affect NDVI values at lower altitudes below 30 m in sunny or cloudy conditions as this study utilized. Therefore, the effect of altitude on NDVI value in this study was considered negligible.

Table 3-4: The application of a standard threshold for all image dates was compared with the application of a custom threshold manually determined for each image date. The average of all gNDVI threshold values visually determined for individual image dates (custom threshold) across all site-years and across all data collection dates at Nasser 2018 were calculated and applied as standard thresholds at Nasser 2018. Correlation between the custom and standard threshold values for green pixel area were calculated to compare their ability to accurately quantify vegetation area.

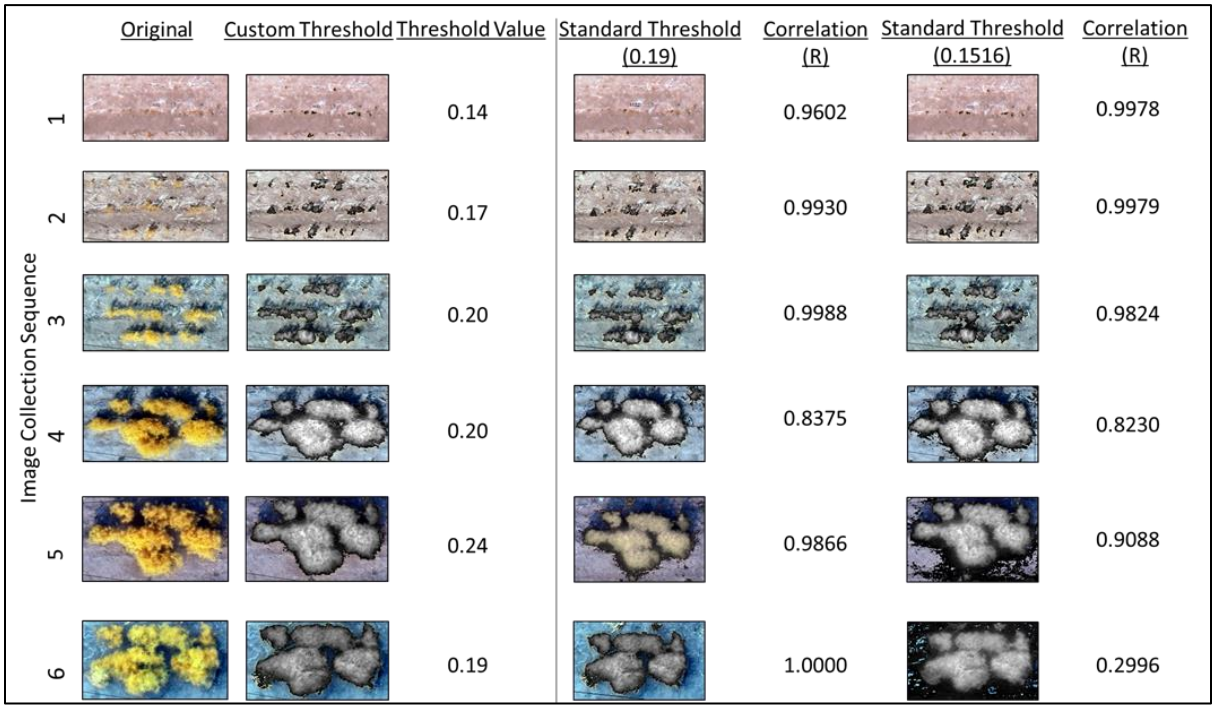

Table 3-5: Biomass sampling dates, flight details, and indices selected for analysis for each site-year.

		Sutherland 2017	Nasser 2017	Rosthern 2017	Nasser 2018	Rosthern 2018
	Seeding Date	2017-05-04	2017-05-30	2017-05-15	2018-05-18	2018-05-11
Sample Collection #1	Date	2017-06-06	2017-06-25	2017-06-12	2018-06-13	2018-06-19
	Spectral Channels	NIR-G-B	NIR-G-B	NIR-G-B	NIR-G-B	NIR-G-B
	Altitude	15m	15m	15m	15m	15m
	Indices Calculated (threshold)	**GNDVI (0.12)**	**GNDVI (0.11)**	**GNDVI (0.21)**	**GNDVI (0.14)**	**GNDVI (0.18)**
Sample Collection #2	Date	2017-06-19	2017-07-05	2017-06-28	2018-06-27	2018-06-28
	Spectral Channels	NIR-G-B	NIR-G-B	NIR-G-B	NIR-G-B	NIR-G-B
	Altitude	20m	20m	15m	15m	20m
	Indices Calculated (threshold)	**GNDVI (0.12)**	**GNDVI (0.12)**	**BNDVI (0.19)**	**BNDVI (0.17)**	**BNDVI (0.23)**
Sample Collection #3	Date	2017-07-05	2017-07-19	2017-07-12	2018-07-10	2018-07-05
	Spectral Channels	NIR-G-B	NIR-G-B	NIR-G-B	NIR-G-B	NIR-G-B
	Altitude	20m	20m	15m	15m	20m
	Indices Calculated (threshold)	**GNDVI (0.30)**	**GNDVI (0.34)**	**BNDVI (0.20)**	**BNDVI (0.20)**	**BNDVI (0.25)**
Sample Collection #4	Date	2017-07-19	2017-08-04	2017-07-26	2018-07-26	2018-07-19
	Spectral Channels	NIR-G-B	NIR-G-B	NIR-G-B	NIR-G-B	NIR-G-B
	Altitude	20m	20m	15m	15m	20m
	Indices Calculated (threshold)	**GNDVI (0.19)**	**GNDVI (0.18)**	**GNDVI (0.18)**	**BNDVI (0.20)**	**BNDVI (0.23)**
Sample Collection #5	Date	2017-08-02	2017-08-17	2017-08-08	2018-08-08	2018-08-01
	Spectral Channels	NIR-G-B	R-G-B	NIR-G-B	NIR-G-B	NIR-G-B
	Altitude	20m	20m	20m	15m	20m
	Indices Calculated (threshold)	**GNDVI (0.09)**	**NGRDI (0.26)**	**GNDVI (0.25)**	**BNDVI (0.24)**	**BNDVI (0.30)**
Sample Collection #6	Date	2017-08-17		2017-08-23	2018-08-23	2018-08-16
	Spectral Channels	R-G-B		NIR-G-B	NIR-G-B	NIR-G-B
	Altitude	20m		20m	20m	15m
	Indices Calculated (threshold)	**NGRDI (0.01)**		**GNDVI (0.20)**	**BNDVI (0.019)**	**BNDVI (0.25)**

3.2.6.2 3-Dimensional Analyses

3-D point clouds were generated utilizing the "point cloud and mesh" option of Pix4D software. 3-D volume was then analyzed using the volume estimation function of Pix4D software (Pix4D Support, 2019). This tool involves a calculation comparing the digital surface model (DSM) and digital terrain model (DTM) from a particular imaging date. Volume information is extrapolated from DSM and DTM information within this manually specified area for each plot by applying a grid based on GSD spacing and determining the volume of each selected cell. Base height of the selected region is derived from the altitude of each user-selected vertex. Plot-bounding polygon vertices were determined manually on a plot-by-plot basis to contain the plot as precisely as possible using the total volume of the selected region as the sum of the volume of each cell within the selected region.

3.3 Statistical Analyses

Package *corrplot* (Wei and Simko, 2017) running in R (R Core Team, 2017) using RStudio version 1.1.456 (RStudio Team, 2016) was utilized to produce correlation matrices displaying Pearson correlation to compare dry weight biomass, wet weight biomass, canopy height, volume, and area of each plot (Figure 3-6b). Leaf area was also included in Sutherland 2017, Nasser 2017, and Nasser 2018 (Figure 3-6a). Site-years were analyzed separately. Function "aov" in R (R Core Team, 2017) run using RStudio version 1.1.456 (RStudio Team, 2016) was utilized to calculate Analysis of Variance (ANOVA) among genotypes for dry weight, wet weight, leaf area, canopy height, vegetation area, and plot volume for each biomass sampling interval at each site-year. It should be noted that there is a risk of Type 1 error due to the calculation of multiple ANOVAs and the high number of *F* tests involved (Clemens, 1975).

3.4 Results and Discussion

3.4.1 Differentiation Among Genotypes Over Time

P-values from ANOVA were calculated to determine differences among genotypes at all site-years and data collection dates for dry weight biomass, wet weight biomass, height, leaf area, vegetation area, and volume (Table 3-6). Genotypes tended to be indistinguishable from one-another early in the growing season for most traits at all site-years. During the middle of the growing season (approximately data collections 4 and 5), it became possible to differentiate genotypes based on most traits evaluated at most site-years. By the end of the growing season genotypes differed for almost all of the measured traits indicating an ability to differentiate genotypes from one-another.

Table 3-6: Analysis of Variance (ANOVA) values for select traits are displayed across all site-years and data collection times. ANOVA was calculated and p-value is displayed for dry weight,wet weight, height, leaf area, area, and volume at each site-year. Biomass collection began two weeks after emergence and was repeated approximately every two weeks until senescence.

	Biomass Collection Time	Dry Weight	Wet Weight	Height	Leaf Area	Area	Volume
Sutherland 2017	Time 1	0.080	0.274	0.140		0.486	0.325
	Time 2	0.806	0.878	0.567	0.640	0.863	0.933
	Time 3	0.455	0.349	0.346	0.852	0.661	0.598
	Time 4	0.130	0.048	0.004	0.629	0.209	0.029
	Time 5	0.007	0.010	0.412	0.736	0.006	0.003
Nasser 2017	Time 1	0.964	0.948	0.131	0.839	0.725	0.366
	Time 2	0.597	0.729		0.747	0.761	0.745
	Time 3	0.923	0.802	0.730	0.486	0.623	0.568
	Time 4	0.933	0.768	0.255		0.095	0.097
	Time 5	0.276	0.008	<0.001	0.022	<0.001	0.005
	Time 6						
Rosthern 2017	Time 1	0.078	0.068	0.011		0.056	0.733
	Time 2	0.004	0.012	0.009		0.008	0.477
	Time 3	0.455	0.051	<0.001		0.069	<0.001
	Time 4	0.022	0.015	<0.001		<0.001	0.008
	Time 5	0.097	0.014	<0.001		0.027	<0.001
	Time 6	<0.001	<0.001	<0.001		<0.001	0.005
Nasser 2018	Time 1	0.365	0.154	<0.001	0.074	0.720	0.623
	Time 2	0.029	0.037	0.708	0.265	0.120	0.499
	Time 3	0.159	0.145	0.019	0.151	0.045	0.071
	Time 4	0.049	0.012	<0.001	0.024	0.165	<0.001
	Time 5	0.004	<0.001	<0.001	0.008	0.006	0.031
	Time 6	0.174	0.0726	0.001		0.144	0.094
Rosthern 2018	Time 1	0.332	<0.001			0.609	0.764
	Time 2	0.344	0.360	0.615		0.085	0.012
	Time 3	0.539	0.351	0.003		0.413	0.002
	Time 4	0.224	0.016	<0.001		<0.001	<0.001
	Time 5	0.007	0.002	<0.001		0.001	0.0356
	Time 6	0.001	<0.001	<0.001		<0.001	<0.001

At all site-years except Nasser 2018, it is noteworthy that differences among genotypes in vegetation area became significant at either similar or earlier sampling times than dry weight biomass. This suggests that, in addition to being faster and simpler to collect, vegetation area

may have more variability due to varietal differences than does dry weight biomass. Although dry weight biomass differed more substantially among genotypes at Nasser 2018, vegetation area still had some utility in differentiating among genotypes at many points during the growing season.

In addition to vegetation area, plot volume also differed significantly among genotypes at mid-to-late points in the growing season. At all site-years, greater differences were generally observed among genotypes based on plot volume than based on dry weight biomass (Table 3-6). Fewer significant differences among genotypes were observed based on dry weight biomass than on plot volume, with differences in dry weight among genotypes appearing at a statistically significant level only sporadically throughout the growing season.

Few significant differences were observed among genotypes based on leaf area (Table 3-6). No differences among genotypes could be identified at any data collection time in Sutherland 2017. Based on these observations, it seems that differences among genotype can be deduced earlier utilizing plot volume than using leaf area. However, at Nasser 2018, both leaf area and plot volume demonstrate statistically significant differences at data collection 4 and 5. At Nasser 2017, time 4 leaf area data were unavailable but significant differences among genotypes could be realized at data collection 5 based on both leaf area and plot volume. Leaf area was not measured at Rosthern 2017 or Rosthern 2018, so data are unavailable for those site-years. More work should be done to definitely compare differences among genotypes based on leaf area vs. plot volume utilizing a larger population with a more complete data set. Regardless, the trend observed suggests that differences among genotype become significant either at a similar time based on plot volume and leaf area, or at an earlier time when based on volume alone. As vegetative material is measured significantly more quickly utilizing less labour and without the need to destroy plant material or rely on sub-sampling, plot volume is suggested as superior to leaf area analysis utilizing a leaf area meter.

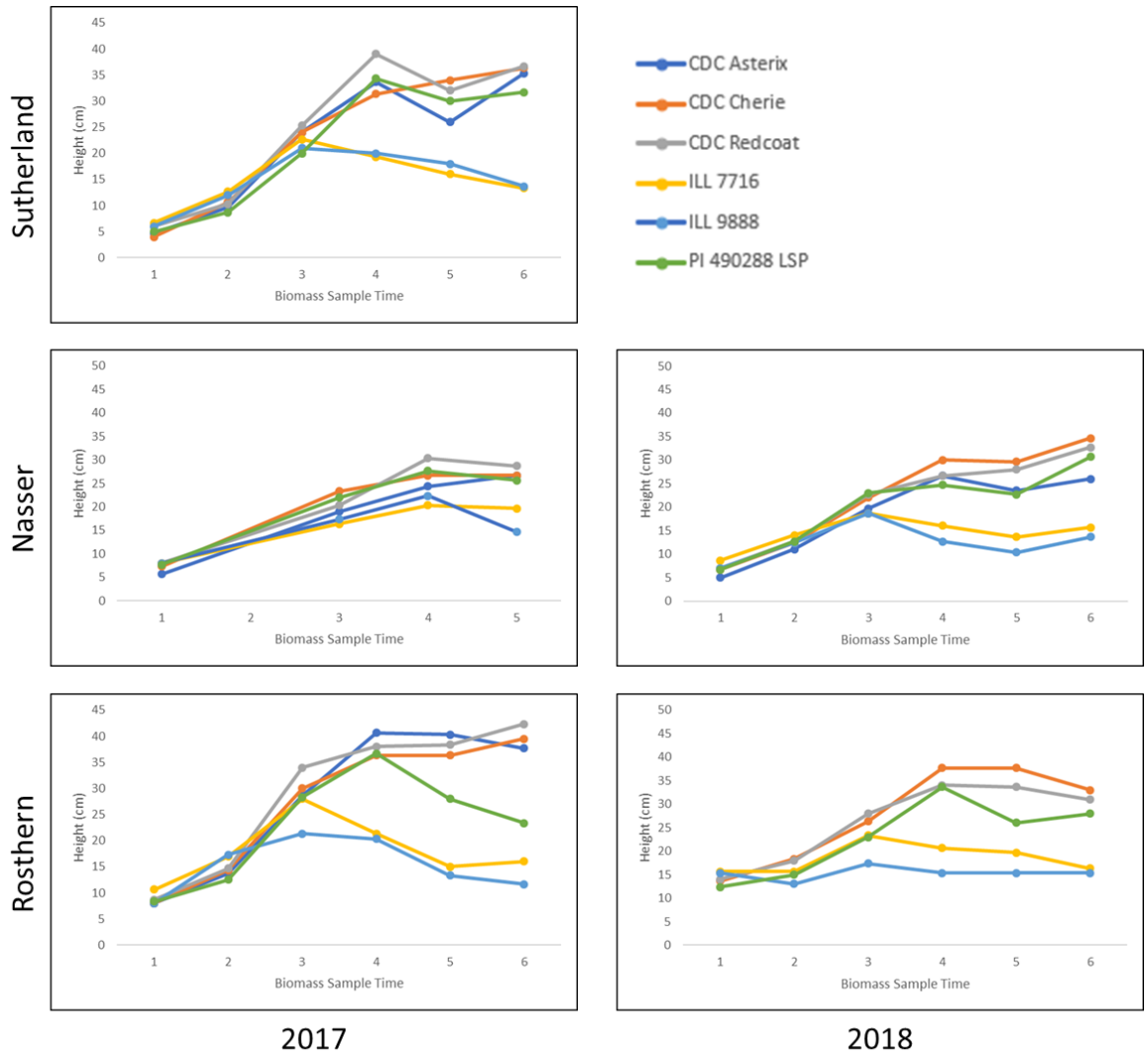

Figure 3-5: Manually measured canopy height of lentil plots collected immediately prior to biomass collection throughout the season at five site-years.

Significant differences among genotypes based on canopy height were observed at many data collection times at several site-years (Figure 3-5). At Rosthern 2017, significant differences among genotype were observed at all data collection times and at Nasser 2018 and Rosthern 2018, genotypes could not be differentiated based on height only at the second data collection time. This trend is similar to that of plot volume and suggests a greater ability to differentiate among genotypes than with dry weight, wet weight, or leaf area. However, canopy height alone should not be expected to be representative of plot biomass due to the large variation in plant

structure and growth habits observed in lentil (Saxena, 2009). Additionally, as canopy height may not be representative of actual stem height due to the tendency of high biomass genotypes to undergo greater amounts of lodging, canopy height alone should not be presumed consistent among different genotypes and varying environments (Hanlan et al., 2006).

3.4.2 Correlation between Wet Weight Biomass and Dry Weight Biomass

The correlation matrices between the measured variables shown in Figures 3-6a and 3-6b at each trial site-year, when viewed over the course of the growing season, give a great deal of insight into the relative efficacy of wet and dry weight biomass for the purpose of plant growth determination. Although not a specific objective of the experiment, it is noteworthy that wet weight biomass and dry weight biomass were highly correlated at most data collection dates during the experiment. The correlation (R) between wet weight biomass and dry weight biomass was greater than 0.95 at 23 of the 29 data collection dates. Additionally, on many occasions, wet weight biomass had greater correlation with calculated volume and area than did dry weigh biomass. In instances where wet weight biomass had a lower correlation with area and volume than did dry weight biomass, the difference was small enough that it was unlikely to lead to different conclusions. Tackenberg (2007) identified similar correlations between dry weight biomass and vegetation area compared to wet weight biomass and vegetation area in grass species. Wet weight biomass had a similar or greater capacity to differentiate among genotypes throughout the growing season at all site-years compared to dry weight biomass (Table 3-6). This suggests that wet weight biomass may be collected in future studies requiring growth rate and/or biomass data in lentil or similar species. It should be recognized, however, plants collected in this experiment were free from dew and large amounts of external moisture which may reduce accuracy and consistency. The collection of wet weight biomass is much more efficient due to the fact that vegetation may be weighed in the field immediately after sample collection negating the need for transportation to a central facility and the cost of operating drying ovens, as well as reducing the potential for data loss due to mismanagement or damage.

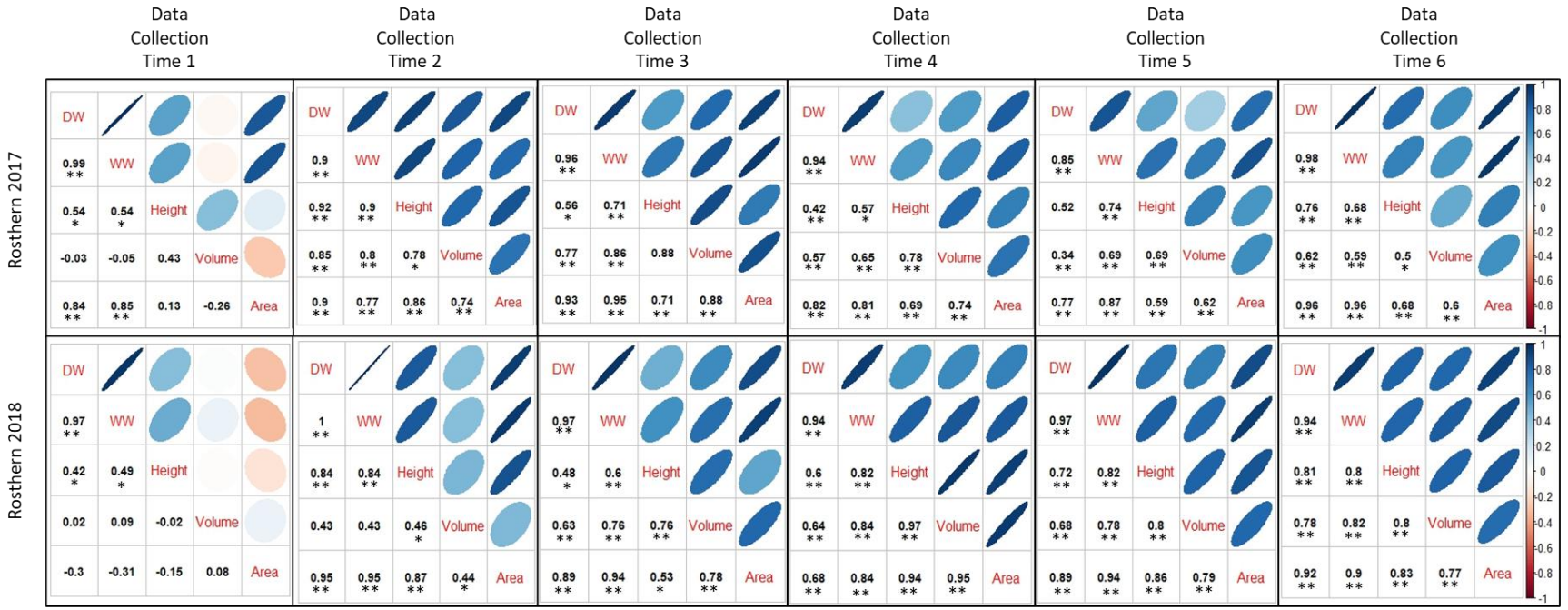

Figure 3-6a: Pearson correlations between wet weight biomass (WW), dry weight biomass (DW), height, plot volume (Volume), and vegetation area (Area) at each data collection time point at each site-year. Ellipses represent Pearson correlation coefficient (R), with perfect correlation being a straight line and zero correlation being a perfect circle. Positive correlations are shown in blue, and negative correlations are shown in red. Significant Pearson correlations having a p-value <0.05 are shown with one asterisk (*), and a p-value of <0.05 with two asterisks (**).

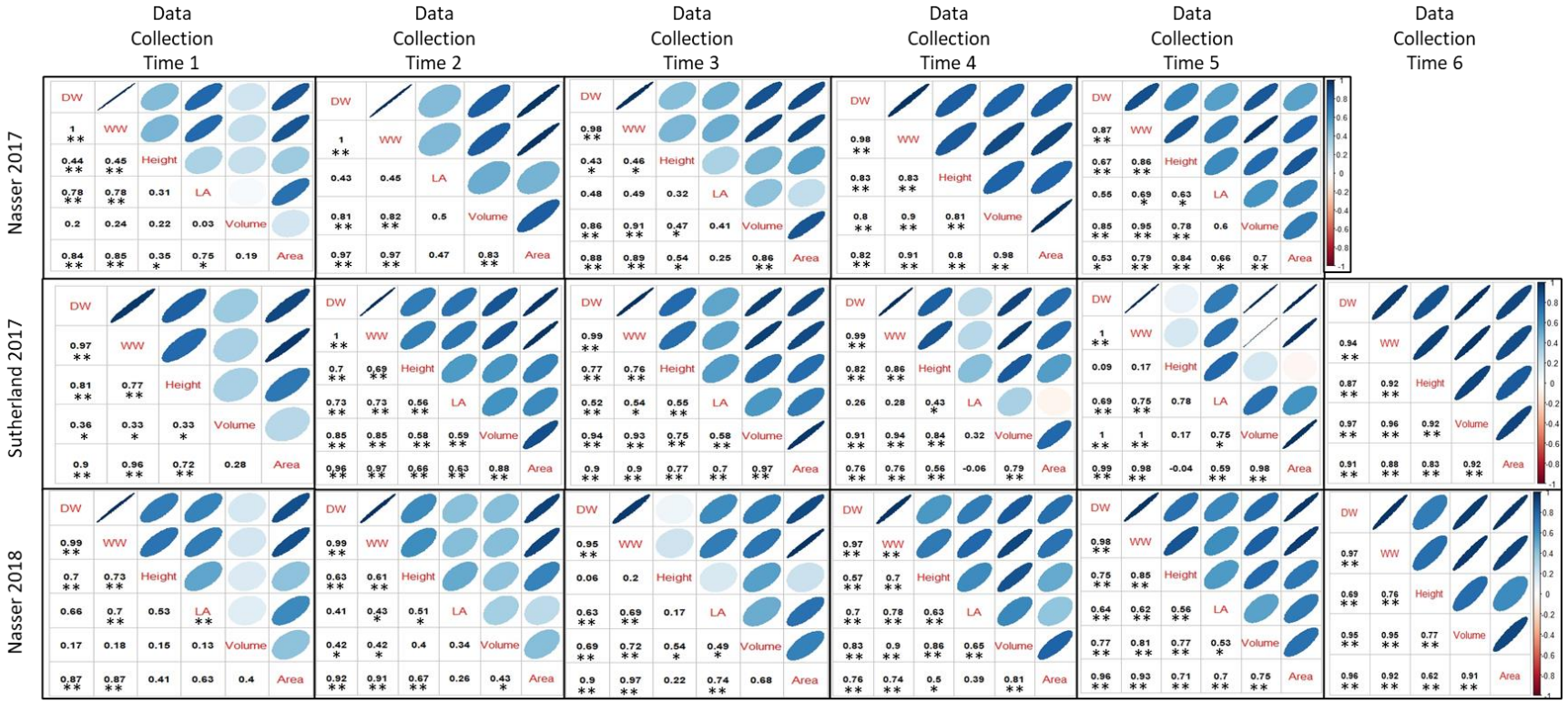

Figure 3-6b: Pearson correlations between wet weight biomass (WW), dry weight biomass (DW), height, leaf area (LA), plot volume (Volume), and vegetation area (Area) at each data collection time point and each site-year. Additionally, LA was measured at Nasser 2017, Sutherland 2017, and Nasser 2018 site-years. Ellipses represent Pearson correlation coefficient (R), with perfect correlation being a straight line and zero correlation being a perfect circle. Positive correlations are shown in blue, and negative correlations are shown in red. Significant Pearson correlations having a p-value <0.05 are shown with one asterisk (*), and a p-value of <0.05 with two asterisks (**).

It should be noted that despite indications that wet weight biomass may be an equal or superior proxy for dry weight biomass, further analysis in this study solely utilized dry weight biomass for clearer comparison with previously published literature. Additionally, there may be greater opportunity for experimental error when wet weight biomass is utilized due to varying internal and external moisture, such as dew or precipitation, on plant material depending on weather and the time of day when the material was collected. It is biologically unsurprising that wet weight biomass was strongly correlated with image-based parameters, as it is expected that lush, moist vegetation should have large, full-expanded leaves to maximize light intercepting and gas exchange capability. Bramley et al. (2015) noted a progressive reduction in destructively measured leaf area and leaf turgor pressure of bread wheat following initiation of water-limited conditions. With a decrease in turgor pressure and leaf area, it is presumed that a decrease in vegetation area and plot volume would result as well. Because the selected genotypes examined were expected to have different GDD requirements to reach various growth stages, as well as due to the potential for varied field conditions throughout the trial, it would seem logical that wet weight biomass should be more highly correlated with vegetation area and plot volume than dry weight biomass. This is expected because these traits are expected to fluctuate to a greater extent under varying conditions and growth stages than dry weight biomass, which is expected to generally increase over the course of the growing season.

3.4.3 Vegetation Area as a Measurement of Plot Biomass

Both wet and dry weight biomass were highly correlated with plot area at many data collection time points throughout the experiment (Figures 3-6a and 3-6b). In a study by Tomasel et al. (2001), foliar area of bunchgrass was evaluated using a chromaticity-based pixel counting method which utilized individual RGB images collected manually from 1.4 m above ground level. The study found highly significant correlation between green pixels and dry weight biomass in field situations without a large amount of overlapping leaves. It is therefore expected that vegetation area will be a useful parameter to estimate lentil biomass early in the growing season before significant vertical growth occurs.

At the first biomass sample timing, correlation between biomass and area was high (>0.84) at all site-years except Rosthern 2018 where there was no noteworthy relationship

(Figures 3-6a and 3-6b). It was likely that image resolution was too low at Rosthern 2018 to sufficiently capture plant material due to small plant size at the first biomass sampling period. At the first biomass collection period, individual plants may have ranged in size from 1-2 cm when viewed from a nadir perspective. As GSD realized for data collection ranged from 4.5-1.0 mm depending on which sensor as utilized and the altitude imagery was collected from (Table 3-5). Significance of the calculated correlations based on p-value also tend to be low early in the growing season. It is likely that this can also be attributed to insufficient resolution to effectively evaluate the small plants early in the growing season. Correlation between volume and area at the first data collection timing is low at all site-years, suggesting that area is a more useful parameter for early-season measurement of plant growth. At collection 3 in Nasser 2017, collection 4 and 5 in Rosthern 2017 and Rosthern 2018, and collection 5 in Sutherland 2017 and Nasser 2018, the correlation between biomass and area experienced a decrease from the trend. Because this mid-season dip in correlation occurred at every site-year, it seems unlikely to be caused by an error in data collection. As Figure 3-5 shows, ILL 9888 and ILL 7716 both abruptly stop increasing and begin to decline in height at the 3rd biomass collection date at all site-years except Nasser 2017. As this occurred at approximately the middle of the growing season at approximately late flowering stage, growth rate was likely high so it is likely that the dip in correlation was due to an increase in plant height which was not accompanied by an increase in plant area. As the season further progressed, plant stems became unable to support the increasing weight of the canopy and lodging occurred. Additionally, leaf and tendril growth were expected to continue in some genotypes after the overall increase in canopy height slowed (Erskine et al., 2009). Collectively, this led to the infilling of inter-row space with vegetation and again increased the correlation between plant biomass and remotely-measured plant area. Using similar methodology in dry bean (*Phaseolus vulgaris*), Sankaran et al. (2018) noted increasing correlation between area and biomass from early to mid-season data collection but significantly reduced correlation during late pod-fill. Similar reduced late-season correlation only occurred at one site-year, Nasser 2017, likely due to a high level of disease late in the growing season that resulted in rapid senescence.

3.4.4 Vegetation Volume as a Measurement of Plot Biomass

Volume correlations with wet and dry biomass followed a generally increasing trend at all site-years except Rosthern 2017 throughout the growing season (Figures 3-6a and 3-6b). Volume was poorly correlated with biomass at the first biomass sampling time at all site-years with the highest correlation being only 0.36 at Sutherland 2017. This low early-season correlation was likely due to insufficient resolution to produce a meaningful volume estimation on the small plant sizes observed. On the second biomass sampling date, the correlation between biomass and volume was reasonably high (>0.80) at all site-years except Rosthern 2018, with a correlation of 0.43, and Nasser 2018 with a correlation of 0.42. For the remainder of the growing season, correlations between biomass and volume remained relatively consistent or slightly increased when observed over time. These findings align with those of Sun et al. (2018), who observed strong correlation between LiDAR point cloud-derived volume of cotton plots with manually measured volume. These findings are also consistent with SfM-based biomass estimation in various herbaceous crops including *Vicia sativa*, *Triticum sativum, Secale cereal, Medicago sativa*, and *Triticosecale* performed by Gil-Docampo et al. (2018) which identified SfM to be a useful tool for biomass estimation in field crops.

Dixit et al. (2017) identified a large variation in HI and biomass in lentil varieties and indicated a need to select both for high HI and for high biomass varieties to identify high-yielding germplasm. Using late-season plot volume measurements combined with predicted or manually-measured seed yield, both above-ground crop biomass and HI parameters may be calculated to allow selection of material with high-yield potential for further analysis and breeding development uses. Currently, evaluation of HI is highly uncommon in plant breeding endeavours due to the enormous time requirement to measure above-ground biomass despite being a highly informative trait for development of efficient crop varieties.

3.4.5 Ability to Estimate Leaf Area using Volume, Area, and Biomass Measurements

Leaf area was measured at Nasser 2017, Sutherland 2017, and Nasser 2018 trials (Figure 3-6a). This study did not aim to investigate the utility of destructively measured leaf area for the

purpose of differentiating among genotypes. It is noteworthy, however, that leaf area measurements had a lower ability to identify statistically significant differences among genotypes when compared to other phenotypic traits analysed (Table 3-6). It is likely that this is, at least in part, due to errors associated with the need to evaluate sub-samples resulting in lower precision rather than the whole plot due to time and cost constraints.

The importance of crop light interception ability for growth and yield is well-documented (Watson, 1958; Monsi and Saeki, 1953; Monsi and Saeki, 2005). Relationships between leaf area with biomass, area, and volume existed in this study, however the correlations between leaf area and any of these parameters were frequently well below 0.60 (Figures 3-6a and 3-6b). The correlations between biomass and destructively sampled leaf area were not greater than the correlations between biomass and remotely-sensed plot area. However, leaf area did correlate more favourably with biomass early in the season than plot area and volume. Remotely-sensed area measurements would likely correlate more highly at early-season time points with higher resolution imagery. At some timepoints early in the growing season, leaf area correlated quite highly with vegetation area (up to R=0.75) while at other time points leaf area and vegetation area did not appear related (Figures 3-6a and 3-6b). Roth et al. (2018) found that by including estimated leaf angle with UAV photogrammetry at various canopy heights in soybean, leaf area index (LAI) estimation tended to be more closely related with destructively measured LAI than with non-destructively measured LAI using a handheld meter. Little literature comparing UAV and manually-derived LAI in small field crops comparable to lentil exists. Tunca et al. (2018) found a strong exponential relationship between UAV-detected NDVI and LAI in sunflower (*Helianthus annuus*) field plots, concluding LAI could be reliably estimated using spectral data from a UAV platform. Differences in the ability to measure LAI of lentil compared to sunflowers are expected, as sunflowers have significantly different plant architecture and more prominent foliage than lentils. Corcoles et al. (2013) compared manually quantified leaf area in onion with UAV photogrammetry-based vegetation area with a coefficient of determination of 0.837 for a linear model, indicating a direct relationship between LAI and groundcover in onion. While onion foliage is closer in size to lentil than sunflower, plant architecture varies significantly between the two crops. It is suspected that the inconsistent relationship between vegetation area and leaf area is due to variability in leaf area among plants chosen for sub-sampling in this study, as large variation was often noted between sub-samples derived from the same plot. Despite the

fact that a sub-sample of only three plants per plot and only three of five site-years were utilized for this study, destructive leaf area measurements were still some of the most time-consuming data points to collect. As a result of the high time requirement and relatively poor results achieved from destructive leaf-area analysis, it is suggested that the need for a high level of accuracy on an individual plant-basis should be weighed against time-savings, ease, and reduced sub-sampling error associated with whole-plot high-throughput phenotyping approaches for measuring plot volume and vegetation area.

3.4.6 Relationship Between Canopy Height and Other Parameters of Plant Growth

Height measurements (Figure 3-5) were collected in this study to clarify the interaction among various plant traits as well as to evaluate the effect of height on estimations of above-ground biomass. As Figure 3-5 shows, height for all genotypes initially increased steadily before decreasing in the middle of the growing season. This decrease in height can be attributed to lodging as stems lose their flexibility and biomass moves to higher levels in the canopy due to pod development and filling. The correlation of height with other parameters is inconsistent, and it is therefore not an ideal predictor of any of biomass or area parameters (Figures 3-6a and 3-6b). Walter et al. (2018) noted strong correlation between above ground biomass and both manually and point cloud-derived plant height measurements. However, the inconsistent correlation of plant height with plant biomass determined in the present study suggests that plant height does have an important effect on plant biomass but is not independently an effective predictor of plant biomass in diverse lentil germplasm.

3.5 Conclusion

Overall, remotely-detected vegetation and plot biomass trends were highly related to various ground-measured parameters that are typically collected in plant research and breeding programs. Results of this experiment indicate vegetation area measured from a UAV may have utility in estimating lentil biomass and be indicative of leaf area early in the growing season. For mid to late-season biomass estimation, plot volume was determined to be a better estimator of plot biomass. Because vegetation area and plot volume parameters can be attained with a single

UAV flight lasting only a few minutes in the field environment, these traits can be evaluated using minimal resources in the field at ideal time-points. Collected images will serve not only for the estimation of plot biomass and groundcover, but may also be used as a field record and perhaps to extrapolate other traits related to plant growth and productivity. Although the time required for image processing and data analysis is not trivial, it can be performed at a convenient time outside of the field environment. Additionally, only a fraction of the processing and analysis procedure requires active user interaction with the software, allowing other tasks to be performed concurrently. It is likely that in the near future, image processing and analysis will be an automated or semi-automated process requiring minimal user inputs (Ahmed et al., 2019).

Although this study was not designed to compare wet weight biomass to dry weight biomass, significant correlation between wet weight biomass and dry weight biomass were observed at most data collection points. Additionally, wet weight biomass was frequently correlated with plot volume to a similar or greater extent than dry weight biomass. It is therefore suggested that wet weight biomass may be a suitable parameter in lieu of dry weight biomass in experiments where efficiency is deemed to be of greater importance than a biological basis for measuring dry weight biomass.

Dry weight biomass was found to be highly correlated with vegetation area throughout most of the growing season. However, the correlation between dry weight biomass and vegetation area was inconsistent during mid-season data collection points at most site-years examined, deeming it inadequate as an estimator of whole-season biomass. Vegetation area was highly correlated with dry weight biomass at early-season data collection points at most site-years, suggesting early-season biomass estimation capability. Although plot volume was less correlated with dry weight biomass at early-season data collection points, its correlation with dry weight biomass increased consistently throughout the growing season at all site-years. These results coincide with observations made by Sun et al. (2018) comparing LiDAR-derived volume with biomass in cotton. By late-season data collection points, plot volume was either similarly or more-highly correlated with dry weight biomass than vegetation area. Due to its consistent improvement in correlation with dry weight biomass throughout the growing season and high correlation with dry weight biomass late in the growing season, it is suggested that plot volume

is an acceptable high-throughput proxy for dry weight biomass of mid to late-season analysis of lentil.

Reasonably high levels of correlation at early-season datapoints suggest a definite relationship between leaf area and vegetation area, despite inconsistent correlation throughout the season (Figures 3-6a and 3-6b). Although further investigation is needed, it is suspected that vegetation area may be a more reliable estimate of overall plot-level photosynthetic potential than destructive leaf area analysis in lentil early in the growing season due to the large sampling error component of destructive leaf area analysis.

4.0 A Novel Approach to Describing Lentil Plant Growth and Development using UAV Imagery

4.1 Introduction

Plant growth rate is an essential component of plant fitness, as rapid growth rate will increase the ability of the crop to compete with other species and to efficiently capture essential resources such as sunlight, carbon dioxide, and water. As above-ground plant material is responsible for sunlight harvesting and gas exchange processes, the quantification of above-ground plant material can give insight into production potential of various crop species (Biere, 1996; Rees et al., 2010).

Evaluation of plant growth rate is typically based off of either height (Holman et al., 2016; Wang et al., 2019) or biomass (Saint Pierre et al., 2012). The collection and measurement of biomass is very tedious and time-consuming, resulting in a significant expense in large plant research and breeding programs. Biomass evaluation in a field setting is inherently destructive to the plant necessitating larger area and more resources (Saint Pierre et al., 2012). While biomass measurements and growth evaluation may be made more easily in indoor, potted environments, plants are unlikely to perform equally to field-based experiment, potentially reducing the utility of results (Bhatnagar-Mathur et al., 2008; Villar et al., 2005; Yang et al., 2010). Cereal crops such as maize and wheat tend to have height that is very highly correlated with biomass (Fernandez et al., 2009). Because of this, simply measuring height can give a very good estimate of biomass. Therefore, by measuring the rate of height increase over a period of time, growth rate may be effectively deduced (Holman et al., 2016; Wang et al., 2019). In bushy crops such as lentil, however, biomass is less correlated with height and the ability to predict biomass based on height alone is reduced. When all plants observed are of the same species and variety and are expected to grow and develop in the same manner, models may be produced to adjust for variation resulting from lateral branching in the horizontal plane (Thomson et al., 1998). In cases where precise morphology of plants is unknown or known to be inconsistent, biomass estimation from height alone would likely result in insufficient accuracy and reproducibility.

The collection of multiple overlapping images with high spatial and temporal resolution is possible with the use of UAV's. Utilizing SfM techniques, this imagery can be utilized to produce high-density 3-D point clouds, from which several parameters can be measured. This

approach has been utilized previously for the measurement of grassland (Wijesingha et al., 2019) and forest/shrub (Alonzo et al., 2018; Jimenez-Brenes et al., 2017; Karpina et al., 2016) biomass. Similar work has utilized 3-D laser scanners to produce 3-D point clouds for analysis (Seidel et al., 2011). While previously published studies utilize SfM techniques to acquire height information (Malambo et al., 2018; Schirrmann et al., 2016; Walter et al., 2018), and utilize height information for calculation of plant growth rate (Shucun and Frelich, 2011), very few consider crop volume. No literature could be found at the time of writing evaluating SfM-derived volume of bushy field crops in a field environment.

Above-ground vegetation biomass, area, and volume are reasonably well-correlated with one-another (Chapter 3) and may be used to obtain generalized inferences among one-another at various times in the growing season. Further analysis has potential to evaluate parameters of biomass, area, and volume basis over time and across different environments. The objective of this experiment was to evaluate the potential for the quantification of plant growth rate utilizing UAV-based imagery collected multiple times throughout the growing season. Rapid, non-destructive evaluation of plant growth rate could be utilized in a variety of plant research and breeding programs to efficiently evaluate material best-suited for particular environments and stresses in a field environment. Furthermore, similar methodology may find utility in larger-scale operations such as prediction of crop yield by producers, crop insurance agencies, and for the purpose of yield monitoring (Marshall et al., 2011).

4.2 See Chapter 3.2 for **Materials and Methods**.

4.3 Statistical Analysis

Statistical analysis was performed utilizing the DRC package (Ritz and Streibig, 2016) run in R (R Core Team, 2017) on RStudio version 1.1.456 (RStudio Team, 2016). Data for dry weight biomass, vegetation area, and plot volume at each site-year was truncated to remove late-season declining values. Three-parameter logistic nonlinear models (Equation 4.1) were constructed independently at each site-year (Figures 4-2, 4-3, and 4-4), with initial above-ground biomass assumed to be zero. These models are frequently utilized in plant biomass modelling

(Paine et al., 2012; Yin et al., 2003). In the three-parameter model (Figure 4-1) *e* represents the G50, or the number of GDD required to accumulate 50 % of maximum growth, parameter *b* represents the growth rate around G50, or growth rate, and parameter *d* represents the upper asymptote of the curve or predicted maximum growth. The three-parameter model utilized is described by equation 4.1, where *b* = slope at *e*, c = lower asymptote = 0, *d* = upper asymptote, and *e* = the effective dose ED50 (Ritz et al., 2015).

$$f(x,(b,c,d,e)) = c + \frac{d-c}{1+\exp\left(b(\log(x)-\log(e))\right)} \qquad (4.1)$$

Parameter estimation in the DRC package is based on the maximum likelihood principle. The "transform-both-sides approach" was executed using a Box-Cox transformation to control variance heterogeneity and help to ensure a normal distribution. (Ritz et al., 2015; Box and Cox, 1964)

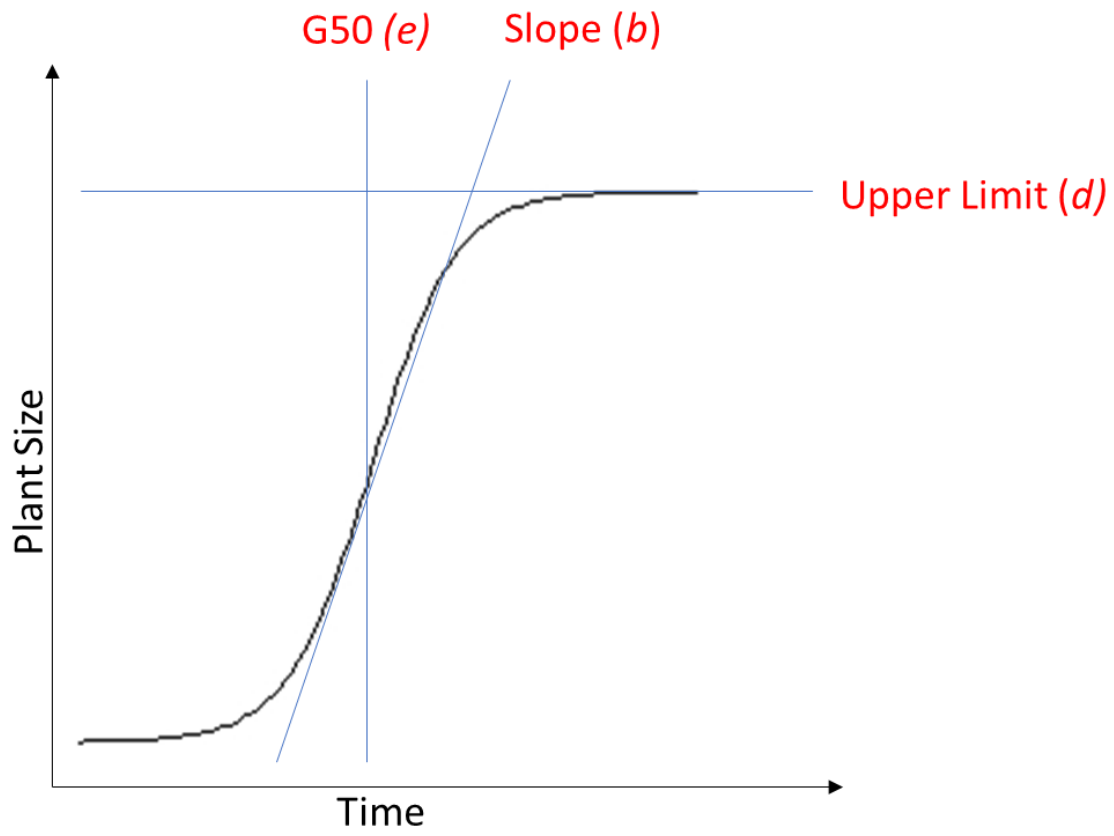

Figure 4-1: A model three-parameter logistic non-linear model representing growth rate (b) at e, maximum predicted growth (d), and G50 (e).

For each site-year, genotypes were analyzed both individually and combined. ANOVA was then performed and used to determine that all site-years except Nasser 2017 showed significant overall difference between the model comparing individual genotypes and the model with genotypes combined at a 5 % significance level. Akaike Information Criterion (AIC) was compared among models at each site-year. AIC-based selection indicated that the model utilizing individual genotypes explained a greater amount of variance in data at all site-years except Nasser 2017. Additionally, models for individual genotypes converged with insignificant lack-of-fit tests at all site-years, except Nasser 2017, indicating acceptable model fit. It was, therefore, determined that a model including individual genotypes should be utilized at Sutherland 2017, Rosthern 2017, Nasser 2018, and Rosthern 2018. Data at Nasser 2017 was best described by combing all genotypes within the model. A lack of significant variance among genotypes was also indicated by ANOVA for several traits (Table 3-6), giving insight regarding temporal differences among genotypes. To handle variance heterogeneity that may be present in the data, R functions *coeftest* and *sandwich* were utilized to obtain robust standard errors (Ritz et al., 2015). P-values for each parameter are shown in Appendices 1, 2, 3, 4, and 5.

4.4 Results and Discussion

4.4.1 Ground-Measured Data

For the purposes of this study, the fitted three-parameter non-linear logistic curve was applied only to a dataset truncated to omit any end-of-season decline in dry weight biomass. As each genotype examined expressed large variation in maturity timing, earlier-maturing genotypes were well past physiological maturity and had completed senescence before the last harvest date. This resulted in a physical loss of some plant components during collection and might have contributed to a false reduction in recorded dry weight biomass. Average dry weight biomass varied substantially among site-years, with most genotypes in Rosthern 2017 experiencing nearly three times the dry weight biomass of those in Nasser 2018. While 1100 to 1200 GDD was calculated at most site-years, it is noteworthy that the Nasser 2017 trial was seeded at a later date in the spring and therefore was only exposed to approximately 800 GDD. It can be assumed that this reduced thermal growth period likely had an effect on the total accumulated biomass. Additionally, the Nasser 2017 trial was planted into loose, heavily cultivated soil and the season

was abnormally dry and warm. Disease that occurred near the end of the growing season caused premature desiccation of the trial. These factors likely contributed to the inability to effectively differentiate among genotypes at Nasser 2017. In most site-years, CDC Redcoat and CDC Asterix were the two largest genotypes, and ILL 9888 and ILL 7716 were the smallest based on the predicted estimate (Figures 4-2 and 4-5).

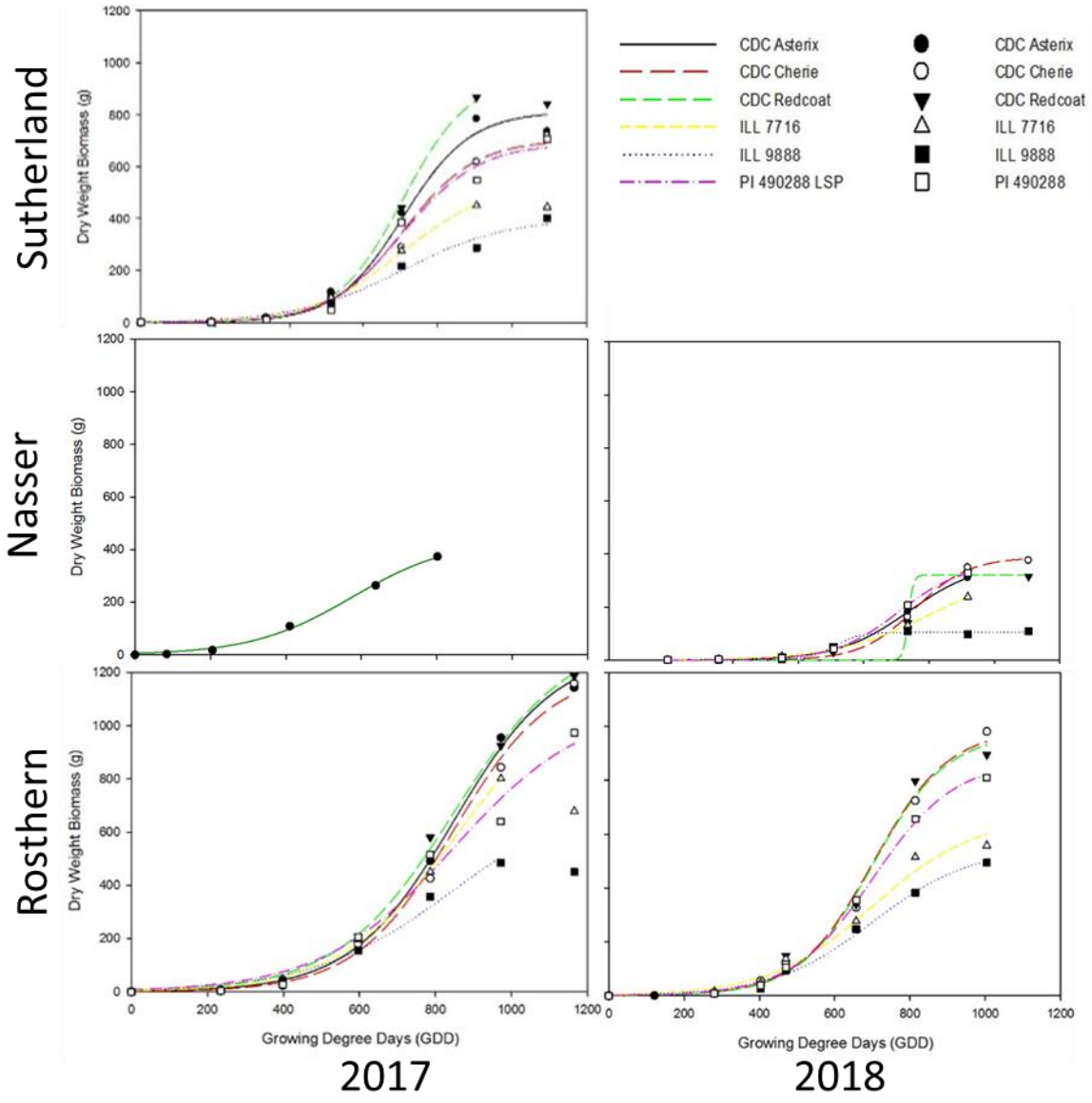

Figure 4-2: 3-parameter growth curves showing dry weight biomass accumulation for each genotype throughout the growing season at each site-year. Data at Nasser 2017 was best described by combing all genotypes within the model.

4.4.2 2-Dimensional Analysis

Two-dimensional imagery was captured and processed to calculate various greenness indices, including gNDVI (Equation 2.3), bNDVI (Equation 2.4), and NGRDI (Equation 2.5). Because these indices could not be compared directly, thresholding was performed to identify green vegetation area by manually identifying pixels having indices values which were representative of green vegetation and performing further analysis only on pixels exceeding that value. The area of pixels that were determined to contain green vegetation was then determined. Accumulation and maximal green pixel area values often differed among genotypes and site-years. Although similarities can be seen in Rosthern 2018 and Nasser 2018 when the order of vegetation area extrapolated from Figure 4-3 is compared to dry weight biomass (Figure 4-2), trends do not clearly match at any site-year. This relatively poor likeness is, at least in part, due to the accumulation of height and density that cannot be accounted for using a 2-D approach which measures groundcover. It should be noted that the 2-D approach does quite consistently identify large, medium, and small genotypes correctly with CDC Redcoat and CDC Asterix generally having the greatest area, and ILL 9888 generally having the lowest area (Figure 4-3). An exception to this occurs in Nasser 2018, where CDC Redcoat was identified as 4th largest in vegetation area where it was also 4th in dry weight biomass (Figure 4-2). This anomaly may be explained by a large standard error estimate for CDC Redcoat in Nasser 2018 in biomass, vegetation area, and plot volume (Figure 4-4). Because the standard error is large in manually-collected biomass as well as remotely-detected vegetation area and plot volume, this variance from the trend is likely to be due to influence from either the environment or G×E interaction, and it has likely been accurately identified using the 2-D and 3-D image analysis approaches.

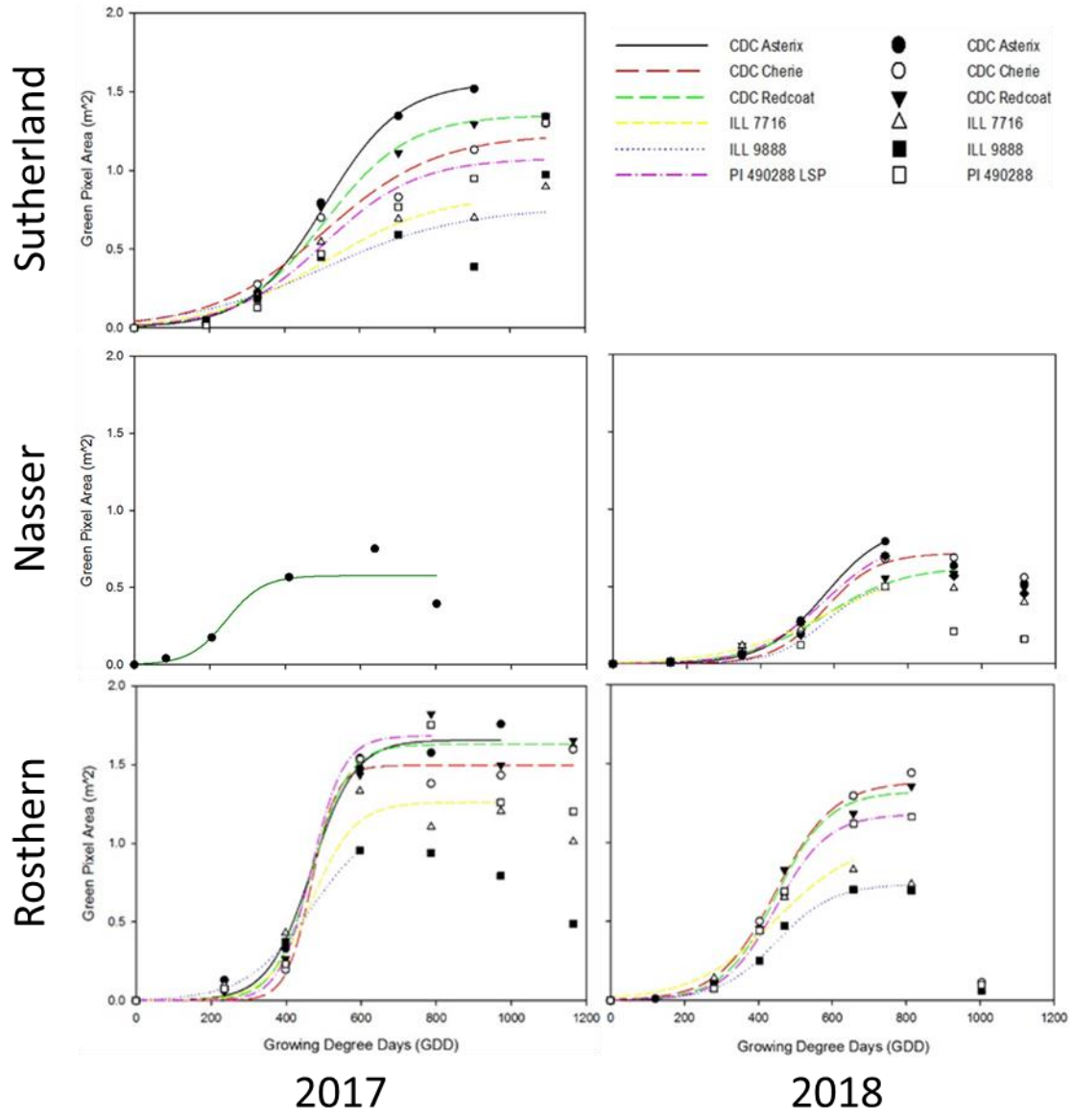

Figure 4-3: 3- parameter growth curves showing Green Pixel Area accumulation for each genotype throughout the growing season at each site-year. Data at Nasser 2017 was best described by combing all genotypes within the model.

G50, or the time required to reach 50 % of total growth, values suggest significant variation among both genotype and environment (Figure 4-7). It is highly probable that differences in seeding time and weather conditions are responsible for significantly different G50 values among site-years. Additionally, there may be G×E interactions occurring which would cause certain genotypes to be differentially suited to specific environments. G50 of manually

measured biomass, G50 of calculated vegetation area, and G50 of calculated plot volume (Figure 4-7) are not consistent among genotypes or site-year, which suggests genetic, environmental, and possibly G × E interaction all have an effect on G50. Overall, G50 of area is significantly lower than G50 of biomass. This indicates that the crop reaches 50 % of total groundcover earlier in the season than 50 % of total biomass. Because rapid groundcover increases competitive ability and resource capturing capability, this trait might have great utility for breeding programs and other crop research initiatives (Kumar et al., 2012; Fedoruk et al., 2011).

Area growth rate, the rate of vegetation area increase, values differ significantly among several genotypes and site-years (Figure 4-5). At Rosthern 2017, CDC Cherie and ILL 7716 have considerably larger area growth rates than other genotypes in the same site-year as well as all other genotypes at all other site-years (Figures 4-4 and 4-5). These large variations in area growth rate are likely indicative of the ideal growing conditions experienced in Rosthern 2017 as well as the ability of CDC Cherie and ILL 7716 to rapidly produce groundcover under such growing conditions.

Seedling vigour and rapid groundcover are essential for the crop to effectively establish with reduced need for weed control by producers (Fedoruk et al., 2011). As such, vigour and groundcover measurements are often obtained manually in crop breeding programs due to their strong relationships with interspecific competitive capabilities, tolerance to biotic and abiotic stresses, and final seed yield (Revilla et al., 1999; Tollenaar and Wu, 1999; Kumar et al., 2012). Similar studies in maize utilizing spectral indices for biomass estimation have been performed attaining high correlation with plant biomass and a high level of repeatability (Montes et al., 2011; Winterhalter et al., 2011).

4.4.3 3-Dimensional Analysis

Large differences in volume accumulation were observed among genotypes and site-years (Figures 4-4, 4-5, and 4-6). Overall, volume growth trends follow a pattern which appears more similar to those observed for dry weight biomass than plot area (Figures 4-3, 4-4, 4-5, and 4-6). This trend is substantiated by the generally high correlation between dry weight, volume, and area shown in Figure 3-6a and 3-6b. The volume data obtained at Rosthern 2018 was poorly

described using the curve chosen for data analysis in this experiment. It is suspected that this is due to the relatively late seeding date followed by ideal growing conditions throughout the season, culminating in a high maturation rate due to sudden onset of disease (Figure 4-4). Between the time of the greatest plot volume and the next image collection date, volume had declined significantly, and data was truncated to avoid false late-season underestimation by the model. When fitted to a three-parameter logistic curve, this resulted a poor fit of the growth curve which resulted in unrealistically large maximum predicted volume and G50 estimations and unrealistically small volume growth rate, or rate of plot volume increase, estimations (Ritz and Streibig, 2012). As the trends shown in Figure 4-4 are based on the maximum observed value prior to data truncation, it is still believed that this approach is useful in estimating plant size and growth parameters. A lack-of-fit test was performed for all site-years and was insignificant for Rosthern 2018 indicating that the model fit the data to an acceptable level, so parameter outputs were considered to be useful for relative comparison among genotypes within the Rosthern 2018 site-year. For the purpose of this experiment, parameter outputs for Rosthern 2018 were not be considered directly comparable to other site-years. Trends based on the maximum measured values for each trait prior to data truncation were instead be utilized for environmental and varietal comparison of Rosthern 2018 (Figure 4-6).

When trends are compared between dry weight biomass and volume (Figures 4-2 and 4-4), genotypes are positioned in a very similar order at most site-years. When considering the model output maximum predicted growth (Figure 4-5), a similar trend can be observed. Overall, CDC Asterix, CDC Redcoat, and CDC Cherie tend to have greater maximum predicted growth. ILL 9888 consistently has the lowest maximum predicted growth, closely followed by ILL 7716. G50 values are relatively similar both among genotypes and among site-years. As standard errors for G50 are quite large at several site-years for all traits examined, it is difficult to make conclusive comparisons (Figure 4-7). However, ILL 7716 and ILL 9888 did tend to have lower G50 values than did CDC Asterix, CDC Cherie, and CDC Redcoat. Overall, G50 is much lower for volume than for biomass (Figure 4-7). This indicates that 50 % of volume was reached earlier than 50 % of biomass was accumulated.

As space-filling ability has important effects on competition and resource harvesting, this may be a useful trait to consider for variety development. Many volume growth rate values have

very large standard errors (Figure 4-5), making comparison inconclusive for many genotypes and site-years. Similar to area growth rate, however, it is noteworthy that many genotypes experienced relatively high volume growth rates in Rosthern 2017. This is indicative of good growing conditions leading to a rapid rate of growth. As volume growth rate determines the rate of volume increase over time, it can be used to describe the rate of 3-D space-filling capability of a genotype. Together with G50 of volume, volume growth rate has potential utility in plant breeding programs for germplasm selection. These traits have the ability to identify germplasm with greater and more rapid early-season growth. Plants that fill space earlier in their lifecycle will have a competitive advantage over weeds as well as greater resource-harvesting capability. A greater ability to acquire and allocate resources (sunlight, carbon dioxide, water, and mineral nutrients) early in the growing season and to remobilize mineral nutrients to developing seed would increase yields (El-Zeadani et al., 2014). Additionally, greater growth and biomass accumulation in times of stress is generally beneficial, and rapid early-season growth may aid in stress-tolerance (Bailey-Serres et al., 2012; Mickelbart et al., 2015).

G50 and GDD required to reach the maximum predicted growth may be more useful parameters for germplasm selection in breeding programs than growth rate at early stages of plant development as growth rate is not expected to vary significantly until the critical density of each genotype has been reached (Deng et al., 2012). The critical density of a crop as described by Deng et al. (2012) may be estimated using G50 values from remotely-evaluated vegetation area or plot volume. Deng et al. (2012) suggested two models that can be used to determine critical density of a crop; a biophysical model which considers plant radius in relation to neighboring plants, and a metabolic model which assumes all plants have a set metabolic rate, which is collectively maximized in a given area when plants are densely packed. Deng et al. (2012) identified a similar initial growth rate in a variety of agricultural crops. Once the critical density was reached, however, growth slowed, with growth of individual plants only occurring when resources were made available by mortality of neighbouring plants. Therefore, the prediction of critical density based off of G50 could be of value to crop research programs with interest in intraspecific competition or seeding density (Andrade et al., 2005), among other topics. Vegetation area and volume parameters may also be useful in predicting the critical density of individual genotypes, giving utility in evaluation the interspecific and intraspecific competitive capabilities of individual genotypes.

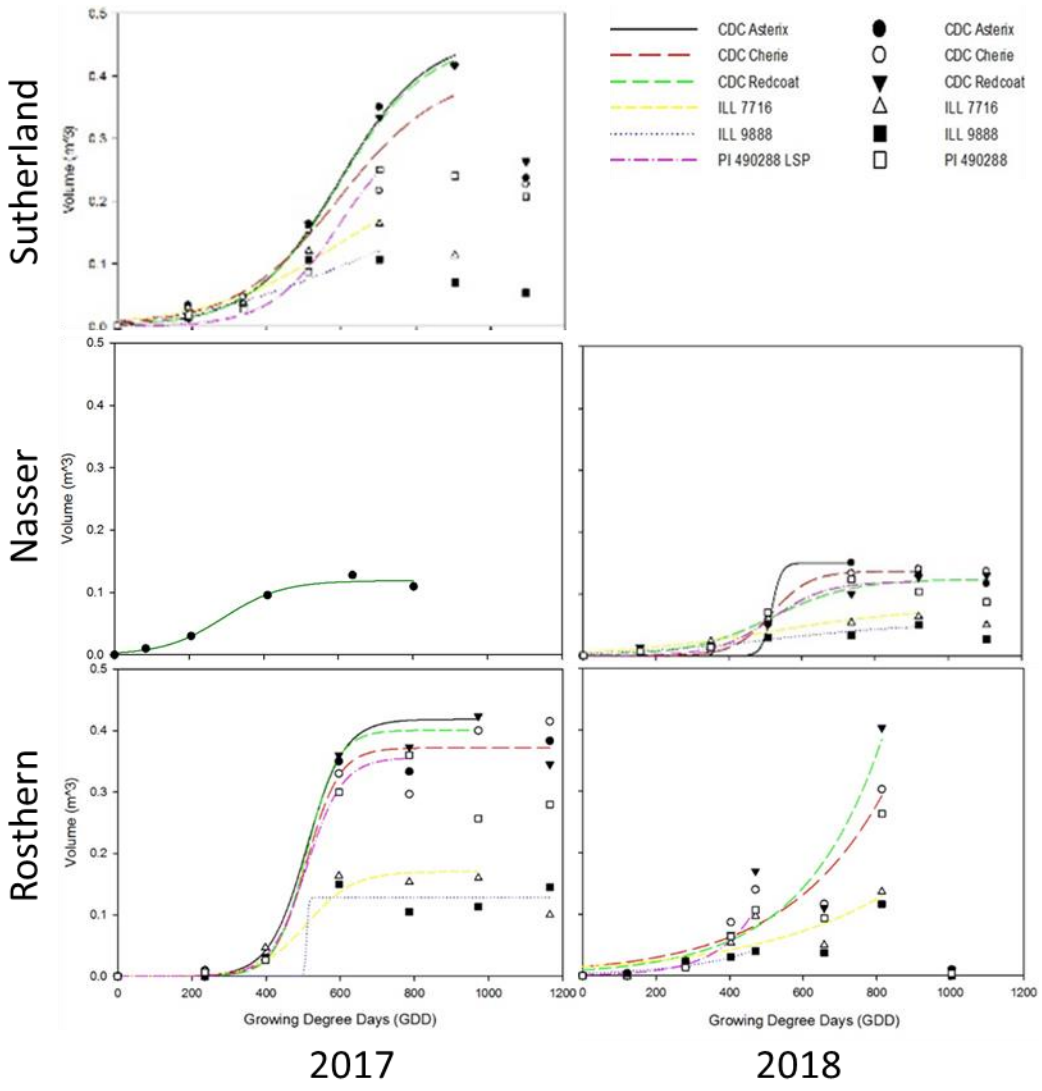

Figure 4-4: 3-parameter growth curves showing volume accumulation for each genotype throughout the growing season at each site-year. Data at Nasser 2017 was best described by combing all genotypes within the model.

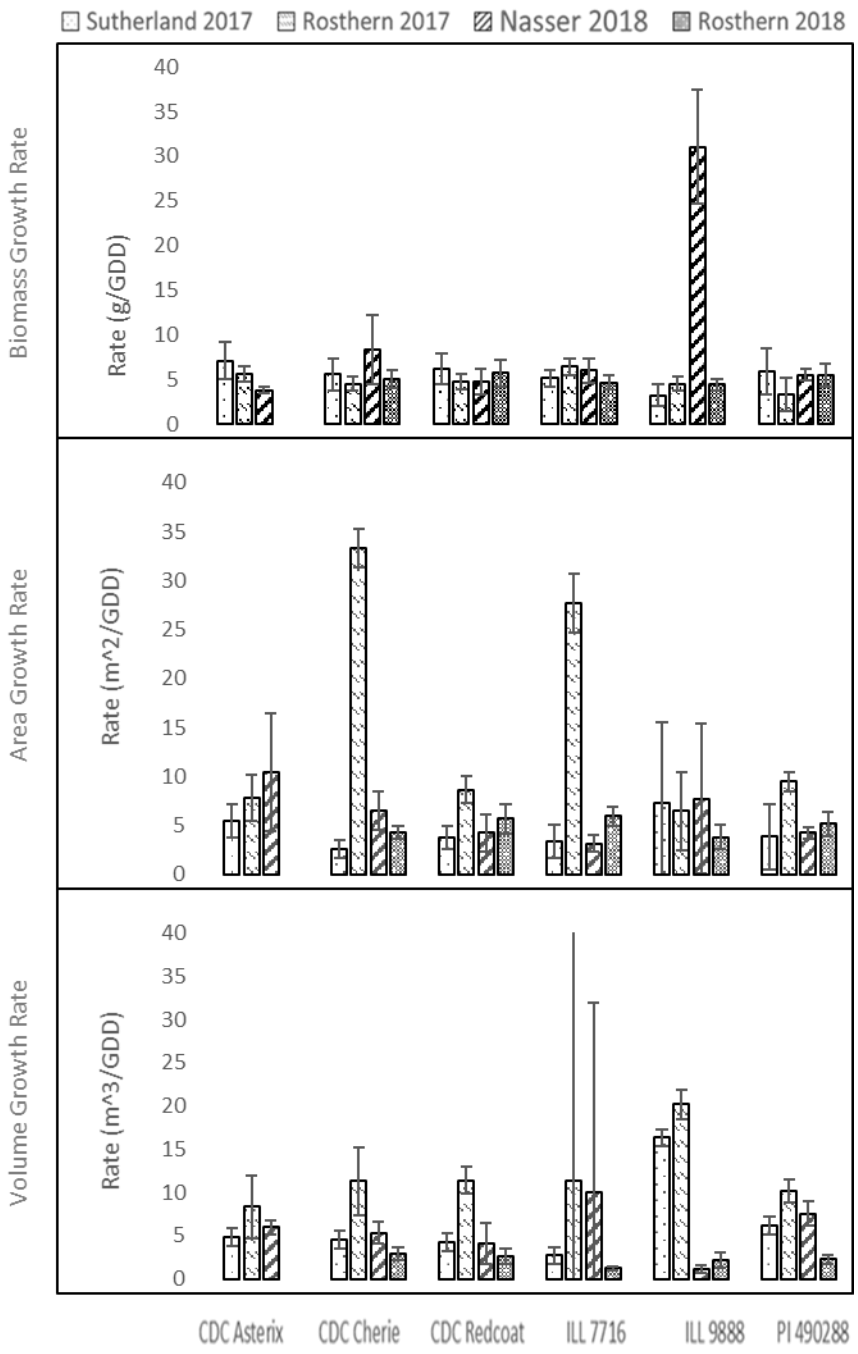

Figure 4-5: Estimated growth rate parameters for dry weight biomass, vegetation area, and plot volume for each genotype at each site-year. Error bars show Standard Error.

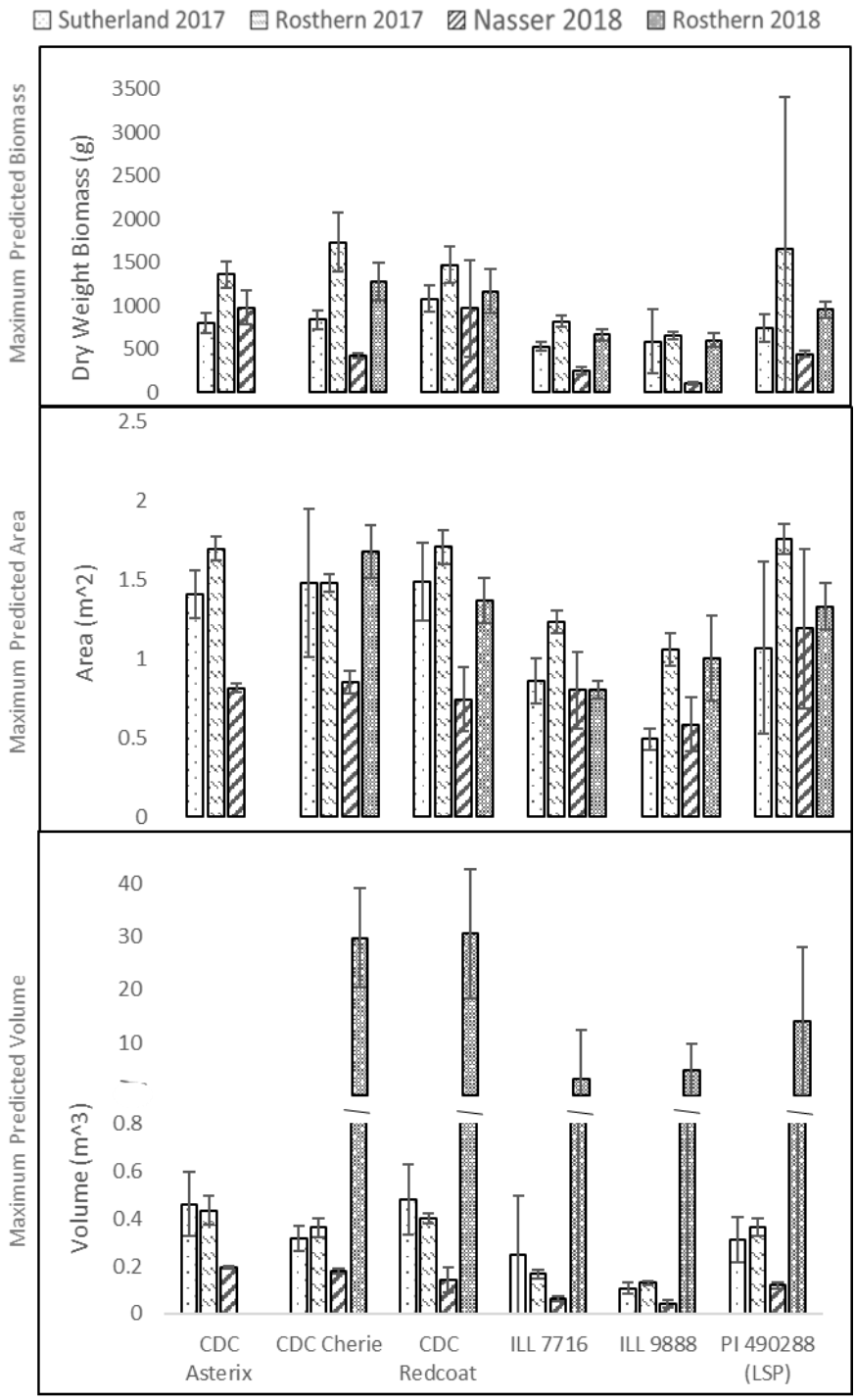

Figure 4-6: Estimated maximum predicted growth parameters for dry weight biomass, vegetation area, and plot volume of each genotype at each site-year. Error bars show Standard Error.

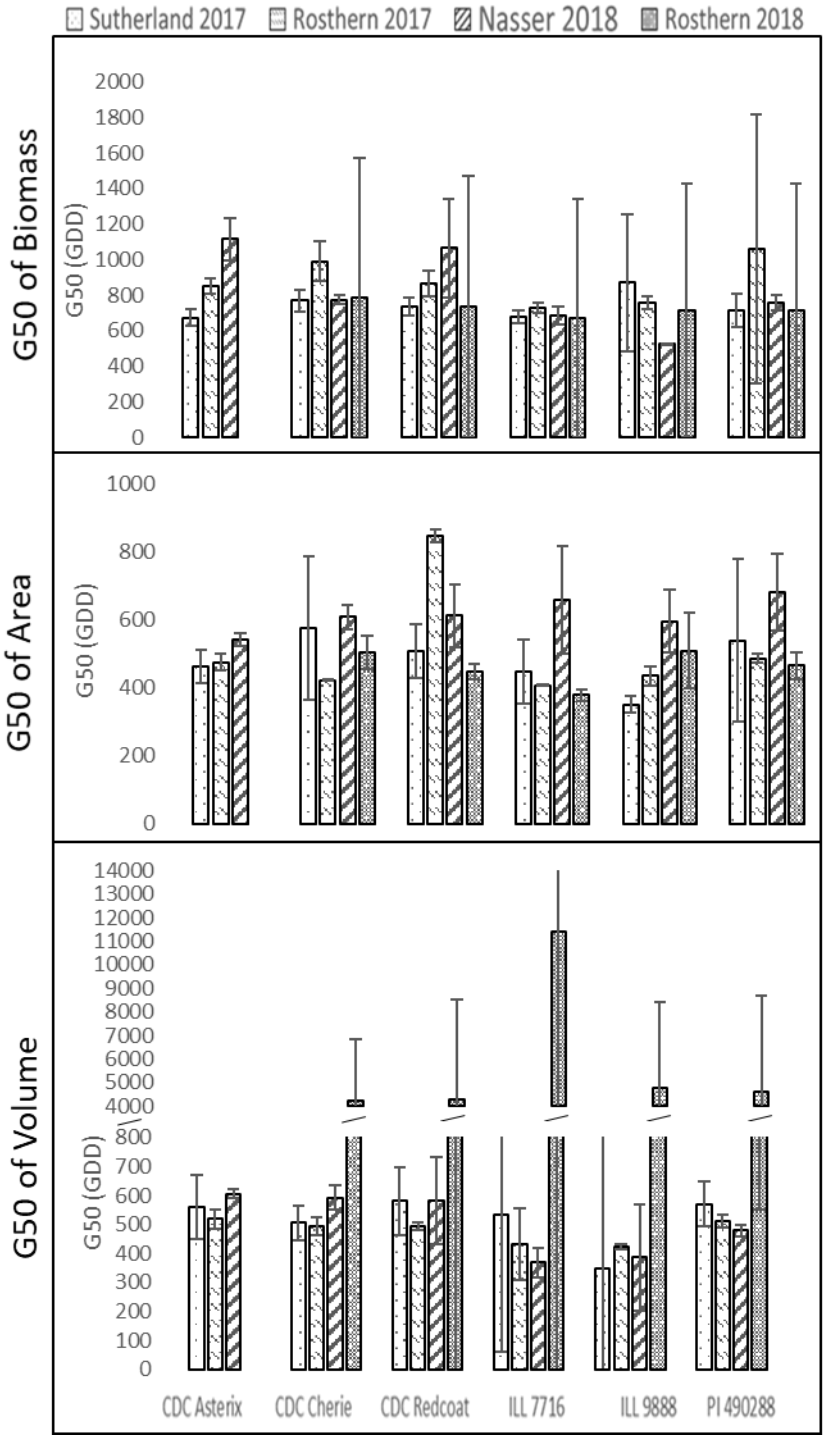

Figure 4-7: Estimate of G50 is shown for dry weight biomass, vegetation area, and plot volume of each genotype at each site-year. Error bars show Standard Error.

4.5 Conclusion

Both vegetation area and plot volume derived from analysis of sequential overhead images collected through the growing season were found to produce trends generally comparable to the accumulation of dry weight biomass throughout the growing season based on visual evaluation of the curves. For generalized experimental data collection purposes, this confirms that vegetation area and plot volume calculated from UAV imagery may useful as a proxy for plant biomass.

Key differences were identified between area, volume, and biomass analyses. Maximum predicted volume was determined to be correlated with end-of-season biomass, and it is proposed that the evaluation of maximum predicted growth relative to other genotypes would be useful in the estimation of end-of-season plant biomass in research programs. Maximum predicted green pixel area may be used to quantify the time to canopy closure, which is a good indicator of early-season competitive potential (Fedoruk et al., 2011). The growth rate parameter of either dry weight biomass, green pixel area, or plot volume may be utilized as an estimation of plant growth rate. The fact that growth rate parameters have a reasonably high likeness when compared among these traits suggests that plant growth rate is similar among dry weight biomass, green pixel area, and plot volume. It is proposed that growth rate calculated from sequential data collection events could be highly useful in a breeding program to evaluate germplasm for desirable rates of growth either throughout the growing season or for the period of a particular physiological growth stage. Area G50 is also useful for the purpose of quantifying rate of canopy closure in 2-D data and Volume G50 is useful in quantifying maximum Volume Growth Rate in 3-D data.

This approach has identified six new traits that were previously unquantifiable in crops with bush-type growth habit without destructive approaches: Area Growth Rate, Area G50, Area Maximum Predicted Growth, Volume Growth Rate, Volume G50, and Volume Maximum Predicted Growth. It is expected that these six new traits will have great potential for use in maximizing efficiency in crop breeding and research programs.

5.0 General Discussion

The ability to evaluate phenotypic parameters associated with plant growth and development is essential for crop physiologists and plant breeders to develop improved crop varieties that may enable higher yields under more sustainable production practices. Manual biomass measurement has historically been used to provide information on crop growth rate. However, manual assessment is so prohibitively time-consuming and labour-intensive that it is rarely performed in large-scale breeding programs. The present study was performed to evaluate novel methods for field-scale evaluation of growth rate and development throughout an entire growing season based on 2-D and 3-D imagery collected from overlapping UAV-based imagery. Vegetation area was deduced from 2-D imagery, and vegetation volume was deduced from SfM-derived 3-D point clouds. Because these data were collected at multiple time-points throughout the growing season, growth rate could also be calculated.

5.1 High Throughput Phenotyping for Plant Growth Traits

The results obtained from this study suggest vegetation area and plot volume traits have great potential in plant research and breeding programs dealing will small, bushy crops such as lentil. Analyzed 2-D imagery data was determined to be effective for non-destructive quantification of early-season biomass and ground cover of lentil which may be converted to a score of early-season vigour as has been done in other species (e.g. Ballari et al., 2016). Analyzed 3-D data was determined to be more effective for non-destructive quantification of late-season biomass. Furthermore, both 2-D and 3-D data enabled calculation of plant growth rate, predicted maximum growth, and growth rate at 50 % of maximum growth (G50), all of which give a tremendous amount of information pertaining to growth and development in field conditions as well as how growth and development interacts with the environment. This ability to determine traits that were previously impossible to accurately quantify non-destructively in small, bushy crop species may allow powerful analyses comparing phenotype with genotype in experiments with larger populations, such as Genome Wide Association Studies (GWAS) (Yang et al., 2014).

Several traits pertaining to growth and development of lentil were quantified based on analysis of 2-D data. Bendig et al. (2014) demonstrated that the use of VIs in prediction of biomass in barley was effective until the booting stage and was not significantly improved by incorporating computed crop height into the model suggesting that 2-D analysis may be sufficient for accurate biomass prediction. While the results of the present study are generally in agreement that 2-D analysis can be used as a proxy for biomass, results were inconsistent throughout the growing season when compared to the 3-D analysis technique. Duan et al. (2017) found a high coefficient of determination (R^2=0.97 for cotton and R^2=0.98 for sorghum (*Sorghum bicolour*)) between orthomosaic-derived groundcover estimates and estimates from a single overhead image, but noted a tendency of orthomosaics-derived groundcover estimates to slightly overestimate actual area when compared to groundcover estimates from a single overhead image in both sorghum and cotton. As the approach utilized in this study relied on a manual, visually-based determination of the thresholding value, it is reasonable that the repeatability of this experiment may be lower than if an OBIA-based automated segmentation approach had been utilized (de Castro et al., 2019). However, because late-season vegetation pixel values varied by only a small amount compared to background pixel values, there was significant risk of area being dramatically over- or under-estimated based on only a small variation of the threshold value selected. It is likely that there is a trade-off between the speed, accuracy, and repeatability of OBIA-based segmentation approaches and the confidence and decision-weighing capabilities of a human operator (Hay and Castilla, 2006). Because of this risk associated with the potential for dramatic over- or under-estimation of area late in the growing season, the manual method of thresholding was preferred to ensure high-quality data that was representative of actual plot parameters. With a highly trained and scrutinized OBIA algorithm in place, there is potential for a further increased efficiency of this high-throughput evaluation approach.

Because green pixel area can be determined relatively cheaply and quickly without damage to vegetation, multiple measurements can be collected through the growing season in applied research programs allowing a calculation of growth rate based on groundcover. This can give insight into light harvesting efficiency and competitive capabilities at early stages in the growing season. In a recent similar study by Moreira et al. (2019), remotely evaluated soybean canopy coverage was identified as a useful trait in early selection, as well as a beneficial

covariate when utilized in yield prediction models. This approach may be of great utility for germplasm selection in breeding programs, or for treatment-response quantification in a wide variety of research endeavors aiming to evaluate biotic or abiotic stress factors.

The 2-D approach quantified groundcover, which may be of great interest when screening for competitive germplasm as early groundcover results in a competitive advantage in a field environment (Nelson et al., 1991) and reduced need for in-crop weed control. Silim et al. (1993) and Shrestha et al. (2005) found a correlation between groundcover and seed yield in lentil, suggesting green area index measurements may have utility in predicting final yield early in the growing season. The critical period for weed control (CPWC), which is the period when the crop is most sensitive to interspecific competition (Kasasian and Seeyave, 1969) in lentil generally ends at the 10-node stage and was found to generally coincide with canopy closure (Fedoruk et al., 2011). A crop capable of rapidly surpassing the CPWC will be able to achieve higher yields with more simple and efficient management strategies.

The 3-D approach to measure volume correlates well with dry weight biomass on most data collection dates, suggesting that vegetation volume estimation from a UAV may be a suitable method of estimating above-ground biomass in lentil. By capturing 3-D information a significantly greater amount of data is present than when using a 2-D approach, resulting in higher correlation with above-ground plant biomass. In the present study, a reduction in correlation between biomass and area occurred approximately mid-season near the end of flower stage (Figures 3-6a and 3-6b). Because this occurred at every site-year, it seems unlikely to be caused by an error in data collection. As Figure 3-5 shows, ILL 9888 and ILL 7716 both abruptly stop increasing and begin to decline in height at the 3rd biomass collection date at all site-years except Nasser 2017. The timing of the decrease coincided with the period of greatest rate of biomass accumulation (Figure 4-2) so it seems likely that the dip in correlation was due to an increase in plant height that was not accompanied by an increase in plant area. As the season further progressed, plant stems became unable to support the increasing weight of the canopy and lodging occurred. Additionally, leaf and tendril growth were expected to continue in some genotypes after the overall increase in canopy height slowed (Erskine et al., 2009). Collectively, this led to the infilling of inter-row space with vegetation and again increased the correlation between plant biomass and remotely-measured plant area. Bendig et al. (2014) examined an

approach to predict biomass in barley based on a model utilizing height information captured using SfM derived point clouds, concluding potential for the method in non-research applications such as in applied agricultural production systems. Tilly et al. (2014) used a similar approach to create a linear regression model of plant height derived from terrestrial laser scanning in paddy rice (*Oryza sativa*) to predict biomass. While both of these studies produced successful results quite similar to the present study, it is likely that analysis of whole plot volume may be more adaptable to different species, as 3-D growth is captured rather than strictly vertical growth. Other research (Holman et al., 2016; Madec et al.,2017) has noted a tendency for SfM photogrammetry-based procedures to consistently underestimate plant height when compared with ground-based measurements and LiDAR. This error may be due to a number of factors, including error resulting in image resolution limitations, GPS accuracy, imperfect algorithms, and faulty ground measurements. However, research by Holman et al. (2016) identified both SfM and LiDAR-based height estimation methods were within 3 cm of ground-based measures in wheat. This level of error may be considered insignificant when considering the increased efficiencies and reduced bias and sampling error possible when compared with manually-measured canopy height measurements. There is a possibility that this consistent underestimation of height would also lead to an underestimation of the vegetation volume determined in this study, and further research will be required to identify the accuracy and consistency of volume estimation in various field crops. It is expected that any underestimation will be consistent across trials and that relative measurements in a trial will be sufficiently accurate for comparison with one-another.

The maximum predicted growth of the curves fit to above-ground biomass, vegetation area, and plot volume generally follow the same trends confirming the potential use of vegetation area and plot volume as proxies for above-ground biomass (Figure 4-6). However, some differences can be seen among biomass, vegetation area and plot volume. Occasional disagreements between trends of these parameters are likely due to the fact that they are, indeed, unique traits. Above-ground biomass will be affected by many factors not considered when determining area and volume including canopy density and the distribution of biomass within the canopy (Whitehead et al., 2000). Vegetation area, in addition, fails to accumulate any information relating to plant height or vertical architecture. Therefore, vegetation area and

volume may be considered unique traits which may be used to describe the growth and development of plants.

As seedlings emerge, the canopy has little height, and most biomass will be in the form of early leaves spreading to capture sunlight, perform photosynthesis, and produce carbohydrates for further growth. This early-emergence stage is a critical period in the life of the plant, because the faster it is able to harvest sunlight, produce carbohydrates, and increase in size, the greater competitive fitness advantage it will have over neighboring plants (Biere, 1996). This early fitness advantage over other plants competing for the same resources can equate to increased biomass, and therefore yield potential, over the entire growing season (Biere, 1996). Speed of germination has historically been utilized to measure seed vigour (Maguire, 1962; Marcos-Filho, 2015). By analyzing the area of green material soon after seedling emergence and over a period of time, seedling growth rate can be calculated. In future work, it is likely also possible to deduce emergence date, and therefore to determine speed of germination as well.

As growth continues, plants merge towards one-another. In crop research, it is common and logical to consider a grouped monoculture on a more general basis at this point in the growing cycle. As individuals in a population continue to grow and intraspecific competition intensifies, self-thinning and self-organization begin to occur under high-density conditions. Self-organization is mediated by changes in the red : far-red ratio of incident light and results in alternate stem inclination along a row of plants, enabling each plant to collect a greater amount of solar energy. This allows an overall increase in production per unit land area (Lopez-Pereira et al., 2017). Self-thinning can be described by:

$$w = C.p^{-3/2} \qquad (5.1)$$

Where p is the density of surviving plants, w is the mean weight of surviving plants, and C varies by species (White and Harper, 1970; Yoda et al., 1963 as cited in White and Harper, 1970).Self-thinning occurs at a predictable rate among a wide variety of species grown in monoculture (White and Harper, 1970; Westoby, 1976) and is due to competition for limited resources, potentially including sunlight (both quality and quantity) and temperature (White and Harper, 1970). As resources become limiting, the smallest individuals are the first mortalities, enable larger ones to grow more quickly (White and Harper, 1970). Because of this natural thinning and

maintenance of plant size, it is logical to view a monoculture plot as a single subject once plants merge, rather than focussing efforts on individual plants.

Growth rate is an essential parameter to understand in various crops, including lentil, due to its demonstrated effect on factors including competitive ability, drought tolerance, and salinity tolerance (Rees et al., 2010, Lachaâl et al., 2002, Ashraf and Waheed, 1990). Both shoot and root size, which are strongly correlated with one another, are important drought-tolerance traits (Sarker et al., 2005). Therefore, selection for larger plants that are capable of efficient resource-harvesting is an important task in plant breeding programs aiming to increase drought, among other stresses, tolerance in lentil. Additionally, plant growth rate can give important indications regarding the effects of various biotic and abiotic conditions experienced throughout the growing season. One abiotic factor affecting plant growth rate is soil fertility. Gulmezoglu and Kayan (2011), for example, found increased nitrogen fertilizer rates to have a positive effect on lentil biomass, seed weight, and nitrogen content of seeds. Whitehead et al. (2000) found lentil biomass to have high correlation with seed yield, suggesting plant growth parameters from various timepoints in the growing season might be useful in identifying yield potential of germplasm. Biomass accumulation at specific physiological stages is known to be a driver of seed yield in several other crops as well. Damisch and Wiberg (1991) suggest that in wheat, selection for high biomass prior to anthesis and maintained growth rates during grain filling are important to achieve high seed yield. A similar trend occurs in rice hybrids, where a high rate of biomass accumulation likely resulting from increased leaf area immediately prior to anthesis is highly correlated with seed yield (Bueno and Lafarge, 2009). Zhang and Flottmann (2016) found canola seed yield to be highly impacted by above-ground biomass and suggested the higher seed yield potential of hybrid varieties could be explained exclusively by differences in biomass, as HI was found to be lower in hybrid varieties than open-pollinated varieties.

5.2 Efficiency of UAV-Based Data Collection

The UAV-based system used for data collection proved to be simple to operate and highly efficient. Most data collection flights in the present study required approximately 10-12 minutes to collect imagery for the 108 70-plant plots. Sun et al. (2018) indicated a data collection time of 6 seconds for each 15-plant plot utilizing a ground-based platform. The UAV-based SfM

approach utilized in this study is much more efficient. Additionally, the use of the UAV platform utilized had no impact on plants, light quality of the image, or compaction of soil as would be expected when utilizing a ground-based platform. Although the UAV utilized did encounter limitations imposed by high winds and active precipitation, the author's experience in this study suggested that UAVs were less impacted by inclement weather conditions than ground-based units due to their reduced data collection time requirements and the fact that they could be deployed regardless of soil and crop conditions. Conversely, ground-based units could typically not be operated for a significant amount of time following rainfall to mitigate the risk of soil compaction, crop damage, and loss of traction by the ground-based unit (White et al., 2012).

As early-season GSD was noted to be inadequate to obtain conclusive results, the procedure utilized was determined to be unable to accurately identify very early crop features. It is therefore suggested that if very early season data is required, acquisition should be performed utilizing either a combination of reduced image-acquisition altitude and a higher-resolution sensor, or a ground-based platform which positions the image-acquisition sensor closer to the crop and has reduced payload weight, data storage, and power consumption limitations.

5.3 Future Research

- Early-season growth parameters such as vegetation area can give insight into plant vigour and germination success, competitive capability, and potential for resource utilization. Very high-resolution imagery is required for this and may be obtained from ground-based systems or very high-resolution cameras on UAV-based platforms flying at ultra-low altitudes. Further investigation should be performed to assess the most practical platform for rapid acquisition of imagery with sufficient resolution to evaluate early-season crop performance. Pena et al. (2018) found a greater ability to estimate biomass of poplar (*Populus* spp.) stands when utilizing a fusion of NDVI and height data obtained using SfM compared to exclusively height information, achieving an R^2 value of 0.540.
- While this study has confirmed that volume information can be efficiently obtained and utilized to describe various crop traits, a protocol must be developed to validate accuracy of volume estimations on crop trials. With a verified calibration protocol, the potential utility of this method of phenotyping could be expanded to production-based applications

and may offer practical benefits to large-scale producers for purposes such as yield estimations, crop damage assessments, or precision agriculture datapoints.

- As this study was performed on a subset of germplasm from the AGILE lentil diversity panel, the techniques described can next be applied to the larger diversity panel. By evaluating plant growth traits on a variety of germplasm, genetic studies such as genome-wide association mapping (GWAS) may be performed to better understand genetic responses to different environments and to identify the genetic control of various traits.
- Further experimentation should be performed to determine differences in wet and dry-weight biomass for evaluation of plant growth in breeding programs. Although the standard for biomass analysis has historically been based on dry weight (Casadesus and Villegas, 2013; Raza et al., 2019), several research, conservation, and industrial projects seek simpler and faster methods of acquiring this information (Helmisaari et al., 2002; Radloff and Ladislav, 2007; Whitbeck and Grace, 2006). As this experiment indicated high correlation between wet weight biomass and vegetation area and plot volume, it seems wet weight biomass would have similar utility to dry weight biomass for the purpose of evaluating plant growth rate. Wet weight biomass can be evaluated in a much shorter time period than dry weight biomass, with reduced transportation requirements and therefore reduced potential for process errors to occur (Cravero et al., 2012). It is essential to determine the relationship between wet and dry wet biomass in field crops, as many image-based high-throughput phenotyping systems will base their data off of fresh material as seen in the field environment (Schirrmann et al., 2016; Tan et al., 2018).

5.4 Final Conclusions

This study has identified several methods with the potential to dramatically increase the efficiency and accuracy of field data collection in plant breeding and research programs using overlapping overhead images that can effectively be processed and analyzed to produce valuable information relating directly to plant growth. Six new traits have been described that can be accurately and efficiently collected from field trials with the use of UAV's or other overhead image-collection systems. These traits are; Area Growth Rate, Area G50, Area Maximum Predicted Growth, Volume Growth Rate, Volume G50, and Volume Maximum Predicted Growth.

Calculated volume was found to correlate well with dry weight biomass, suggesting that the 3-D point-cloud based approach may be useful in the rapid estimation of plant biomass from a UAV platform. Calculated area is also correlated with plant biomass indicating possible utility in estimating biomass from 2-D imagery. However, it is likely that calculated area would have greater utility in capturing early-season rate of groundcover than in measuring late-season biomass. Due to high costs and time commitments associated with the collection of conventional growth rate parameters such as sequential biomass, leaf area, and light interception, collection of these traits is highly limited in practical plant research and breeding initiatives. This study has indicated strong relationships between biomass accumulation and remotely-sensed vegetation area and volume, suggesting that these traits may serve as a good proxy for biomass measurement. As well as being time and cost-effective compared to conventional growth-rate analysis techniques, these methods may allow early and mid-season selection of desirable growth traits and contribute to a diversified approach to future plant research and crop breeding initiatives.

7.0 Appendices

Appendix 1: P-values are displayed for parameter estimates of biomass, area, and volume at Sutherland 2017 (Figures 4-2, 4-3, 4-4, 4-5, 4-6, and 4-7).

	Parameter	Genotype	Biomass p-value	Area p-value	Volume p-value
Sutherland 2017	b	CDC Asterix	0.0010783**	0.0106606*	0.0545018.
	b	CDC Cherie	0.0075081**	0.0448616*	0.0245172*
	b	CDC Redcoat	0.0002363***	0.0226625*	0.0413735*
	b	ILL 7716	0.0247735*	0.1856161	0.6144765
	b	ILL 9888	0.1226977	0.5084299	0.978569
	b	PI 490288 LSP	0.0058059**	0.1480549	0.2150047
	d	CDC Asterix	< 2.2e-16***	0.00000000000000002158***	0.00002469***
	d	CDC Cherie	0.0000002355***	0.0094595**	0.00000000006617***
	d	CDC Redcoat	0.00000000000004659***	0.0000001472***	0.0003888***
	d	ILL 7716	0.000002608***	0.0002548***	0.6235544
	d	ILL 9888	0.2160101	0.000005606***	0.0288056*
	d	PI 490288 LSP	0.000000008287***	0.0098095**	0.0012181**
	e	CDC Asterix	< 2.2e-16***	< 2.2e-16***	0.0000000006881***
	e	CDC Cherie	< 2.2e-16***	0.0122504*	0.00000000000882***
	e	CDC Redcoat	< 2.2e-16***	0.000000006274***	0.0000004175***
	e	ILL 7716	0.00000000000004259***	0.0003936***	0.5596982
	e	ILL 9888	0.0775739.	0.0000005507***	0.6425453
	e	PI 490288 LSP	< 2.2e-16***	0.0007874***	0.00000001271***

Appendix 2: P-values are displayed for parameter estimates of biomass, area, and volume at Rosthern 2017 (Figures 4-2, 4-3, 4-4, 4-5, 4-6, and 4-7).

	Parameter	Genotype	Biomass p-value	Area p-value	Volume p-value
Rosthern 2017	b	CDC Asterix	0.00002139***	0.0001129***	0.0129345*
	b	CDC Cherie	0.0001336***	0.8447085	0.0168705*
	b	CDC Redcoat	0.00001137***	0.000002154***	0.0045896**
	b	ILL 7716	0.000259***	0.8450369	0.7562458
	b	ILL 9888	0.0410868*	0.1517675	0.6892332
	b	PI 490288 LSP	0.0010412**	0.00002314***	0.0098845**
	d	CDC Asterix	0.00000000001392***	< 2.2e-16***	< 2.2e-16***
	d	CDC Cherie	0.0013187**	< 2.2e-16***	< 2.2e-16***
	d	CDC Redcoat	0.00000001446***	< 2.2e-16***	< 2.2e-16***
	d	ILL 7716	< 2.2e-16***	< 2.2e-16***	0.000001256***
	d	ILL 9888	0.002717**	0.00000006961***	0.00000003987***
	d	PI 490288 LSP	0.0538398.	< 2.2e-16***	< 2.2e-16***
	e	CDC Asterix	< 2.2e-16***	< 2.2e-16***	< 2.2e-16***
	e	CDC Cherie	0.000000001536***	0.0008463***	< 2.2e-16***
	e	CDC Redcoat	< 2.2e-16***	< 2.2e-16***	< 2.2e-16***
	e	ILL 7716	< 2.2e-16***	0.000000000002267***	0.0007469***
	e	ILL 9888	0.0000005206***	0.00000000000000002672***	0.0000000324***
	e	PI 490288 LSP	0.0022866**	< 2.2e-16***	< 2.2e-16***

Appendix 3: P-values are displayed for parameter estimates of biomass, area, and volume at Nasser 2018 (Figures 4-2, 4-3, 4-4, 4-5, 4-6, and 4-7).

	Parameter	Genotype	Biomass p-value	Area p-value	Volume p-value
Nasser 2018	b	CDC Asterix	0.00005098***	0.2068709	0.00128**
	b	CDC Cherie	0.0017183**	0.0109888*	0.002111**
	b	CDC Redcoat	0.00003343***	0.0389078*	0.015443*
	b	ILL 7716	0.001551**	0.0440525*	0.652909
	b	ILL 9888	0.9361405	0.0562488.	0.413948
	b	PI 490288 LSP	0.00002214***	0.1629725	0.042982*
	d	CDC Asterix	0.0710893.	0.00000000000003065***	0.0000000005822***
	d	CDC Cherie	< 2.2e-16***	0.000001443***	0.0000000001361***
	d	CDC Redcoat	0.019189*	0.0004356***	0.00000003343***
	d	ILL 7716	0.00000000001018***	0.0346268*	0.00000001974***
	d	ILL 9888	0.00000000000007574***	0.000000003352***	0.928423
	d	PI 490288 LSP	0.0000000002027***	0.3713966	0.0000000000000001128***
	e	CDC Asterix	0.0004119***	< 2.2e-16***	< 2.2e-16***
	e	CDC Cherie	< 2.2e-16***	3.791E-16***	< 2.2e-16***
	e	CDC Redcoat	0.0000001434***	0.00000008311***	0.00000000006771***
	e	ILL 7716	< 2.2e-16***	0.0059821**	0.000000001479***
	e	ILL 9888	0.0123912*	< 2.2e-16***	0.937999
	e	PI 490288 LSP	< 2.2e-16***	0.0853904.	< 2.2e-16***

Appendix 4: P-values are displayed for parameter estimates of biomass, area, and volume at Nasser 2017 (Figures 4-2, 4-3, 4-4, 4-5, 4-6, and 4-7).

	Parameter	Genotype	Biomass p-value	Area p-value	Volume p-value
Nasser 2017	b	CDC Asterix	0.20404	0.0656461.	0.0866435.
	b	CDC Cherie	0.17161	0.5434208	0.1454995
	b	CDC Redcoat	0.12928	0.0572646.	0.1222986
	b	ILL 7716	0.92097	0.6948322	0.5887951
	b	ILL 9888	0.37814	0.485527	0.6098003
	b	PI 490288 LSP	0.18512	0.220733	0.3641058
	d	CDC Asterix	0.63243	0.0001057***	0.00005252***
	d	CDC Cherie	0.61201	0.0000001735***	0.0010251**
	d	CDC Redcoat	0.23779	0.000006478***	0.000002108***
	d	ILL 7716	0.00000000003091***	0.0006082***	0.0044956**
	d	ILL 9888	0.63576	0.0482207*	0.6880613
	d	PI 490288 LSP	0.79658	0.0495049*	0.3927459
	e	CDC Asterix	0.52618	0.00006232***	0.0001391***
	e	CDC Cherie	0.4513	0.005127**	0.0009101***
	e	CDC Redcoat	0.09491.	0.000001436***	0.00000006275***
	e	ILL 7716	0.0000000007845***	0.0035725**	0.0064826**
	e	ILL 9888	0.55967	0.1558248	0.8042223
	e	PI 490288 LSP	0.66425	0.036055*	0.4397135

Appendix 5: P-values are displayed for parameter estimates of biomass, area, and volume at Rosthern 2018 (Figures 4-2, 4-3, 4-4, 4-5, 4-6, and 4-7).

	Parameter	Genotype	Biomass p-value	Area p-value	Volume p-value
Rosthern 2018	b	CDC Cherie	0.000007894***	0.00009475***	0.0100064*
	b	CDC Redcoat	0.00001084***	0.0013014**	0.0036068**
	b	ILL 7716	0.0001397***	0.0036547**	0.3986955
	b	ILL 9888	0.0023239**	0.0632386.	0.5371942
	b	PI 490288 LSP	0.000009695***	0.0009274***	0.0532361.
	d	CDC Cherie	0.00000002998***	0.0000000005052***	0.0055806**
	d	CDC Redcoat	0.000000000003424***	< 2.2e-16***	0.0002387***
	d	ILL 7716	0.000000003641***	< 2.2e-16***	0.00009433***
	d	ILL 9888	0.00009302***	0.010909*	0.1947455
	d	PI 490288 LSP	0.000000000005386***	0.000000000001125***	0.0074611**
	e	CDC Cherie	< 2.2e-16***	2.481E-16***	0.0007708***
	e	CDC Redcoat	< 2.2e-16***	< 2.2e-16***	0.000005776***
	e	ILL 7716	< 2.2e-16***	< 2.2e-16***	0.0006491***
	e	ILL 9888	0.000000001293***	0.000243***	0.179438
	e	PI 490288 LSP	< 2.2e-16***	< 2.2e-16***	0.0014262**

6.0 References

Agriculture and Agri-Food Canada. 2018. Plant Gene Resources of Canada. Available from: https://pgrc.agr.gc.ca/about-propos_e.html. Accessed November 1, 2019.

Ahmed I, Eramian M, Ovsyannikov I, Van der Kamp W, Nielsen K, Duddu H, Rumali A, Shirtliffe S, Bett K. 2019. Automatic detection and segmentation of lentil crop breeding plots from multi-spectral images captured by UAV-mounted camera. IEEE Work App Comp. 1673-1681.

Alba O. 2019. Integrating the organic arsenal for weed control in field pea and lentil (M.Sc. Thesis). University of Saskatchewan.

Alonzo M, Anderson H-E, Morton D, Cook B. 2018. Quantifying boreal forest structure and composition using UAV structure from motion. Forests. 9(3): 119.

Andrade F, Sadras V, Vega C, Echarte L. 2005. Physiological determinants of crop growth and yield in maize, sunflower, and soybean. J. Crop Improv.14:1-2.

Andrade-Sanchez P, Gore M, Heun J, Thorp K, Carmo-Silva A, French A, Salvucci M, White J. 2013. Development and evaluation of a field-based high-throughput phenotyping platform. Funct. Plant Biol. 41: 68-79.

Araus J and Cairns J. 2014. Field high-throughput phenotyping: the new crop breeding frontier. Trends Plant Sci. 19(1): 52-61.

Ashraf M and Waheed A. 1990. Screening of local/exotic accessions of lentil (*Lens culinaris* Medic.) for salt tolerance at two growth stages. Plant and Soil. 128: 167-176.

Bai G, Ge Y, Scoby D, Leavitt B, Stoerger V, Kirchgessner N, Irmak S, Graef G, Schnable J, Awada T. 2019. NU-Spidercam: a large-scale, cable-driven, integrated sensing and robotic system for advanced phenotyping, remote sensing, and agronomic research. Comput. Electron. Agr. 160: 71-81.

Bailey-Serres J, Lee, SC, Brinton E. 2012. Waterproofing crops: effective flooding survival strategies. Plant Physiol. 160(4): 1698-1709.

Ballari D, Orellana D, Acosta E, Espinoza A, Morocho V. 2016. UAV monitoring for environmental management in Galapagos Islands. ISPRS Archives. XLI-B1.

Bekkering, E. 2015. Pulses in Canada. Statistics Canada. Catalogue no. 96-324-X-No. 007. ISSN:0-662-35659-4. Available from: http://www.statcan.gc.ca/pub/96-325-x/2014001/article/14041-eng.pdf. Accessed November 2017.

Bendig J, Bolten A, Bennertz S, Broscheit J, Eichfuss S, Bareth G. 2014. Estimating biomass of barley using crop surface models (CSMs) derived from UAV-based RGB imaging. Remote Sens. 6(11): 10395-10412.

Bendig J, Yu K, Aasen H, Bolten A, Bennertz S, Broscheit J, Gnyp M, Bareth G. 2015. Combining UAV-based plant height from crop surface models, visible, and near infrared vegetation indices for biomass monitoring in barley. Int. J. Appl. Earth Obs. Geoinf. 39: 79-87.

Bhatnagar-Mathur P, Vadez V, Sharma K. 2008. Transgenic approaches for abiotic stress tolerance in plants: retrospect and perspectives. Plant Cell Rep. 27: 411-424.

Biere A. 1996. Intra-specific variation in relative growth rate: impact on competitive ability and performance of *Lychnis flos-cuculi* in habitats differing in soil fertility. Plant and Soil. 182: 313-327.

Blum A, Mayer J, Gozlan G. 1983. Associations between plant production and some physiological components of drought resistance in wheat. Plant Cell Environ. 6: 219-225.

Boote K and Sinclair T. 2006. Significant discoveries and our changing perspective on research. Crop Physiology. Crop Sci. 46:2270-2277.

Box G and Cox D. 1964. An analysis of transformations. J. Royal Stat. Soc. 26(2): 211-252.

Brachi B, Faure N, Horton M, Flahauw E, Vazquez A, Nordborg M, Bergelson J, Cuguen J, Roux F. 2010. Linkage and association mapping of *Arabidopsis thaliana* flowering time in nature. PLoS Genet. 6(5):e1000940

Bramley H, Bitter R, Zimmermann G, Zimmermann U. 2015. Simultaneous recording of diurnal changes in leaf turgor pressure and stem water status of bread wheat reveal variation in hydraulic mechanisms in response to drought. Funct. Plant Biol. 42(10): 1001-1009.

Brede B, Lau A, Bartholomeus H, Kooistra L. 2017. Comparing RIEGL RiCOPTER UAV LiDAR derived canopy height and DBH with terrestrial LiDAR. Sensors. 17(10): 2371.

Breunig MM, Kriegel HP, Ng RT, Sander J. 2000. LOF: identifying density-based local outliers. Sigmod Rec. 29(2): 93-104.

Bueno C and Lafarge T. 2009. Higher crop performance of rice hybrids than of elite inbreds in the tropics: 1. Hybrids accumulate more biomass during each phenological phase. Field Crops Res. 112(2-3): 229-237.

Busemeyer L, Mentrup D, Moller K, Wunder E, Alheit K, Hahn V, Maurer H P, Reif J, Wurschum T, Muller J, Rahe F, Ruckelshausen A. 2013. BreedVision – a multi-sensor platform for non-destructive field-based phenotyping in plant breeding. Sensors. 13(3): 2830-2847.

Calera A, Martinez C, Melia J. 2001. Technical note: A procedure for obtaining green plant cover: relation to NDVI in a case study for barley. Int. J. Remote Sens. 22(17): 3357-3362.

Calvini R, Amigo J, Ulrici A. 2017. Transferring results from NIR-hyperspectral to NIR-multispectral imaging systems: a filter-based simulation applied to the classification of Arabica and Robusta green coffee. Anal. Chim. Acta. 967: 33-41.

Canadian Food Inspection Agency. 2019. Variety Registration Application Form. Retrieved from: https://www.inspection.gc.ca/plants/variety-registration/registration-procedures/application-form/eng/1363059428910/1363059623297. Accessed November 1, 2019.

Cardon L and Bell J. 2001. Association study designs for complex diseases. Nature Reviews. Genetics. 2(2): 91-0.

Casadesus J and Villegas D. 2013. Conventional digital cameras as a tool for assessing leaf area index and biomass for cereal breeding. J. Integr. Plant Biol. 56(1): 7-14.

de Castro A, Rallo P, Suarez M, Torres-Sanchez J, Casanova L, Jimenez-Brenes F, Morales-Sillero A, Jimenez M, Lopez-Granados F. 2019. High-throughput system for the early quantification of major architectural traits in olive breeding trials using UAV images and OBIA techniques. Front. Plant Sci. 10: 1472.

Chappelle E and Kim M. 1992. Ratio analysis of reflectance spectra (RARS): an algorithm for the remote estimation of the concentrations of chlorophyll a, chlorophyll b, and carotenoids in soybean leaves. Remote Sens. Environ. 39: 239-247.

Chen X, Vosman B, Visser RG, van der Vlugt R, Broekgaarden C. 2012a. High throughput phenotyping for aphid resistance in large plant collections. Plant Methods. 8:33.

Chen Z, Devereux B, Gao B, Amable G. 2012b. Aupward-fusion urban DTM generating method using airborne Lidar data. ISPRS J Photogramm Remote Sens. 72: 121-130.

Clemens B. 1975. 375: Type I error rates when multiple comparison procedures follow a significant F test of ANOVA. Biometrics 31: 229-232.

Comar A, Burger P, de Solan B, Baret F, Daumard F, Hanocq J. 2012. A semi-automatic system for high throughput phenotyping wheat cultivars in-field conditions: description and first results. Funct. Plant Biol. 39(11): 914-924.

Condit H. 1970. The spectral reflectance of American soils. Photogramm. Eng. 955-966.

Corcoles J, Ortega J, Hernandez D, Moreno M. 2013. Estimation of leaf area index in onion (*Allium cepa* L.) using an unmanned aerial vehicle. Biosyst. Eng. 115: 31-42.

Crain J, Wei Y, Ill J B, Thompson S, Alderman P, Reynolds M, Zhang N, Poland J. 2016. Development and deployment of a portable field phenotyping platform. Crop Sci. 56: 965-975.

Cravero V, Martin E, Crippa I, Anido F, Garcia S, Cointry E. 2012. Fresh biomass production and partitioning of aboveground growth in the three botanical varieties of *Cynara cardunculus* L. Ind. Crops Prod.37(1): 253-258.

Damisch W and Wiberg A. 1991. Biomass yield-a topical issue in modern wheat breeding programmes. Plant Breeding. 107: 11-17.

Daniel I, Atinsola K, Ajala M, Popoola A. 2017. Phenotyping a tomato breeding population by manual field evaluation and digital imaging analysis. Int J Plant Breed Genet. 11(1): 19-24.

Daughtry C, McMurtrey J, Chappelle E, Hunter W, and Steiner J. 1996. Measuring crop residue cover using remote sensing techniques. Theor. Appl. Climatol. 54: 17-26.

Deery D, Rebetzke G, Jimenez-Berni J, James R, Condon A, Bovill W, Hutchinson P, Scarrow J, Davy R, Furbank R. 2016. Methodology for high-throughput field phenotyping of canopy temperature using airborne thermography. Front. Plant Sci. 7: 1808.

Deng J, Zuo W, Wang Z, Fan Z, Ji M, Wang G, Ran J, Zhao C, Liu J, Niklas K, Hammond S, Brown J. 2012. Insights into plant size-density relationships from models and agricultural crops. Proc. Natl. Acad. Sci. U.S.A. 109(22): 8600-8605.

Dixit G, Kumar A, Parihar A. 2017. Variability for harvest index and biomass in lentil (*Lens culinaris* Medik) varieties. Legume Res. 40(6): 1093-1096.

Donald C and Hamblin J. 1976. The biological yield and harvest index of cereals as agronomic and plant breeding criteria. Adv. Agron. 28: 361-405.

Doneus M, Verhoeven G, Fera M, Briese C, Kucera M, Neubauer W. 2011. From deposit to

point cloud – a study of low-cost computer vision approaches for the straightforward documentation of archaeological excavations. Geoinformatics FCE CTU. 6: 81-88.

Dongwei X, Zhigang D, Yang Z, Tang Q, Sun J, Yang X, Song X, Lu Y, Zhao D, Zhang L, Su J. 2018. Genomic variations and association study of agronomic traits in flax. BMC Genomics. 19:512.

Duan T, Zheng B, Guo W, Ninomiya S, Guo Y, Chapman S. 2017. Comparison of ground cover estimates from experiment plots in cotton, sorghum and sugarcane based on images and ortho-mosaics captured by UAV. Funct. Plant Biol. 44:169-183.

Duveiller G and Defourny P. 2010. A conceptual framework to define the spatial resolution requirements for agricultural monitoring using remote sensing. Remote Sens. of Environ. 114(11): 2637-2650.

El-Zeadani H, Puteh AB, Mondal MMA, Selamat A, Ahmad ZA, Shalgam MM. 2014. Seed growth rate, seed filling period and yield responses of soybean (*Glycine max*) to plant densities at specific reproductive growth stages. Int. J. Agric. Biol. 16(5): 923-928.

Elliot N, Mirik M, Yang Z, Dvorak T, Rao M, Michels J, Walker T, Catana V, Phoofolo M, Giles K, Royer T. 2007. Airborne multi-spectral remote sensing of Russian wheat aphid injury to wheat. Southwestern Entomol. 32(4): 213-220.

Environment Canada. 2018. Climate normals 1981-2010. Saskatoon Diefenbaker Airport. [Online] Available at: http://climate.weather.gc.ca/historical_data/search_historic_data_e.html. Accessed December 18, 2018.

Environment Canada. 2018. Climate normals 1981-2010. Prince Albert Airport. [Online] [Online] Available at: http://climate.weather.gc.ca/historical_data/search_historic_data_e.html. Accessed December 18, 2018.

Erskine W. 1983. Relationship between the yield of seed and straw in lentil. Field Crops Res. 7:115-121.

Erskine W, Muehlbaur F, Sarker A, Sharma B (eds.). 2009a. Pages 4-12. In: *The Lentil: botany, production, and uses. Wallingford*: CABI.

Erskine W, Muehlbaur F, Sarker A, Sharma B (eds). 2009b. Pages 38-41. In: *The Lentil: botany,*

production, and uses. Wallingford: CABI.

ESRI 2015. ArcGIS desktop: release 10. Redlands, CA: Environmental Systems Research Institute.

Estep L, Terrie G, Davis B. 2004. Technical note: crop stress detection using ARVIS hyperspectral imagery and artificial neural networks. Int. J. Remote Sens. 25(22): 4999-5004.

FAO. 2009. How to feed the world 2050. Available From: http://www.fao.org/fileadmin/templates/wsfs/docs/Issues_papers/HLEF2050_Global_Agriculture.pdf. Accessed December 14, 2018.

FAOSTAT. 2017. Countries by commodity. Available from: http://www.fao.org/faostat/en/#rankings/countries_by_commodity. Accessed June 16, 2019.

FAOSTAT. 2016. Countries by commodity. Available from: http://www.fao.org/faostat/en/#rankings/countries_by_commodity. Accessed June 16, 2019.

Fedoruk L, Johnson E, Shirtliffe S. 2011. The critical period of weed control for lentil in western Canada. Weed Sci. 59: 517-526.

Felipe-Garcia B, Hernandez-Lopez D, Lerma J. 2012. Analysis of the ground sample distance on large photogrammetric surveys. Applied Geomatics. 4(4): 231-244.

Furbank R. 2009. Plant Phenomics: from gene to form and function. Funct. Plant biol. 36: v-vi.

Fernandez M, Becraft P, Yin Y, Lubberstedt T. 2009. From dwarves to giants? Plant height manipulation for biomass yield. Trends Plant Sci. 14(8): 454-461.

Gao B. 1996. NDWI- a normalized difference water index for remote sensing of vegetation liquid water from space. Remote Sens. Environ. 58(3): 257-266.

Gausman H. 1977. Reflectance of leaf components. Remote Sens. Environ. 6: 1-9.

Government of Saskatchewan. 2018. 2018 Specialty crop report. Available from: saskatchewan.ca/crops. Accessed January 1, 2020.

Morgan G, Baumann P, Chandler J. 2001. Competitive impact of palmer amaranth (*Amaranthus palmeri*) on cotton (*Gossypium hirsutum*) development and yield. Weed Technol. 15(3): 408-412.

Ge Y, Bai G, Stoerger V, Schnable J. 2016. Temporal dynamics of maize plant growth, water

use, and leaf water content using automated high throughput RGB and hyperspectral imaging. Comput. Electron. Agr. 127: 625-632.

Gomez-Candon D, Virlet N, Labbe S, Jolivot A, Regnard J. 2016. Field phenotyping of water stress at tree scale by UAV-sense imagery: new insights for thermal acquisition and calibration. Precis. Agric. 16(6):786-800.

Gonzalez-Dugo V, Lopez-Lopez M, Espadafor M, Orgaz F, Testi L, Zarco-Tejada P, Lorite I, Fereres E. 2019. Transpiration from canopy temperature: implications for the assessment of crop yield in almond orchards. Eur. J.Agron. 105: 78-85.

Government of Canada. 2019. Flying your drone safely and legally. [Online] Available at: https://www.tc.gc.ca/en/services/aviation/drone-safety/flying-drone-safely-legally.html. Accessed February 1, 2019.

Grüner E, Astor T, Wachendorf M. 2019. Biomass prediction of heterogeneous temperate grasslands using and SfM approach based on UAV imaging. Agronomy. 9: 54.

Gulmezoglu N and Kayan N. 2011. Dry matter and nitrogen accumulation during vegetative and grain filling of lentil (*Lens culinaris* Medic.) as affected by nitrogen rates. Not. Bot. Horti. Agrobo. 39(2): 196-202.

Gil-Docampo M, Arza-Garcia M, Ortiz-Sanz J, Martinez-Rodriguez S, Marcos-Robles J, Sanchez-Sastre L. 2018. Above-ground biomass estimation of arable crops using UAV-based SfM photogrammetry. Geocarto Int. DOI: 10.1080/10106049.2018.1552322

Golzarian G, Frick R, Rajendran K, Berger B, Roy S, Tester M, Lun D. 2011. Accurate inference of shoot biomass from high-throughput images of cereal plants. Plant Methods. 7:2.

Haghighattalab A, Perez L, Mondal S, Singh D, Schinstock D, Rutkoski J, Ortiz-Monasterio I, Singh R, Goodin D, Poland J. 2016. Application of unmanned aerial systems for high throughput phenotyping of large wheat breeding nurseries. Plant Methods. 12:35.

Haile TA, Heidecker T, Wright D, Neupane S, Ramsay L, Vandenberg A, Bett KE. 2019. Genomic selection for lentil breeding: empirical evidence. The Plant Genome. Accepted November 20, 2019. Also currently available on BioRxiv at: https://www.biorxiv.org/content/10.1101/608406v1?rss=1

Han L, Yang G, Dai H, Yang H, Xu B, Li H, Long H, Li Z, Yang X, Zhao C. 2019. Combining self-organizing maps and biplot analysis to preselect maize phenotypic components based on UAV high-throughput phenotyping platform. Plant Methods. 15:57.

Hanlan T, Ball R, Vandenberg A. 2006. Crop growth and biomass partitioning to yield in short-season lentil. Can J Plant Sci. 86(1): 109-119.

Helmisaari H-S, Makkonen K, Kellomaki S, Valtonen E, Malkonen E. 2002. Below-and above-ground biomass, production and use in Scots pine stands in eastern Finland. Forest Ecol. Manag.1-3: 317-326.

Herwitz S, Johnson L, Arvesen J, Higgins T, Leung J, Dunagan S. 2002. Precision agriculture as a commercial application for solar-powered unmanned aerial vehicles. AIAA's 1st Technical Conference and Workshop on Unmanned Aerospace Vehicles. 2002-3404.

Hay G and Castilla G. 2006. Object-based image analysis: strengths, weaknesses, opportunities, and threats (SWOT). OBIA 2006: ISPRS Archives.

Heurich M. 2008. Automatic recognition and measurement of single trees based on data from airborne laser scanning over the richly structured national forests of the Bavarian Forest national park. Forest Ecol Manag. 255(7): 2416-2433.

Hill A, Breschan J, Mandallaz D. 2014. Accuracy assessment of timber volume maps using forest inventory data and LiDAR canopy height models. Forests. 5: 2253-2275.

Hill S, Stephenson D, Taylor B. 1987. Almont yield in relation to tree size. Scientia Horticulturae. 33: 97-111.

Hoffmann H, Nieto H, Jensen R, Guzinski R, Zarco-Tejada P, Friborg T. 2016. Estimating evaporation with thermal UAV data and two-source energy balance models. Hydrol. Earth Syst. Sci. 20: 697-713.

Holman F, Riche A, Michalski A, Castle M, Wooster M, Hawkesford M. 2016. High throughput field phenotyping of wheat plant height and growth rate in field plot trials using UAV based remote sensing. Remote Sens. 8(12): 1-24.

Hu P, Chapman S, Wang X, Potgieter A, Duan T, Jordan D, Guo Y, Zheng B. 2018. Estimation of plant height using a high throughput phenotyping platform based on unmanned aerial vehicle and self-calibration: example for sorghum breeding. Eur J. Agron. 95: 24-32.

Huang Y, Yuan L, Reddy K, Zhang J. 2016. In-situ plant hyperspectral sensing for early detection of soybean injury from dicamba. Biosyst. Eng. 149: 51-59.

Hunt E, Doraiswamy P, McMurtrey J, Daughtry C, Perry E, Akhmedov B. 2013. A visible band index for remote sensing leaf chlorophyll content at the canopy scale. Int. J. Appl. Earth Obs. Geoinf. 21: 103-112.

Ingvarsson P and Street N. 2011. Association genetics of complex traits in plants. New Phytol. 189: 909-922.

Innes J. 1988. Forest health surveys: problems in assessing observer objectivity. Can. J. For. Res. 18:560-567.

Inoue Y, Morinaga S, Tomita A. 2000. A blimp-based remote sensing system for low-altitude monitoring of plant variables: a preliminary experiment for agricultural and ecological applications. Int. J. Remote Sens.. 21(2): 379-385.

Jiang Y, Li C, Paterson A. 2016. High throughput phenotyping of cotton plant height using depth images under field conditions. Comput Electron Agr. 130: 57-68.

Jimenez-Beril J, Deery D, Rozas-Larraondo P, Condon A, Rebetzke G, James R, Bovill W, Furbank R, Sirault X. 2018. High throughput determination of plant height, ground cover, and above-ground biomass in wheat with LiDAR. Front. in Plant Sci. 9:237.

Jimenez-Brenes F, Lopez-Granados F, de Castro A, Torres-Sanchez J, Serrano N, Pina J. 2017. Quantifying pruning impacts on olive tree architecture and annual canopy growth by using UAV-based 3D modelling. Plant Methods. 13(55):1-15

Jogloy C, Jaisil P, Akkasaeng C, Kesmala T, Jogloy S. 2011. Heritability and correlation for components of crop partitioning in advanced generations of peanut crosses. Asian J. Plant Sci. 10(1): 60-66.

Karpina M, Jarzabek-Rychard M, Tymkow P, Borkowski A. 2016. UAV-based automatic tree growth measurement for biomass estimation. ISPRS Archives. XLI: B8.

Kasasian L and Seeyave J. 1969. Critical periods for weed competition. PANS. 15(2): 208-212.

Kipp S, Mistele B, Baresel P, Schmidhalter U. 2014. High-throughput phenotyping early plant vigour of winter wheat. Eur. J. Agron. 52(B): 271-278.

Kirchgessner N, Liebisch F, Yu K, Pfeifer J, Friedli M, Hund A, Walter A. 2016. The ETH field phenotyping platform FIP: a cable-suspended multi-sensor system. Funct Plant Biol. 44(1): 154-168.

Kumar A and Tripathi R. 1990. Relationships between leaf water potential, canopy temperature and transpiration in irrigated and nonirrigated wheat. J. Agron. Crop Sci. 166: 19-23.

Kumar J, Basu P, Srivastava E, Chaturvedi S, Nadarajan N, Kumar S. 2012. Phenotyping of traits imparting drought tolerance in lentil. Crop Pasture Sci. 63(6): 547-554.

Khan Z, Chopin J, Cai J, Eichi V, Haefele S, Miklavcic S. 2018. Quantitative estimation of

wheat phenotyping traits using ground and aerial imagery. Remote Sens. 10(6): 950.

Lachaâl M, Grignon C, Hajji M. 2002. Growth rate affects salt sensitivity in two lentil populations. J. Plant Nutr. 25(12): 2613-2625.

Lande R and Thompson R. 1989. Efficiency of marker-assisted selection in the improvement of quantitative traits. Genetics, 124 (3): 743-756.

Leeper A, Chan S, Salisburry K. 2011. Point clouds can be represented as implicit surfaces for constraint-based haptic rendering. 2012 Ieee Symp Comp Commu. 12847416.

Lelong C, Burger P, Jubelin G, Roux B, Labbe S, Baret F. 2008. Assessment of unmanned aerial vehicles imagery for quantitative monitoring of wheat crop in small plots. Sensors. 8(5): 3557-3585.

Lev-Yadun S, Gopher A, Abbo S. 2000. The cradle of agriculture. Science. 288: 1602-1603.

Lopez-Pereira M, Sadras V, Batista W, Casal J, Hall A. 2017. Light-mediated self-organization of sunflower stands increases oil yield in the field. PNAS. 114(30): 7975-7980.

Ma J, Kirkpatrick T, Rothrock C, Brye K. 2013. Effects of soil compaction and *Meloidogyne incognita* on cotton root architecture and plant growth. J. Nematol. 45(2): 112-121.

Madec S, Baret F, de Solan B, Thomas S, Dutartre D, Jezequel S, Hemmerlé M, Colombeau G, Comar A. 2017. High-throughput phenotyping of plant height: comparing unmanned aerial vehicles and ground LiDAR estimates. Front. Plant Sci. 8: 1-14.

Maguire JD. 1962. The physiological potential of soybean seeds treated with thiamethoxam and submitted to storage. Crop Science. 2(2): 176-177.

Malambo L, Popescu S, Murray S, Putman E, Pugh N, Horne D, Richardson G, Sheridan R, Rooney W, Avant R, Vidrine M, McCutchen B, Baltensperger D, Bishop M. 2018. Multitemporal field-based plant height estimation using 3D point clouds generated from small unmanned aerial systems high-resolution imagery. Int. J. Appl. Earth Obs. Geoinformation. 64: 31-42.

Maleki A, Mozafari V, Naseri R, Tahmasebi A, Mirzaeiheydari M. 2014. Leaf water relationships and canopy temperature as criteria to distinguish maize hybrids under drought stress. J. Stress Physiol. Biochem. 10(2): 266-274.

Marcos-Filho J. 2015. Seed vigor testing: an overview of the past, present and future perspective. Sci. Agric. 74(4): 363-374.

Marshall M, Husak G, Michaelsen J, Funk C, Pedreros D, Adoum A. 2011. Testing a high-

resolution satellite interpretation technique for crop area monitoring in developing countries. Int. J. Remote Sens. 32(23): 7997-8012.

McMaster G and Wilhelm W. 1997. Growing degree days: one equation, two interpretations. Agric. For. Meteorol. 87: 291-300.

Mewes T, Franke J, Menz G. 2009. Data reduction of hyperspectral remote sensing data for crop stress detection using different band selection methods. International Geoscience and Remote Sensing Symposium (IGARSS). 3(5418292): III463-III466.

Miko G, Nemeth A. 2013. Combined communication and radio navigation systems for small UAVs. 23rd International Conference Radioelektronika. 13580694. DOI: 10.1109/10.1109/RadioElek.2013.6530932RadioElek.2013.6530932

Mickelbart M, Hasegawa PM, Bailey-Serres J. 2015. Genetic mechanisms of abiotic stress tolerance that translate to crop yield stability. Nat. Rev. Genet. 16(4): 237-251.

Miladinović J, Vidić M, Đorđević V, Balešević-Tubić S. 2015. New trends in plant breeding-example of soybean. Genetika. 47(1): 131-142.

Moreira F, Hearst A, Cherkauer K, Rainey K. 2019. Improving the efficiency of soybean breeding with high-throughput canopy phenotyping. Plant Methods. 15: 139.

Monsi M and Saeki T. 1953. The light factor in plant communities and its importance for dry matter production. Japan J.Botany. 14: 22-52.

Monsi M and Saeki T. 2005. On the factor light in plant communities and its importance for matter production. Ann. Bot. 95: 549-567.

Montes J, Technow F, Dhillon B, Mauch F, Melchinger A. 2011. High-throughput non-destructive biomass determination during early plant development in maize under field conditions. Field Crops Res. 121(2): 268-273.

Muhammed H, 2005. Hyperspectral crop reflectance data for characterizing and estimating fungal disease severity in wheat. Biosyst. Eng. 91(1): 9-20.

Neitzel F and Klonowski J. 2011. Mobile 3D mapping with a low-cost UAV system. Int. Arch. Photogramm. Remote Sens. Spat. Inf. Sci. 38-1:39-44.

Nelson W, Kahn B, Roberts B. 1991. Screening cover crops for use in conservation tillage systems for vegetables following spring plowing. Hortsci. 26(7): 860-862.

Neumann K. 2008. Trends for digital aerial mapping cameras. Int. Arch. Photogramm. Remote Sens. Spat. Inf. 37(B1): 551-554.

Neumann K, Klukas C, Friedel S, Rishbeck P, Chen D, Entzian A, Sterin N, Graner A, Kilian B. 2015. Dissecting spatiotemporal biomass accumulation in barley under different water regimes using high-throughput image analysis. Plant Cell Environ. 38:1980-1996.

Neupane S. 2019. Flowering time response of diverse lentil (*Lens Culinaris* Medik.) germplasm grown in multiple environments (unpublished master's thesis). University of Saskatchewan, Saskatoon, Canada.

Otsu N. 1979. A threshold selection method from gray-level histograms. IEEE Trans. Syst. Man Cybern. 9(1): 62-66.

Paine CE, Marthews TR, Vogt DR, Purves D, Rees M, Hector A, Turnbull LA. 2012. How to fit nonlinear plant growth models and calculate growth rates: an update for ecologists. Methods Ecol. Evol. 3:245-256.

Pena J, Castro A, Torres-Sanchez J, Andujar D, San Martin C, Dorado J, Fernamdez-Qintanilla C, Lopez-Granados F. 2018. Estimating tree height and biomass of a poplar plantation with image-based UAV technology. AIMS Agriculture and Food. 3(3): 313-326.

Pettorelli N, Vik J, Mysterud A, Gaillard J, Tucker C, Stenseth N. 2005. Using the satellite-derived NDVI to assess ecological responses to environmental change. Trends Ecol. Evol. 20(9): 503-510.

Pix4D Support. 2019. How Pix4Dmapper calculates the volume? [Online] Available From: support.pix4d.com/hc/en-us/articles/202559239-How-Pix4Dmapper-calculates-the-Volume-. Accessed February 4, 2019.

Proctor C and He Y. 2015. Workflow for building a hyperspectral UAV: challenges and opportunities. Int. Arch. Photogramm. Remote Sens. Spat. Inf. Sci. 40(1): 415-419.

R Core Team. 2017. R: a language and environment for statistical computing. R Foundation for Statistical Computing, Vienna, Austria. URL https://www.R-project.org/.

Radloff F and Ladislav M. 2007. A quick and robust method for biomass estimation in structurally diverse vegetation. J. Veg. Sci. 18: 719-724.

Raza M, Feng L, Iqbal N, Ahmed M, Chen Y, Khalid M, Din A, Khan A, Ijaz W, Hussain A, Jamil M, Naeem M, Bhutto S, Ansar M, Yang F, Yang W. 2019. Growth and development of soybean under changing light environments in relay intercropping system. PeerJ. 7:e7262.

Reynolds D, Baret F, Welcker C, Bostrom A, Ball J, Cellini F, Lorence A, Chawade A, Khafif

M, Noshita K, Mueller-Linow M, Zhou J, Tardieu F. 2019. What is cost-efficient phenotyping? Optimizing costs for different scenarios. Plant Science. 284: 14-22.

Rasmussen J, Ntakos G, Nielsen J, Svensgaard J, Poulsen R, Christensen S. 2016. Are vegetation indices derived from consumer-grade cameras mounted on UAVs sufficiently reliable for assessing experimental plots? Eur. J. Agron. 74: 75-92.

Rees M, Osborne C, Woodward I, Hulme S, Turnbull L, Taylor S. 2010. Partitioning the components of relative growth rate: how important is plant size variation? Am. Nat. 176(6): E152-E161).

Revilla P, Butron A, Malvar R, Ordas A. 1999. Relationships among kernel weight, early vigour, and growth in Maize. Crop Sci. 39(3): 654-658.

Ritz C and Streibig J. 2012. Dose response curves and other nonlinear curves in weed science and ecotoxicology with the add-on package drc in R. Available from: www. bioassay.dk. Accessed November 11, 2019.

Ritz C, Baty F, Streibig J, and Gerhard D. 2015. Dose-response analysis using R. PLoS ONE 10(12): e0146021.

Ritz C and Strebig J. 2016. Package "drc". Available from: https://cran.rproject.org/web/packages/drc/drc.pdf. Accessed December 10, 2018.

Roth L, Aasen H, Walter A, Liebisch F. 2018. Extracting leaf area index using geometry effects-a new perspective on high-resolution unmanned aerial system photography. ISPRS J. Photogramm. Remote Sens. 141: 161-175.

RStudio Team. 2016. RStudio: integrated development for R. RStudio Inc., Boston, MA. Available from: http://www.rstudio.com. Accessed December 10, 2018.

Sadras V, Lake L, Leonforte A, McMurray L, Paull J. 2013. Screening field pea for adaptation to water and heat stress: associations between yield, crop growth rate and seed abortion. Field Crops Res. 150: 63-73.

Saint Pierre C, Crossa J, Bonnett D, Yamaguchi-Shinozaki K, Reynolds M. 2012. Phenotyping transgenic wheat for drought resistance. J. Exp. Bot. 63(5): 1799-1808.

Sandhu and Singh. 2007. Chapter 1: In: History and Origin. Yadav S, McNeil D, Stevenson P. (eds.) *Lentil: An ancient crop for modern times*. Springer Netherlands.

Sankaran S, Khot L, Espinoza C, Jarolmasjed S, Sathuvalli V, Vandemark G, Miklas P, Carter

A, Pumphrey M, Knowles N, Pavek M. 2015. Low-altitude, high-resolution aerial imaging systems for row and field crop phenotyping: a review. Europ J Agronomy. 70: 112-123.

Sankaran S, Zhou J, Khot L, Trapp J, Mndolwa E, and Miklas P. 2018. High-throughout field phenotyping in dry bean using small unmanned aerial vehicle based multispectral imagery. Comput. Electron. Agr. 151: 84-92.

Sarker A, Erskine W, Singh M. 2005. Variation in shoot and root characteristics and their association with drought tolerance in lentil landraces. Genet. Resour. Crop Evol. 52: 89-97.

Sarker A and Erskine W. 2006. Recent progress in ancient lentil. J. Agr. Sci. 144: 19-29.

Saxena, M. C. 2009. Plant morphology, anatomy, and growth habit. Pages 34-46. In Erskine, W., Muehlbauer, F.J., Sarker, A. & Sharma, B. eds. The lentil: Botany, production and uses. Wallingford: CABI.

Schirrmann M, Hamdorf A, Garz A, Ustyuzhanin A, Dammer K-H. 2016. Estimating wheat biomass by combining image clustering with crop height. Comput. Electron. Agr. 121: 374-384.

Scipy Community. Updated October 25, 2017. Available From: https://docs.scipy.org/doc/scipy/reference/generated/scipy.spatial.ConvexHull.html. Accessed December 1, 2017.

Senthilnath J, Kandukuri M, Dokania A, Ramesh K. 2017. Application of UAV imaging platform for vegetation analysis based on spectral-spatial methods. Comp. Electron. Agr. 140: 8-24.

Shendure J and Hanlee J. 2008. Next-generation DNA sequencing. Nature Biotechnol. 26: 1135-1145.

Seidel D, Beyer F, Hertel D, Fleck S, Leuschner C. 2011. 3D-laser scanning: a non-destructive method for studying above-ground biomass and growth of juvenile trees. Agr. Forest. Meteorol. 151(10): 1305-1311.

Shrestha R, Siddique K, Turner N, Turner D, Berger J. 2005. Growth and seed yield of lentil (*Lens culinaris* Medikus) genotypes of West Asian and South Asian origin and crossbreds between the two under rainfed conditions in Nepal. Aust. J. Agric. Res. 56: 971-981.

Shucun S and Frelich L. 2011. Flowering phenology and height growth pattern are associated with maximum plant height, relative growth rate and tissue mass density in herbaceous grassland species. J. Ecol. 99: 901-1000.

Sieberth T, Wackrow R, Chandler J. 2014. Motion blur disturbs - the influence of motion-blurred images in photogrammetry. Photogramm. Rec. 29(148): 434-453.

Silim S, Saxena M, Erskine W. 1993. Adaptation of lentil to the Mediterranean environment. I. Factors affecting seed yield under drought conditions. Expl. Agric. 29: 9-19.

SKSIS Working Group. 2018. Saskatchewan Soil Information System – SKSIS. A. Bedard-Haughn, M. Bentham, P. Krug, K. Walters, U. Jamsrandorj, and J. Kiss, eds. [Online]. Available: sksis.usask.ca. Accessed May 5, 2020.

Slavov G, Nipper R, Robson P, Farrar K, Allison G, Bosch M, Clifton-Brown J, Donnison I, Jensen E. 2013. Genome-wide association studies and prediction of 17 traits related to phenology, biomass and cell wall composition in the energy grass *Miscanthis sinensis*. New Phytol. 201: 1227-1239.

Snavely N, Seitz S, Szeliski R. 2007. Modeling the world from internet photo collections. Int. J. Comput. Vis. 80:189-219.

Sole A and Valanzano A. 1996. Digital Terrain Modelling. In: *Geographical Information Systems in Hydrology*. Singh V.P., Fiorentino M. (eds). Vol 26. Springer. Dordrecht.

Sonnante G, Hammer K, Pignone D. 2009. From the cradle of agriculture a handful of lentils: history of domestication. Rend. Lencei. 20: 21-37.

Sun S, Li C, Paterson A, Jiang Y, Xu R, Robertson J, Snider J, Chee P. 2018. In-field high throughput phenotyping and cotton plant growth analysis using LiDAR. Front. Plant Sci. 9(16): 1-17.

Tackenberg O. 2007. A new method for non-destructive measurement of biomass, growth rates, vertical biomass distribution and dry matter content based on digital image analysis. Ann. Bot. 99(4): 777-783.

Tan C, Zhang Q, Zhou J, Du Y, Wang D, Luo M, Zhang H, Guo W. 2018. Remotely assessing above-ground fresh biomass weight of wheat based on the combinations of pair vegetation indexes from HJ-CCD images. Cluster Comput. DOI: https://doi-org.cyber.usask.ca/10.1007/s10586-018-2614-0

Thomson E, Mirza SN, Afzal J. 1998. Technical note: predicting the components of aerial

biomass of fourwing saltbrush from shrub height and volume. J. Range Manage. 51: 323-325.

Tilly N, Hoffmeister D, Cao Q, Huang S, Lenz-Wiedemann V, Miao Y, Bareth G. 2014. Multitemporal crop surface models: accurate plant height measurement and biomass estimation with terrestrial laser scanning in paddy rice. J. Appl. Remote Sens. 8(1): 083671.

Tilman D, Balzer C, Hill J, Befort B. 2011. Global food demand and the sustainable intensification of agriculture. PNAS. 108(50): 20260-20264.

Tollenaar M and Wu J. 1999. Yield improvement in temperate maize is attributable to greater stress tolerance. Crop Sci. 39: 1597-1604.

Tomasel F, Paruelo J, Abras G, Ballarin V, Moler E. 2001. A chromaticity-based technique for estimation of above-ground plant biomass. Appl. Veg. Sci. 4: 207-212.

Torres-Sanchez J, Lopez-Granados F, Serrano N, and Arquero O, Pena J. 2015. High-throughput 3-D monitoring of agricultural-tree plantations with unmanned aerial vehicle (UAV) technology. PLoS ONE. DOI:10.1371/journal.pone.0130479

Tunca E, Koksal E, Cetin S, Ekiz N, Balde H. 2018. Yield and leaf area index estimations for sunflower plants using unmanned aerial vehicle images. Environ. Monit. Assess. 190:682.

Tullu A, Tar'an B, Warkentin T, Vandenberg A. 2008. Construction of an intraspecific linkage map and QTL analysis for earliness and plant height in lentil. Crop Sci. 48: 2254-2264.

Ullman S. 1979. The interpretation of structure from motion. Proc. R. Soc. Lond. B. Biol. Sci. 203 (113):405-426.

Underwood J, Hung C, Whelan B, Sukkarieh S. 2016. Mapping almond orchard canopy volume, flowers, fruit, and yield using lidar and vision sensors. Comput. Electron. Agr. 130: 83-96.

Verhoeven G, Doneus M, Brisese C, Vermuelen F. 2012. Mapping by matching: a computer vision-based approach to fast and accurate georeferencing of archaeological aerial photographs. J Archaeol Sci. 39:7:2060-2070.

Villar R, Maranon T, Quero J, Panadero P, Arenas F, Lambers H. 2005. Variation in relative

growth rate of 20 *aegilops* species (Poaceae) in the field: The importance of net assimilation rate or specific leaf area depends on the time scale. Plant and Soil. 272: 11-27.

Virlet N, Sabermanesh K, Sadeghi-Tehran P, Hawkesford M. 2017. Field Scanalyzer: an automated robotic field phenotyping platform for detailed crop monitoring. Funct. Plant Biol. 44: 143-153.

Wallace L, Lucieer A, Malenovsky Z, Turner D, and Vopenka P. 2016. Assessment of forest structure using two UAV techniques: a comparison of airborne laser scanning and structure from motion (SfM) point clouds. Forests. 7:62.

Walter J, Edwards J, McDonald G, Kuchel H. 2018. Photogrammetry for the estimation of wheat biomass and harvest index. Field Crops Res. 21: 165-174.

Wanscher J. 1975. An analysis of Wilhelm Johannsen's genetical term "genotype" 1909-26. Hereditas. 79:1-4.

Wang X, Zhang R, Song W, Han L, Liu X, Sun X, Luo M, Chen K, Zhang Y, Yang H, Yang G, Zhao Y, Zhao J. 2019. Dynamic plant height QTL revealed in maize through remote sensing phenotyping using a high-throughput unmanned aerial vehicle (UAV). Scientific Reports. 9: 3458.

Watson D. 1958. The dependence of net assimilation rate on leaf-area index. Ann. Bot. 22:85.

Wei T and Simko V. 2017. R package "corrplot": visualization of a correlation matrix (Version 0.84). Available from: https://github.com/taiyun/corrplot. Accessed October 10, 2018.

Westoby M. 1976. Self-thinning in *Trifolium subterraneum* not affected by cultivar shape. Aust. J. Ecol. 1: 245-247.

Westoby M, Brasington J, Glasser N, Hambrey M, Reynolds J. 2012. Structure-from-motion photogrammetry: A low cost, effective tool for geoscience applications. Geomorphology. 179: 300-314.

Whitbeck M and Grace J. 2006. Evaluation of non-destructive methods for estimating biomass in marshes of the upper Texas, USA coast. Wetlands. 26(1): 278-282.

White J and Harper J. 1970. Correlated changes in plant size and number in plant populations. J. Ecol. 58(2): 467-485.

White J, Andrade-Sanchez P, Gore M, Bronson K, Coffelt T, Conley M, Feldmann K, French A, Heun J, Hunsaker

D, Jenks M, Kimball B, Roth R, Strand R, Thorp K, Wall G, Wang G. 2012. Field-based phenomics for plant genetics research. Field Crops Res. 133: 101-112.

White J and Conley M. 2013. A flexible, low-cost cart for proximal sensing. Crop Sci. 53: 1646-1649.

Whitehead S, Summerfield R, Muehlbauer F, Coyne C, Ellis R, Wheeler T. 2000. Crop improvement and the accumulation and partitioning of biomass and nitrogen in lentil. Crop Sci. 40: 110-120.

Wijesingha J, Moeckel T, Hensgen F, Wachendorf F. 2019. Evaluation of 3-D point cloud-based models for the prediction of grassland biomass. Int. J. Appl. Earth Obs, 78: 352-259.

Winterhalter L, Mistele B, Jampatong S, Schmidhalter U. 2011. High-throughput sensing of aerial biomass and above-ground nitrogen uptake in the vegetative stage of well-watered and drought stressed tropical maize hybrids. Crop Sci. 51: 479-489.

Xinhua Y, McClure A, Hayes R. 2011. Improvement in regression of corn yield with plant height using relative data. J. Sci. Food Agric. 91(14): 2606-2612.

Xu R, Li C, Velni J M. 2018. Development of an autonomous ground robot for field high throughput phenotyping. IFAC PapersOnLine. 51-17L 70-74.

Yang S, Vanderbeld B, Wan J, Huang Y. 2010. Narrowing down the targets: towards successful genetic engineering of drought-tolerant crops. Mol. Plant. 3(3): 469-490.

Yang C and Everitt J. 2011. Using spectral distance, spectral angle and plant abundance derived from hyperspectral imagery to characterize crop yield variation. Precis. Agric. 13(1): 62-75.

Yang W, Guo Z, Huang C, Duan L, Chen G, Jiang N, Feng H, Xie W, Lian X, Wang G, Luo Q, Zhang Q, Liu Q, Xiong L. 2014. Combining high-throughput phenotyping and genome-wide association studies to reveal natural genetic variation in rice. Nat. Commun. 5: 5087.

Yin X, Goudriaan J, Lantinga E, Vos J, Spiertz H. 2003. Flexible sigmoid function of determinate growth. Ann. Bot. 91: 361-371.

Yuan H, Wang N, Bennet R, Burditt D, Cannon A, Chamberkin K. 2018a. Development of a ground-based peanut canopy phenotyping system. IFAC PapersOnLine. 51(17): 162-165.

Yuan W, Li J, Bhatta M, Shi Y, Baenziger P, Ge Y. 2018b. Wheat height estimation using LiDAR in comparison to ultrasonic sensor and UAS. Sensors. 18(11): 3731.

Yue J, Tian Q, Dong X, Xu K, Zhou C. 2019. Using hyperspectral crop residue angle index to estimate maize and winter-wheat residue cover: a laboratory study. Remote Sens. 11(7): 807.

Zhang H and Flottmann S. 2016. Seed yield of canola (*Brassica napus* L.) is determined primarily by biomass in a high-yielding environment. Crop Pasture Sci. 67: 369-380.